Behavior of Steel Drop-In Connections

Evaluated Utilizing Digital Image Correlation

by

Emily Caroline Doody

A thesis submitted to the Graduate Faculty of
Auburn University
in partial fulfillment of the
requirements for the Degree of
Master of Science in Civil Engineering

Auburn, Alabama
December 14, 2024

Keywords: steel connection, simple connection, shear connection, DIC, steel industry

Approved by

Dr. Matthew Yarnold, Chair, Associate Professor of Civil Engineering
Dr. Kadir Sener, Assistant Professor of Civil Engineering
Dr. Robert Barnes, Professor of Civil Engineering

Abstract

A safer and more efficient drop-in shear connection (compared to conventional shear tab and double angle connections) has been proposed for implementation in the commercial and residential steel frame building industry. This effort is part of the American Institute of Steel Construction's (AISC's) Need for Speed Initiative to reduce the steel construction cycle by 50%. The objective of this thesis is to aid in the development of a future design process for the proposed connection by evaluating the behavior of its various components, specifically the connection angles, girder top flange, and column web, through full-scale testing. Eleven various drop-in connections were tested in realistic girder-to-column and beam-to-column test setups at Auburn University's Advanced Structural Engineering Laboratory. Six girder top flanges and eight angles were observed and analyzed utilizing Digital Image Correlation (DIC), an established optical technique that allows for the visualization of complete strain fields on a specimen's surface. As well, two-column webs were observed via DIC for a typical one-sided beam-to-column connection, like that which is utilized for an exterior beam in a building.

Testing revealed various ductile failure modes, such as transverse and longitudinal bending of the girder's top flange, allowing for large plastic deformations to occur before ultimate failure. It was determined, through surface strains observed on the vertical angle legs, that the current AISC equation to determine single-angle leg shear strength would be adequate for the design of the tested connection angles. Finally, when utilizing a one-sided beam-to-column connection in which the angles are attached to the column web, plastic deformation of the web may occur and should be checked.

Acknowledgments

I would like to express my gratitude to my advisor and principal investigator (PI), Matthew Yarnold, Ph.D., co-principal investigator, Kadir Sener, Ph.D., and fellow researcher, Robel Alemayehu, Ph.D., for their support in my studies and understanding of structural engineering, as well as the guidance and the abundance of contributed knowledge they have put towards this research project. Thank you to AISC and the industry panel members for their time, recommendations, and donated material that has allowed this novel connection to be excelled forward.

As a student who was given the opportunity to pursue my bachelor's and master's degrees at the same institution, I am extremely thankful to the professors who both sparked my interest in structural engineering during undergrad and continued to encourage me throughout my graduate studies. Thank you to all who belong to the Auburn family. You have provided me with experiences and friendships that only the Loveliest Village on the Plains could have. I am especially grateful for those who call the Advanced Structural Engineering Laboratory (ASEL) their second home, which without their kindness and comic relief throughout long days of studying or working in the high bay, graduate school would not have been nearly as enjoyable.

Thank you to my parents, Bill and Leslie Doody, and brother, Mitchell Doody, for their constant encouragement, unwavering love, and sincere interest in my studies and research. Above all else, I thank my Savior, Jesus Christ, for my salvation and for being the One who placed all the above people into my life, allowing me to grow in both faith and wisdom.

Table of Contents

List of Tables

List of Figures

Chapter 1: Introduction

1.1 Background

Structural steel has remained a competitive choice as the primary structural framing material in the United States for many years and for various reasons. The American Institute of Steel Construction (AISC), a century-old non-profit technical institute and advocate of the American steel industry, implemented the Need for Speed Initiative with an ambitious goal of decreasing the overall steel construction cycle timeline by half by 2025. Utilizing a large team of researchers, fabricators, steel erectors, and industry panelists, various innovative ideas were proposed to aid in the completion of this goal through new inventions and redevelopment of current practices.

With a focus on the one aspect that many structures have in common, shear connections, the new drop-in connection seeks to increase erection speed in the field, specifically for residential and commercial steel systems. The shear tab is predominantly used as the connection of choice for designers due to its conventional and reliable design. This connection consists of a prefabricated plate that is shop-welded to a column and field-bolted (with a designer-specified number of bolts) to the web of a beam (AISC, 2022). Figure 1 illustrates the field erection of a shear tab connection. While simplicity is advantageous in this industry, for steel erectors, the shear tab erection process is an inefficient use of time as the beam must be rigged to and upheld by a crane until both sides of the beam have been successfully connected. This process may be further exaggerated for larger shear reactions due to the multitude of bolts specified.

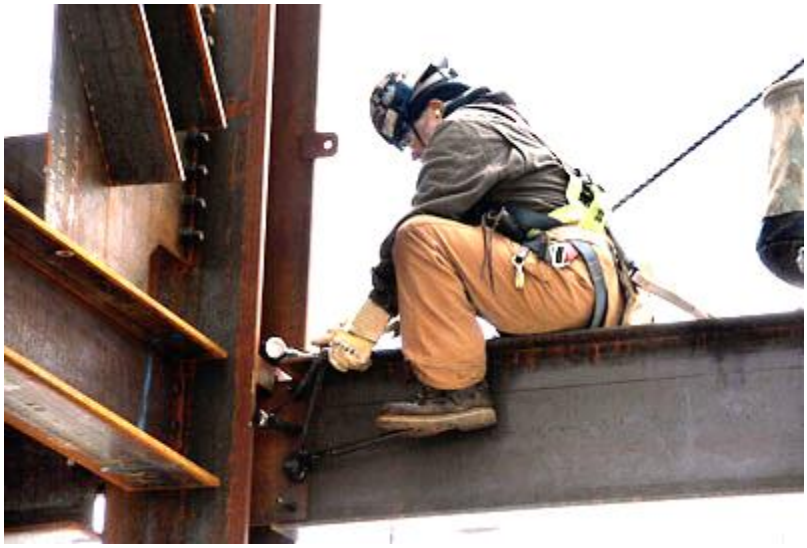

Figure 1: Iron Worker Erecting a Beam with Shear Tab Connection (Boake)

Matthew Yarnold, Ph.D., P.E. and Kadir Sener, Ph.D., P.E. envisioned a shear connection that would employ common practices and materials already familiar to those in the steel industry. The drop-in connection, shown in Figure 2, utilizes two prefabricated steel angles that are shop-welded to a column flange or web. During erection, the beam or girder, featuring a coped bottom flange, is “dropped” or “knifed” between the two angles, creating immediate stability during the erection process. A crane is no longer required to suspend the beam once it has been placed. Two bolts are then placed and tightened in prefabricated holes featured in the beam’s top flange and angles.

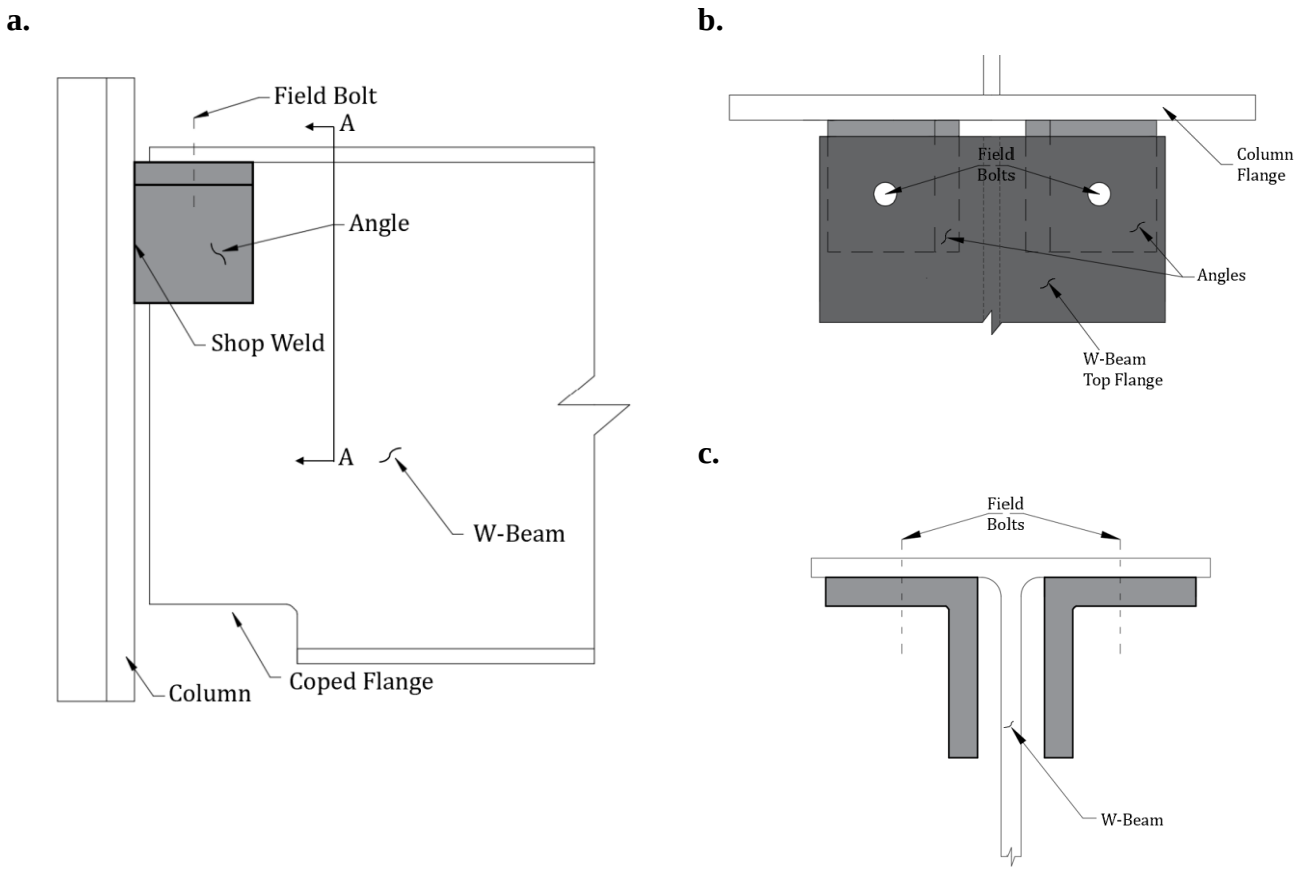

Figure 2: SpeedConnect Drop-In Connection (a) Elevation View (b) Plan View and (c) Cross-Section A-A

While more time and resources may be required during the fabrication process due to welding of the angles to the column and coping of the beam's bottom flange, the overall time required to achieve a positive connection in the field is less than that of the shear tab because of the inherent stability of the beam upon drop-in. As well, the current design proposal specifies two bolts for a singular connection, far fewer than would be anticipated for a shear tab of similar shear capacity. The orientation and location of the bolts are also greatly beneficial for erectors due to their ease of access.

1.2 Objectives

This project was funded by AISC to investigate the proposed drop-in connection for future implementation in the structural steel industry. The primary goal of the research described in this thesis is to aid in the development of a future design process via the following:

- Identify geometric limitations and propose a simple standardized process to be considered before strength design.
- Identify and discuss plastic deformations of the girder top flange
- Identify and discuss plastic deformations of the vertical legs of the connection angles.
- Recommend probable yield line locations of the girder/beam top flange for use in future design equations and yield line analysis.
- Evaluate the shear strain experienced in the vertical angle leg during testing.
- Identify the plastic deformation in a column web due to a drop-in beam-to-column connection.

1.3 Experimental Approach

This study consisted of the investigation of the proposed drop-in connection through full-scale connection testing at the Advanced Structural Engineering Laboratory at Auburn University. Nine girder-to-column drop-in connections, two beam-to-column drop-in connections, and an industry-standard shear tab were tested and investigated via Digital Image Correlation (DIC).

Prior to testing, a representative building layout was chosen for use as the benchmark building in which all connections would be designed accordingly, resulting in industry-typical connection sizes and shear capacities. A team of industry panelists was consulted to determine best practices, ensuring the likelihood of implementation in the field. Table 1 provides the full

list of project panel members. A testing matrix and test setup were then developed to best utilize donated materials in an efficient way. As well, a DIC instrumentation plan was created to properly assess the different connection components: the girder top flange, vertical angle leg, and column web.

Table 1: Project Panel Members

Name	**Company/Institution**
Devin Huber	AISC
Carlo Lini	AISC
Eric Bolin	AISC
Erin Conaway	AISC
Larry Kruth	AISC (retired)
Bo Dowswell	ARC International
W. Duff Zimmerman	Cooper Steel
Matthew Trammell	Trammell Engineering Group, LLC
Keith Palmer	Simpson Gumpertz & Heger
Larry Muir	Consultant (former Cives/AISC)
Brian Volpe	Cives Steel
Tom Kuznick	Herrick Steel (retired)
Victor Shneur	Lejeune Steel (retired)
Doug Abernathy	NAFCO

For full-scale testing, all connections were shop-welded to a stiff stub column web or flange, and each drop-in connection was made with one of four angle sections and one of two bearing lengths. Six tests were performed, in which two connections, one on each end of the girder/beam, were tested at the same time via a connecting wide-flange section. Two wide-flange sections, both of which are commonly used in the commercial and residential steel frame

industry, were utilized. In total, for a girder-to-column connection, six girder top flange regions, eight drop-in connection vertical angles, and one shear tab were assessed via DIC. For a smaller beam-to-column connection, two column webs were assessed via DIC.

1.4 Organization of Thesis

This thesis is organized as follows. Chapter 2 discusses various requirements for a connection to be considered simple or pinned for analysis, current simple shear connections, and the basics of DIC and its use in structural testing. Chapter 3 provides a detailed overview of each connection design, preliminary design considerations, the experimental testing setup, specimen fabrication and preparation, and DIC verification. Geometric considerations are also discussed in this chapter. Chapter 4 presents and discusses all test results through DIC data. Various figures, tables, and images are utilized to adequately capture the discussed specimen behavior. The final recommendations and conclusions derived from this research are stated in Chapter 5.

Chapter 2: Literature Review

2.1 Introduction

Simple shear connections are easily found in all areas of the steel industry, especially at the girder-column interface of a commercial or residential building. This chapter outlines the current simple shear connection requirements in the AISC *Steel Construction Manual and Specification for Structural Steel Buildings*, common shear connections, and DIC basics and application in research.

2.2 Steel Shear Connections

2.2.1 Connection Classification

All connections can be subdivided into three categories, which can best be characterized and defined by the moment-rotation behavior of the connection. A connection may be classified as fully restrained or rigid if the angle between the beam and supporting element (such as a column) remains constant in which a significant bending moment is then developed at the connection; a simple or flexible (idealized as a hinge) connection develops little to no moment and allows for sufficient rotation while a partially-restrained or semi-rigid connection is defined as an intermediate case between a simple and rigid connection (AISC, 2022). Properties of simple connections are emphasized herein due to the expected behavior of the drop-in connection.

The defining behavioral characteristics of a connection are stiffness, strength, and ductility, and are shown in the moment-rotation diagram in Figure 3. Connection stiffness, due to the onset of non-linear behavior at low loads, is not determined by its initial stiffness but is instead defined by the secant stiffness, K_s (AISC, 2022; Bjorhovde et al., 1990). This stiffness is

defined in equation 2.1 as the ratio of the bending moment and relative rotation of the connection at service loads.

$$K_s = \frac{M_s}{\theta_s} \qquad 2.1$$

Where:

M_s= moment at service loads

θ_s= rotation at service loads

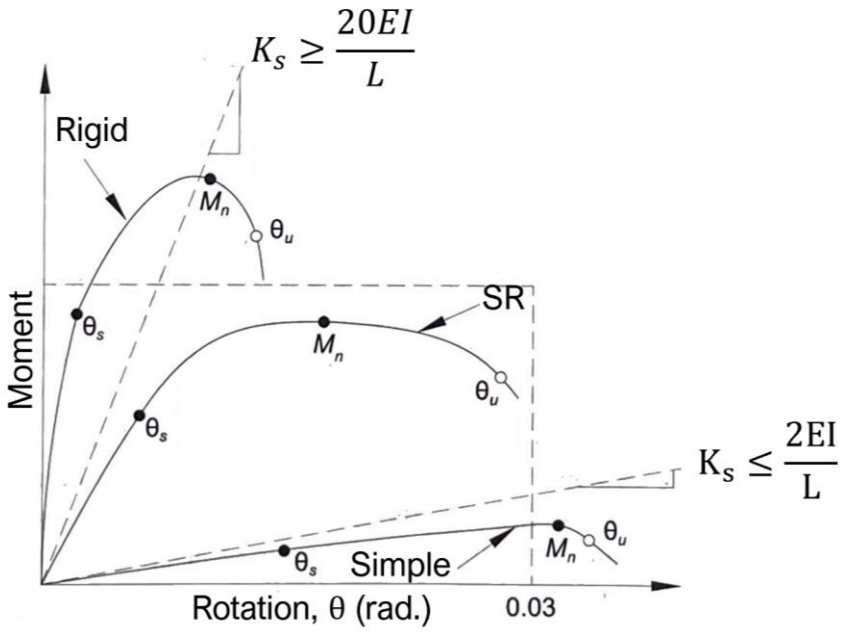

Figure 3: Moment-Rotation Diagram of Connections

In testing noted by Astaneh (1989), it was observed that highly stressed areas of the connection yielded under the combined effect of shear and moment. These yielded areas proceeded to lose their stiffness, inducing a reduction in the global rotational stiffness of the connection and a decrease in the produced moment at the connection. As well, a non-linear response is observed after the elastic limit of the beam is reached, in which a small amount of shear disproportionately increases the end rotation (Astaneh, 1989). To allow for this shedding of

moment and increase in rotation, the secant stiffness should remain limited and must satisfy equation 2.2 (AISC, 2022).

$$\frac{K_s L}{EI} \leq 2 \qquad 2.2$$

Where:

K_s = secant stiffness

EI = bending rigidity of the beam

L = length of beam

Connection strength is defined as the maximum or peak moment it is capable of carrying, M_n, and is based on an analysis of the ultimate limit state of the connection or testing. Connections that transfer less than 20% of the full plastic moment of the beam at a rotation of 0.02 radians can be considered to have no flexural strength and assumed a simple connection (AISC, 2022; Astaneh, 1989; Bjorhovde et al., 1990).

Connection ductility, or rotational capacity, is defined as the rotation that corresponds to either (a) a reduction of the resisting strength (M_n) by 20 percent or (b) the connection has deformed beyond 0.03 radians. This available rotation capacity should then be compared to the rotation required at the strength-limit state, considering a non-linear analysis of the connection. If an accurate analysis is not available, a conservative rotational capacity of 0.03 radians is considered adequate; 0.03 radians is roughly equivalent to the end rotation of a beam whose span is 24 times its depth and is uniformly loaded with the maximum design load (AISC, 2022; Muir & Thornton, 2011). Again, as this rotation increases in the connection, the rate of increase in moment produced will steadily taper off; however, the shear forces will continue to rise in proportion to the applied load. Overall, a simple connection is designed to provide sufficient

strength to transfer the end reaction of a beam whilst also providing enough end rotation and negligible end moments to qualify as a simply supported beam (Astaneh, 1989; Astaneh et al., 1989).

2.2.2 Common Shear Connections

The following simple shear connections are distinctly recognized and easily designed utilizing simple design tables in the AISC manual: double-angle connections, seated connections, and single-plate connections (AISC, 2022). Though each connection has varying behaviors and design limit states according to the geometry and components used, there are several design considerations that apply to all previously listed. Each connection must develop a plastic hinge, allowing for sufficient rotation as it is idealized as a pinned support; the location of this hinge occurs at the most flexible point within the connection and will vary according to the connection and its components. This location of the hinge will also determine the shear forces and bending moments for the design of the individual elements (Geschwinder et al., 2017). For simple beam connections, the permissible tolerance for beam underrun or overrun must be considered; while tolerances are not typically considered in strength design, they should be considered for fit-up purposes. Typically, for a beam-to-column connection, beams are set a nominal one-half inch from the column face to accommodate for this tolerance; when considering edge distance from the bolt hole to the edge of a member, the distance used in calculations should be one-quarter of an inch smaller due to the possibility of an under-run beam length yielding at a lower strength (AISC, 2022; Geschwinder et al., 2017).

2.2.2.1 Double-Angle Connections

Double-angle connections are very common connections used in steel construction. They consist of two angles; one leg of each angle is bolted or welded to the supporting member (such as a column web or flange), and the opposing leg is bolted or welded to the web of the supported beam. Two examples of this connection are shown in Figure 4. They are easily fabricated and are most suitable when the end shear reaction is large and a singular angle is not sufficient. It is also a relatively compact connection that is generally contained within the flanges of the supported beam and is regularly used at the beam-to-column-web interface (AISC, 2022). However, multiple in-field and shop practices must be considered prior to installation in the field, such as when determining the element in which the angles will be shop-connected, coping of the beam in-shop, or if the bolt holes will be short-slotted to allow for adjustments among others. For example, if the angles are shop-attached to a column flange in what is called a knifed connection, the supported beam flange must be coped, and an erection clearance must be provided to allow for adjustments. As well, when double-angle connections are to be installed back-to-back, especially at the column web, adjustments must be made, such as staggering the angles (AISC, 2022; Geschwinder et al., 2017).

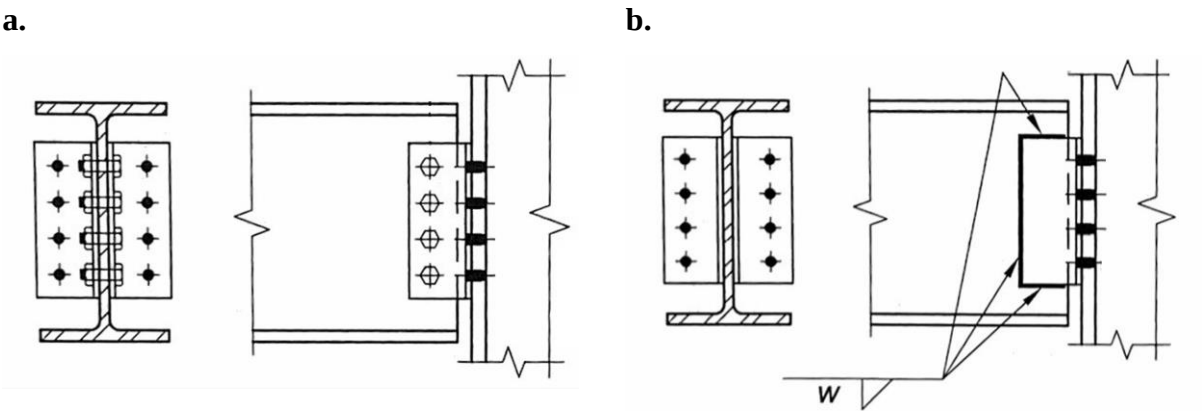

Figure 4: Double Angle Connections (a) Bolted-Bolted and (b) Bolted-Welded (AISC, 2022)

Forces in a double-angle connection are transferred through shear in the bolts, angles, supporting member web or flange, and the web of the supported member. A multitude of limit states are considered in the design of a bolted-bolted double-angle connection: shear rupture of the bolts and angles, bolt bearing and tearout on the beam web and supporting member, shear yielding of the beam web and angles, block shear on the coped beam web and angles, and coped beam flexural strength. An additional limit state of weld rupture considering eccentric loading must be checked if the connection utilizes welding in addition to bolts (AISC, 2022; Geschwinder et al., 2017). Otherwise, the eccentricity on the supported side of the connection may be neglected if a single vertical row of bolts with a distance from the face of the supported member not exceeding three inches is used. To provide adequate flexibility, the thickness of the angles is limited, and a weld should never be utilized at the topmost part of the angles (AISC, 2022).

2.2.2.2 Seated Connections

Another common shear connection utilized is the seated connection. Both stiffened and unstiffened seated connections consist of few components in which a beam is seated on top of an angle that is welded or bolted to the supporting member; a stiffened seated connection utilizes a seat plate and a stiffening element, such as a plate, structural tee, or pair of angles (AISC, 2022; Geschwinder et al., 2017). An example of these connections is shown in Figure 5. For design simplicity, AISC design procedures assume the use of two high-strength bolts to attach the angle to the bottom flange of the beam, as well as a singular plastic hinge formation in the connection. This assumption of a singular hinge leads to a conservative estimate, though: two hinges are actually formed in flexural yielding of the angle (AISC, 2022; Carter et al., 1997; Chen et al., 1997).

a.

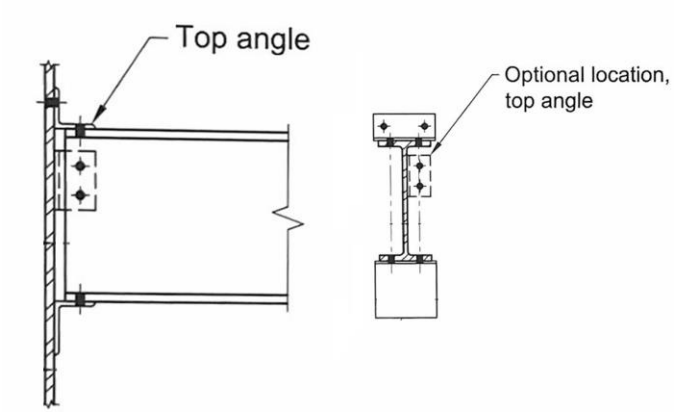

b.

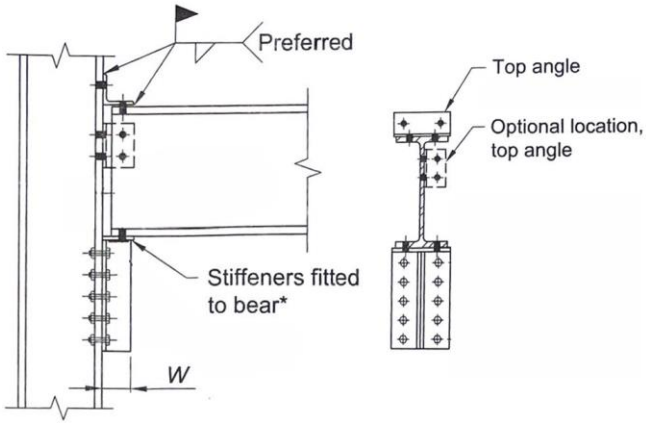

Figure 5: Seated Connections (a) Unstiffened and (b) Stiffened (AISC, 2022)

All force in an unstiffened seated connection is assumed to be transferred through the bearing of the beam on the angle seat and subsequently through the connection of the seat to the supporting member. In a stiffened seated connection, the stiffening element and connection to the supporting member are assumed to carry the entire end reaction (AISC, 2022; Chen et al., 1997; Geschwinder et al., 2017). For stability purposes, another angle, typically a ¼ in.-thick angle with a 4-in. vertical leg, is connected to the supporting member and in one of two optional locations of the beam, the top flange of the beam or the beam's web. This stability angle may be bolted to both members or line-welded to the toe of each angle leg at either the supporting

member or the beam; minimal welding is required to provide adequate flexibility and rotation for a simple connection. Though this angle is not designed for strength requirements, testing has concluded that the top angle carries a substantial end reaction, and the exclusion of it may result in an unconservative estimate of the beam web buckling capacity in both stiffened and unstiffened seated connections (Roeder & Dailey, 1989).

The application of the seated connection in the steel industry is common, as there are multiple advantages; the angles are easily prefabricated and attached to the column or supporting member in the shop, and they can be utilized on both column flanges and webs. If adequate clearance is provided, it can be attached to the web of a supporting girder. However, multiple member tolerances must be consulted in design geometry to ensure proper fit and elevation in the field. Since the bottom flange of a beam typically establishes the plane of reference for a seated connection, tolerance in beam depth may result in variation in elevation of the top flange across multiple spans; while this is non-consequential for a concrete slab or metal deck, it may be of concern when utilizing a steel-plate or grating floor. When utilizing a bolt for the top stabilization angle, it is recommended that due to overrun and underrun in the beam length, slotted-bolt holes are utilized for ease and economy in fabrication and erection. If the top angle is shop-welded, it must provide proper clearance; this angle can also be welded in the field to ignore any variations in beam depth (AISC, 2022).

Unstiffened seated connections generally perform well as simple connections as the angle can sufficiently rotate about the bottom of the beam without imposing any significant moment in the column and has relatively few limit states to consider. Due to the flexibility of the unstiffened angle, this connection is most commonly used with small shear end reactions (Geschwinder et al., 2017). The design limit states for an unstiffened seated connection include the following:

web local yielding and crippling due to bearing, seat angle flexural and shear yielding, and bolt or weld shear with considered eccentricity (AISC, 2022; Geschwinder et al., 2017). Web crippling is an atypical limit state to be checked for other shear connections, as seated connections utilize bearing to transfer the shear force, unlike in a shear tab or double angle connection.

In design, the minimum required bearing length of web yielding and crippling is first determined and is a function of the web thickness, flange thickness, and beam depth. A thin web will result in a larger required bearing length compared to a beam with a thicker web; as minimum bearing lengths can be relatively small due to the small end reaction and flexibility of the angle, a minimum bearing length taken as the value of k_{det} is required. The required and minimum angle thickness is determined based on the flexural and shear yielding of the angle. The assumed critical section location for an unstiffened seated connection is at the fillet edge of the outstanding leg; an eccentricity of the distance from this critical section to the bolt centerline (located at half the bearing length) is assumed for an unstiffened angle, and an eccentricity of 80% of the length of the stiffener parallel to the beam web is considered for the stiffened seated connection. Finally, the weld and/or bolt groups must be designed with the applicable and previously described eccentricity. As a stiffened seated connection is typically only utilized when the unstiffened angle is insufficient for a large end reaction, an additional limit state of punching shear in the supporting member must be checked for a stiffened seated connection (AISC, 2022; Ellifritt & Sputo, 1999; Geschwinder et al., 2017).

2.2.2.3 Shear Tab Connections

Single-plate connections, typically referred to as shear tabs, consist of a plate that is fillet welded (on both sides) to a support and field-bolted to the web of a beam or supported member

(AISC, 2022; Muir & Thornton, 2011). An example of this connection is shown in Figure 6. Shear tabs are widely used in the steel framing industry and are perceived as a preferred connection due to the reduced material use and labor requirements compared to the previously discussed simple shear connections, ease in fabrication, and ample clearance provided for erection. However, as previously discussed in Chapter 1, the erection process is timely. In testing, this connection has proven rather complex and must be checked against multiple limit states. Design considerations to achieve the assumed rotation for a simple connection must also be taken into account (Astaneh et al., 1989). Due to the many limit states, a conventional configuration with prescriptive geometry and physical limitations has been produced in the AISC specification so that only five limit states need to be considered (AISC, 2022; Geschwinder et al., 2017; Muir & Thornton, 2011).

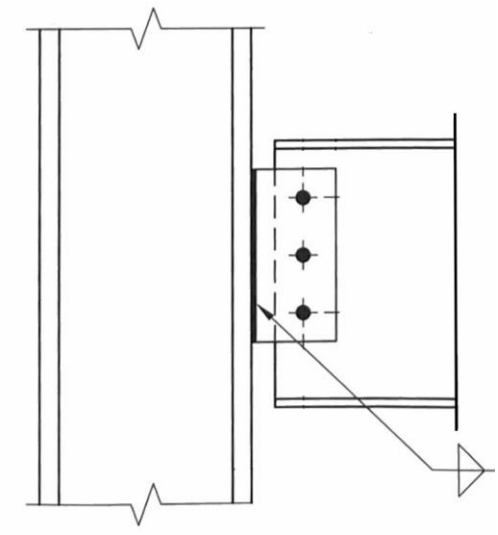

Figure 6: Shear Tab (AISC, 2022)

The following limit states (eleven in total) must be checked for the design of a shear tab that does not meet the requirements of the conventional design:

- shear rupture of the bolts considering eccentricity

- bearing and shear yielding of the supported beam web
- bearing and tearout of the plate
- flexural rupture and elastic yield moment of the plate
- shear yielding and rupture of the plate
- block shear rupture of the plate
- buckling of the plate
- plastic flexural yielding with the shear reaction of the plate
- weld rupture considering eccentricity

To accommodate for the requisite beam end rotations of a simple connection, a shear tab (connected to a rigid support) with standard holes utilizes a combination of the following: plate flexural yielding, bolt deformation, and bolt plowing in which local yielding of the plate allows for elongation in the bolt holes (Muir & Thornton, 2011). For the conventional configuration, an upper-bound distance between the bolts and the weld is defined such that buckling of the plate does not govern (AISC, 2022; Muir & Thornton, 2004; Muir & Thornton, 2011). This limiting distance allows for only a small area over which yielding may occur; therefore, plate yielding is usually not considered a sufficient means of accommodating the simple beam end rotation (Astaneh et al., 1989; Muir & Thornton, 2011). This means that the two remaining methods to achieve proper rotation are bolt deformation and bolt plowing, both of which must be activated for significant horizontal movements like that required in a deep connection. For example, a deep shear tab of 12 rows of single bolts results in a horizontal translation of almost half an inch at a rotation of 0.03 radians. This movement cannot solely come from bolt deformation as it would exhaust the capacity of the bolt; even the minimal deformation required by a two-bolt connection would utilize 60% of the bolts' capacity if bolt plowing is not initiated (Muir & Thornton, 2011).

To allow for bolt plowing without extreme deformation or shearing of the bolt, limitations are placed on the stiffness of the plate by limiting its thickness, i.e., a deeper connection will require a thinner plate to allow for greater elongation of the bolt holes. The weld is also designed to allow for flexible and ductile behavior considering eccentricity; a maximum limit is placed on the weld (as a ratio of the plate thickness) to ensure that full yielding of the plate will initiate before weld rupture (AISC, 2022; Astaneh et al., 1989; Muir & Thornton, 2011).

2.3 Digital Image Correlation

As the holistic behavior of the connection elements is of primary interest in this thesis, a practical means of measuring the mechanical properties (deformations and strains) of a large area was paramount. Strain gauges, while of common use in a laboratory setting, can only measure properties at a specific location in which the gauge is placed, meaning that the researcher must conclude where a strain field or strains of notable importance will occur before testing occurs. Though finite element analysis had been performed within this study by Robel Alemayehu, Ph.D. and provided insight into probable strain field formation, the large areas of interest and improbability of placing the strain gauges directly where deformation would occur in testing led to primary utilization of DIC.

2.3.1 Basics of DIC

DIC is a non-contact optical method that utilizes photographic images and a mathematical correlation technique to measure deformations, displacements, and strain on a prepared specimen that is subjected to a load. Two main branches of DIC will be further discussed, 2D and 3D, both of which fundamentally track displacement in the same way (Correlated Solutions, 2020a).

A 2D-DIC setup consists of a singular camera that photographs the full field of interest. Due to this monocular vision, out-of-plane motion is unable to be detected, and the object is assumed to be planar, parallel to, and at a constant distance to the visual sensor during the entire test (Correlated Solutions, 2020a; Sutton et al., 2009). Any change in the size of a region on the specimen (due to both in or out-of-plane movement) will be reflected as strain in the results. For example, if the specimen moves towards the camera, it will become larger in the image and result in a tensile strain bias, and vice versa if it moves away from the camera, creating a compressive strain bias. On the other hand, like human vision and our ability to perceive depth, 3D-DIC utilizes stereo-imaging (two cameras) to perceive 3D information and any out-of-plane motions that occur, eliminating strain bias due to movement (Correlated Solutions, 2020a).

Both 2D and 3D-DIC track local and global movement via the same process of temporal matching. Given a point and its uniqueness in the undeformed reference image, the system tracks a point (in the form of a pixel in the image) on the test specimen's surface throughout time and across the deformed images. Due to this required uniqueness of a point, a pattern with certain properties must be applied to the surface; this pattern will not interfere with correlation as it is adhered to the surface and deforms with the surface (Sutton et al., 2009). Typically, a base coat of white matte paint is applied to the specimen with a secondary black ink speckle pattern, resulting in a high contrast pattern that provides high information content. The surface should be isotropic without a noticeable orientation, random in placement, have sufficient variation, and be of relatively uniform speckle sizing (Correlated Solutions, 2020a, 2023; Jones & Iadicola, 2018; Sutton et al., 2009).

As each point is inherently not distinguishable from another point, a grouping of pixels around a point is used to distinguish the specific point. This surrounding neighborhood of pixels

is called a subset and is user-defined according to the speckle pattern; a subset should be large enough to allow for a point to be recognized from another but should remain small enough to provide good spatial resolution (Correlated Solutions, 2020a). To establish the various points (in memory), each pixel in the image is assigned to a gray-level natural integer ranging from 0 to 255, a black pixel is assigned a number of 0 and a white pixel is assigned a number of 255 (Correlated Solutions, 2020a, 2021; Sutton et al., 2009). An example of this is shown in Figure 7.

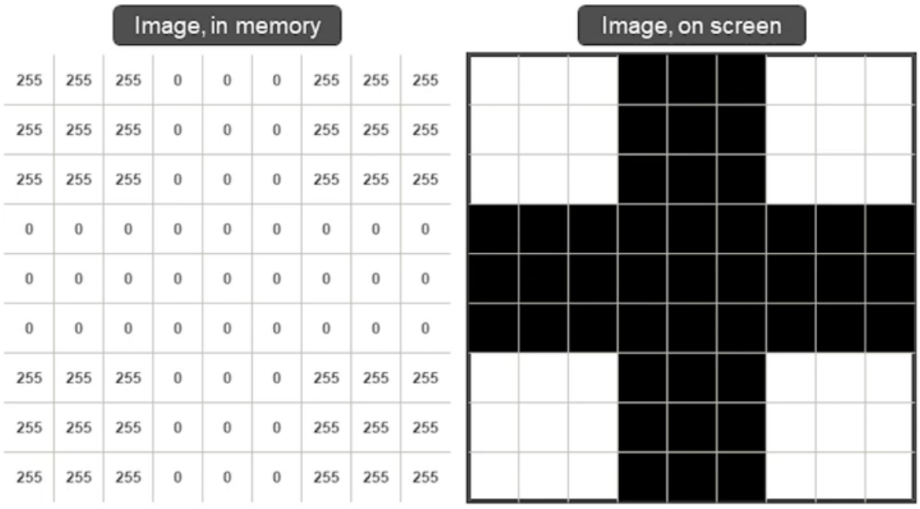

Figure 7: Assigning Gray Scale to Reference Image (Correlated Solutions, 2020a)

As the specimen's surface moves, the pixel number at that specific point (in memory) will adjust accordingly. This is shown in Figure 8 in which the deformed image has shifted to the right and up one pixel, causing the same shift in memory. In reality, the specimen doesn't move in pixel increments, therefore a grey level interpolation (not shown in the figure) is utilized to represent a field of discrete grey levels as a continuous spline. By default, an 8-tap spline is used as it typically results in more accurate displacement information (Correlated Solutions, 2020a; Sutton et al., 2009).

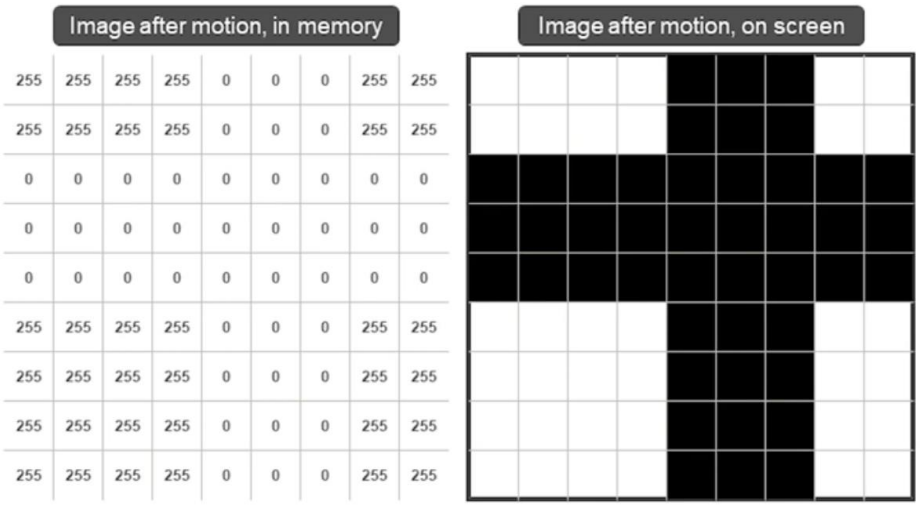

Figure 8: Adjusting Gray Scale to Deformed Image (Correlated Solutions, 2020a)

Utilizing the user-defined subset, the DIC system can track where each dot from the reference image has moved. This is shown in Figure 9 in which the red pixel in the original image is what is being "looked for" utilizing the surrounding pixels through subset matching.

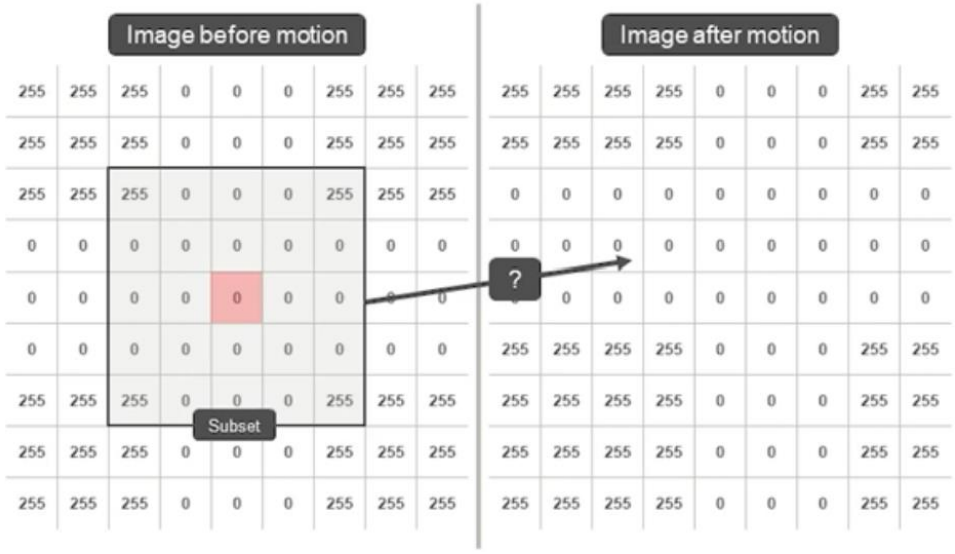

Figure 9: Subset Matching (Correlated Solutions, 2020a)

To find the proper subset match in the deformed image, a classic correlation function is utilized to check several possible matches. This function is a sum of the squared differences

(SSD) of the pixel values, in which a smaller value indicates greater similarity in the subset considered. If the function, shown in Figure 10, results in a high error, another point is considered until the lowest error possible is achieved. Ideally, a correlation function of 0 means a perfect match; however, in reality, a result of 0 is not possible due to the corruption of the image caused by noise (Correlated Solutions, 2020a; Sutton et al., 2009).

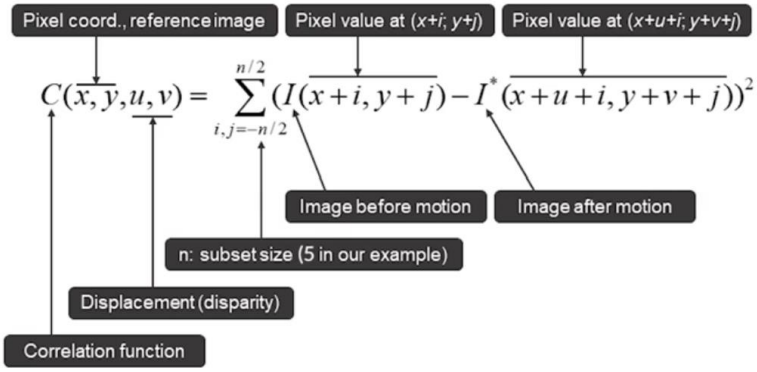

Figure 10: Correlation Function (Correlated Solutions, 2020a)

During subset matching, there are other considerations that the algorithm accounts for such as photometric mapping and subset shape function. Photometric transformations are utilized in the correlation function as the patterns on a specimen become lighter or darker due to expansion and compression or the exposure times change (Correlated Solutions, 2020a; Jones & Iadicola, 2018). It cannot, however, correct major lighting changes due to glares or shadows cast onto the specimen (Correlated Solutions, 2020c). In the reference image, a subset is square; as the specimen moves, the subset changes shape and does not remain a square. A subset shape function accounts for this change in the shape of the subset (Correlated Solutions, 2020a; Jones & Iadicola, 2018). Once the subset is successfully matched, the system can measure surface displacement relative to the reference image, leading to the formation of vector fields and strain maps (McCormick & Lord, 2010).

For a 3D-DIC analysis, further correlation occurs as stereo-imaging is utilized to form a 3D model of the specimen. The overall process is shown in Figure 11 and is similar to 2D-DIC analysis; to begin the analysis, the two images produced at the same time, for example, an image from Camera A (Picture A1) and an image from Camera B (Picture B1) taken at time equal to 1 second, are compared and the points on Picture A1 are matched to points on Picture B1 through stereo-correlation via stereo-triangulation to create a 3D point.

a. **b.**

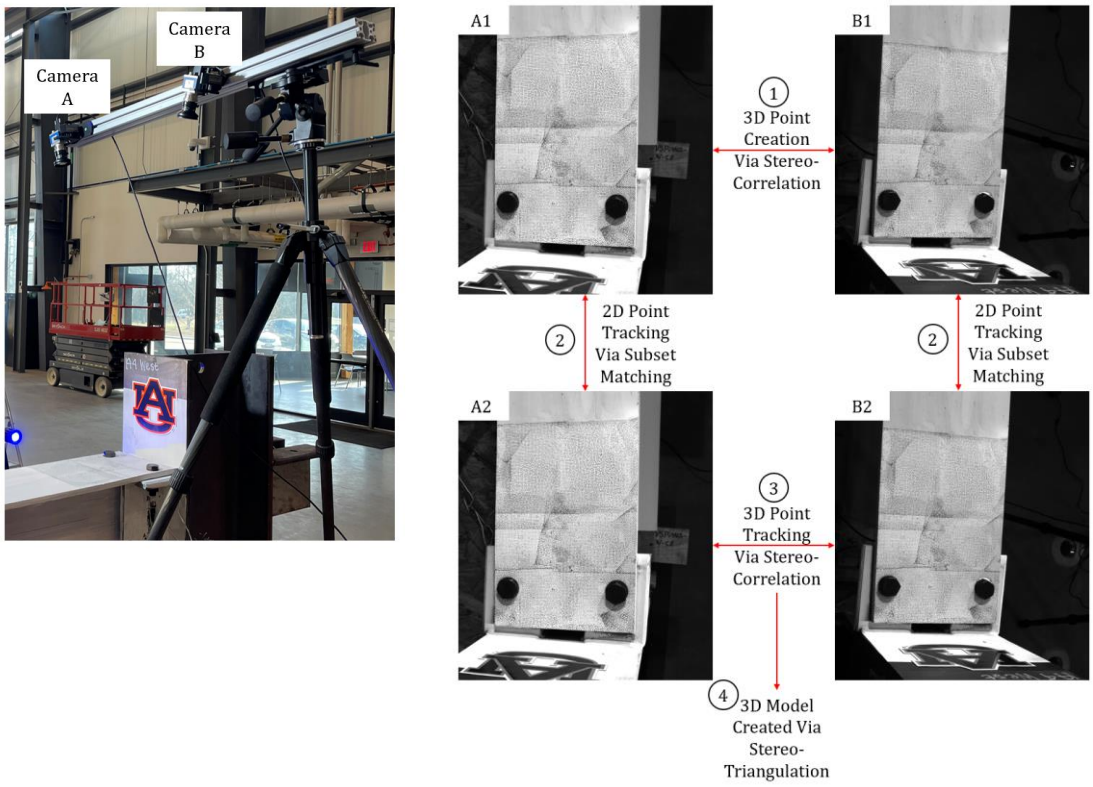

Figure 11: 3D DIC Process (a) Example Stereo-Rig and (b) Example Process

Stereo-triangulation uses the known locations of the sensors to compute the intersection of two optical rays (Epipolar Projection Lines) to locate features on the 3D specimen and define 3D points (Correlated Solutions, 2020a, 2021; Sutton et al., 2009). To do this, the optical rays must be in a common coordinate system; this is done by calibrating the stereo-rig (two-camera

system) via imaging of calibration targets in various arbitrary motions, shown in Figure 12 (Correlated Solutions, 2020a, 2020c).

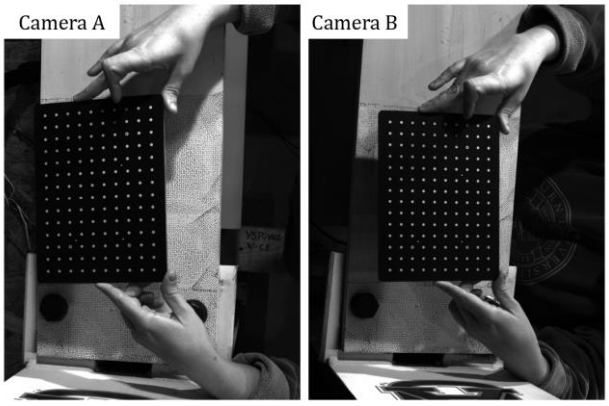

Figure 12: Calibration Photo Example

Calibration is a shape-measurement process that builds the model of the stereo-rig parameters using the shape of the calibration target. All calibration parameters are extracted from the calibration images alone and a transfer function is then built from the pair of 2D images (Correlated Solutions, 2020a). Calibration targets have a known spacing and are imaged in various arbitrary movements to calculate extrinsic properties of the cameras, like angle and distance. Intrinsic properties of the sensors, such as distortion, focal length, etc. are also utilized in the stereo-triangulation process (Correlated Solutions, 2020a; Jones & Iadicola, 2018).

After the subsets of both images taken at the same time (A1 and B1 in Figure 11) are matched via stereo-correlation to create 3D points, subset matching occurs for each subsequent image (A1 to A2 and B1 to B2) to track the subset deformation (Correlated Solutions, 2020a). This subset matching process is the same as described in the 2D-DIC analysis. Stereo-triangulation is then used to build the deformed 3D model. As the full field displacement of each point is known, strains can be computed. For each data point, three neighboring data points are assessed to compute the strain; this point density is called the step size and can be adjusted by the

user (Correlated Solutions, 2020a, 2020c, 2021; Sutton et al., 2009). Various strain tensors are available in the system as well as user-input equations.

2.3.2 DIC Use in Structural Engineering

Though Digital Image Correlation (DIC) has been in use since the 1980s, its use in both the laboratory and field setting has greatly increased in recent years; in fact, the quantity of published research papers utilizing DIC in civil engineering has more than tripled from 2010 to 2020 (Mousa et al., 2023). This influx of DIC use can be attributed to the advancement of optical sensors (like cameras) and the computational capacity of computers. As high-resolution cameras are continuously improving, the increasing pixel density, spatial resolution, and frame rate have allowed for a broader array of specimens to be analyzed, from large structural frames undergoing dynamic loading to small structural components like joints (Desai, 2016; Mousa et al., 2023; Shih & Sung, 2014). DIC's portability, accuracy, full-field analysis, and non-contact method have made it a great option both in the laboratory and field compared to other conventional options that can only measure results at a discrete number of locations and require more laborious activity for installation (Niezrecki et al., 2018; Oats et al., 2022).

Many studies have been performed on various structures to confirm the accuracy of DIC through comparison to strain gauges and other established methods. These studies include but are not limited to, in-the-field evaluation of existing structures, such as bridges, and analysis of structural connection components in the laboratory setting. Though a greater variation in DIC versus strain gauge results are more likely to occur in the field (though still minimal), due to external circumstances such as weather and ground movement, laboratory experiments have resulted in higher accuracy of DIC use (Blikharsky & Kopiika, 2024; Elhadary et al., 2024; Niezrecki et al., 2018; Oats et al., 2022).

Chapter 3: Methodology

3.1 Introduction

The overarching objective of this research was to evaluate the behavior and deformations of the girder top flange, connection angle, and column web of drop-in shear connections through DIC in full-scale testing. To adequately capture a representative range of behavior, nine girder-to-column drop-in connections, one girder-to-column shear tab, and two beam-to-column drop-in connections were tested in a total of six tests. This chapter provides an overview of the specimen and connection design, geometric constraints to be considered before strength design, testing preparation, setup, and procedure. Also, verification of the DIC system and the post-testing data analysis procedure are included.

3.2 Connection Design

To provide an industry-suitable connection design, a benchmark building from AISC's steel solutions center, *"Office: Conventional Steel Framing Study"*, was selected (AISC, 2018). As seen in Figure 13, a W24x48 girder with a span length of 30' and spacing of 45'-6" was determined to be an appropriate girder for the drop-in connection. The provided loadings result in a factored beam-column force of 39 kips and a girder-column force of 78 kips. Utilizing the same benchmark building design loads and a modified smaller building layout, a W16x36 with a girder spacing and span length of 30' was chosen to investigate a relatively small girder-column connection with a factored reaction of 52 kips. A stocky column size of W14x82 was chosen to provide adequate flange width and minimal column bending. See Appendix E for loading calculations.

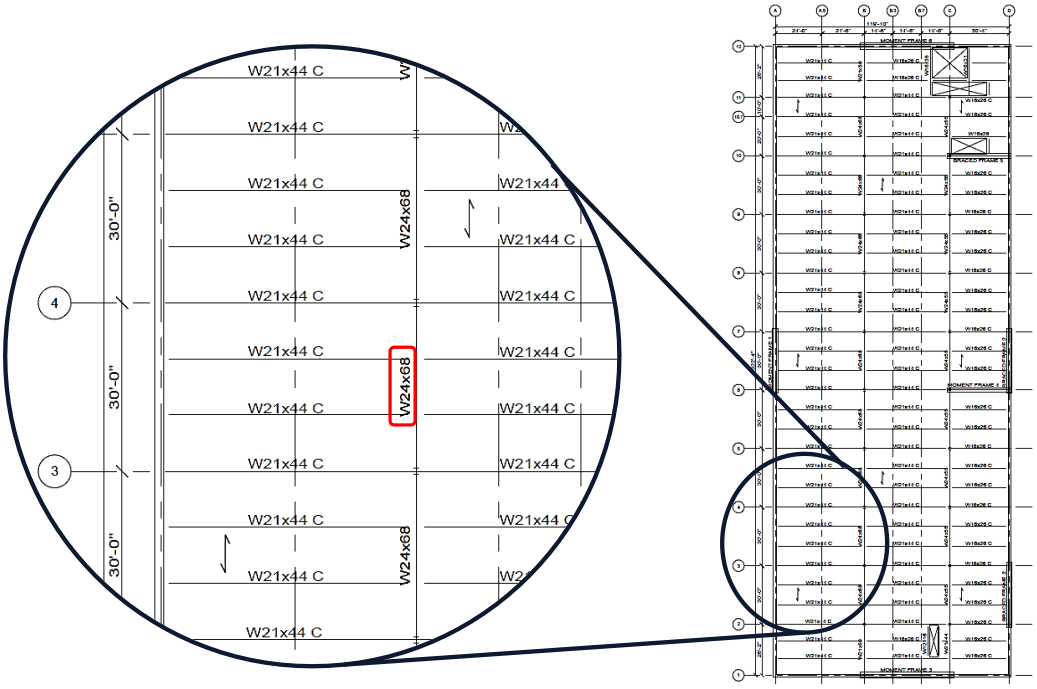

Figure 13: Girder Selected from Office Benchmark Building (AISC, 2018)

A benchmark girder-column drop-in connection and conventional shear tab were designed for the W24x68 and W16x36 girders utilizing the AISC V.16 *Steel Construction Manual* (AISC, 2022). An elevation view of these connections is shown in Figure 14 and Figure 16. In addition, Figure 15 shows a cross-sectional and plan view of the W24x68 benchmark drop-in connection. All drop-in connections varied in one or more of the following to provide a range of behavior: angle size, bearing length, weld geometry and thickness, beam/girder size, and angle orientation. The final connection design summary is found in subsection 3.2.2.

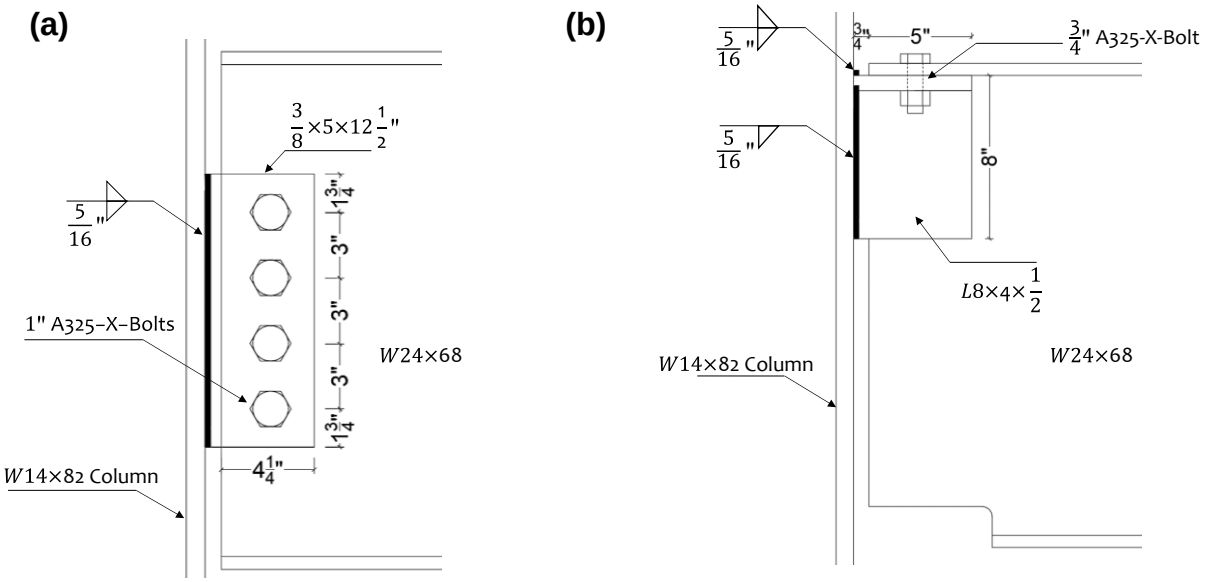

Figure 14: W24x68 Benchmark Designs for a Girder-Column (a) Shear Tab Connection and (b) Drop-In Connection

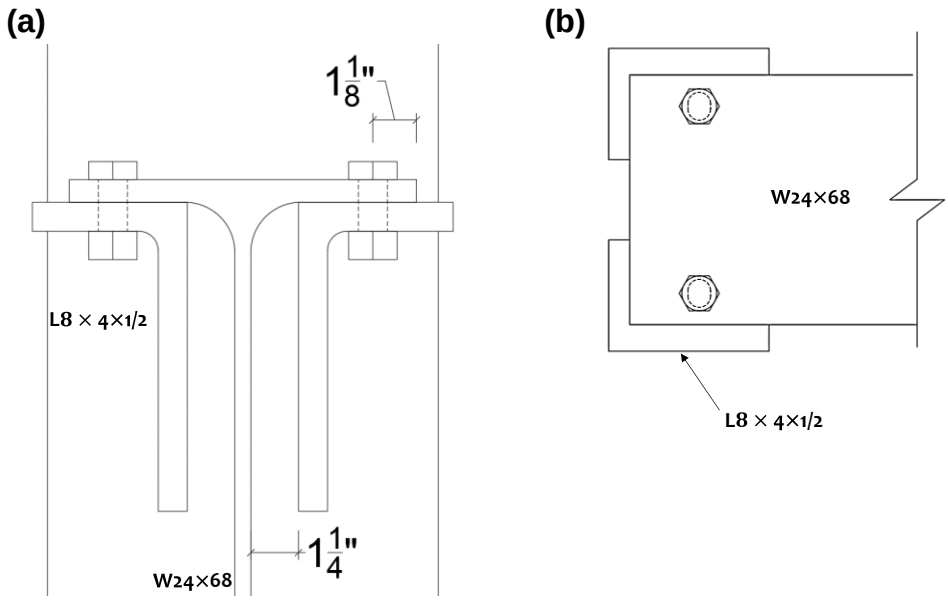

Figure 15: W24x68 Benchmark Drop-In Girder-Column Connection (a) Section View and (b) Plan View

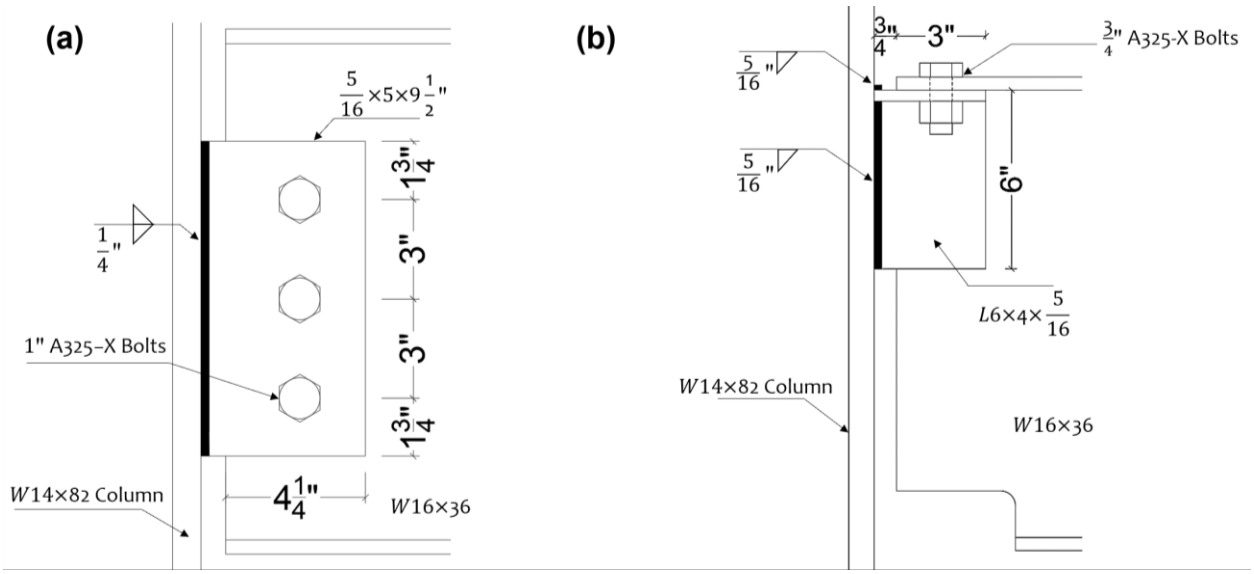

Figure 16: W16x36 Benchmark Designs for a Girder-Column (a) Shear Tab Connection and (b) Drop-In Connection

3.2.1 Considerations in Design

During the preliminary design of the drop-in connection, the general geometry of the connection elements was first considered to ensure proper fit-up during erection. The connection must allow for the minimum edge distance of the angle and girder/beam, as well as the entering and tightening clearance to be satisfied (AISC, 2022). Figure 17 shows all considered geometric constraints and their associated references.

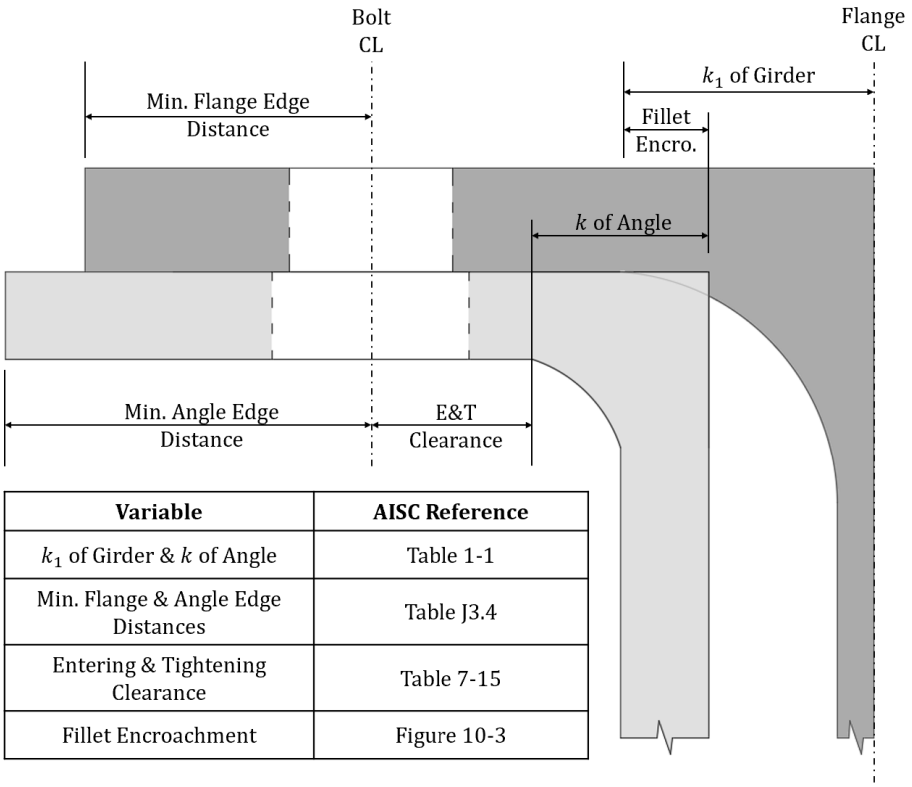

Variable	AISC Reference
k_1 of Girder & k of Angle	Table 1-1
Min. Flange & Angle Edge Distances	Table J3.4
Entering & Tightening Clearance	Table 7-15
Fillet Encroachment	Figure 10-3

Figure 17: Considered Geometric Constraints

It is of importance to know that, in general, a girder/beam with a relatively small flange width and/or a large fillet zone (k_1) will produce a limited number of acceptable angle sections due to scant transverse length available to be seated on the angle. To increase this transverse length and subsequently decrease the transverse distance between the angles, one may take advantage of AISC's fillet encroachment, the maximum of which is listed in Fig. 10-3 of the AISC Steel Manual according to the difference between k_1 and half the web thickness of the girder/beam section (AISC, 2022). For this project, fillet encroachment was not utilized in the design of the drop-in connections. The angles were transversely spaced at two times the AISC listed k_1 value for the associated girder/beam. For simplification of future design, Figure 18 shows the steps considered when choosing an angle section that will satisfy geometric constraints with a known girder/beam section and bolt size. An asterisk notes the subsequent

limitations determined at the choice chosen each step, i.e.: the bolt size chosen directly influences the bole hole dimensions, entering and tightening clearance, and minimum edge distance required. As well, it assumes the bolt will be located at the distance required by the entering & tightening clearance from the fillet end of the angle. To further prove that geometric compatibility does not eliminate many possible W-Sections and/or angle sections and therefore is probable to be implemented in the field, a preliminary design side-study was performed utilizing industry common sections and the common bolt size of 7/8 in. It was determined that approximately 70% of all AISC angles with both legs greater than or equal to a length of three inches (110 possible angle sections) were geometrically compatible with all W16 to W30 sections equal to or less than 100 pounds per linear foot and with a flange width greater than six inches.

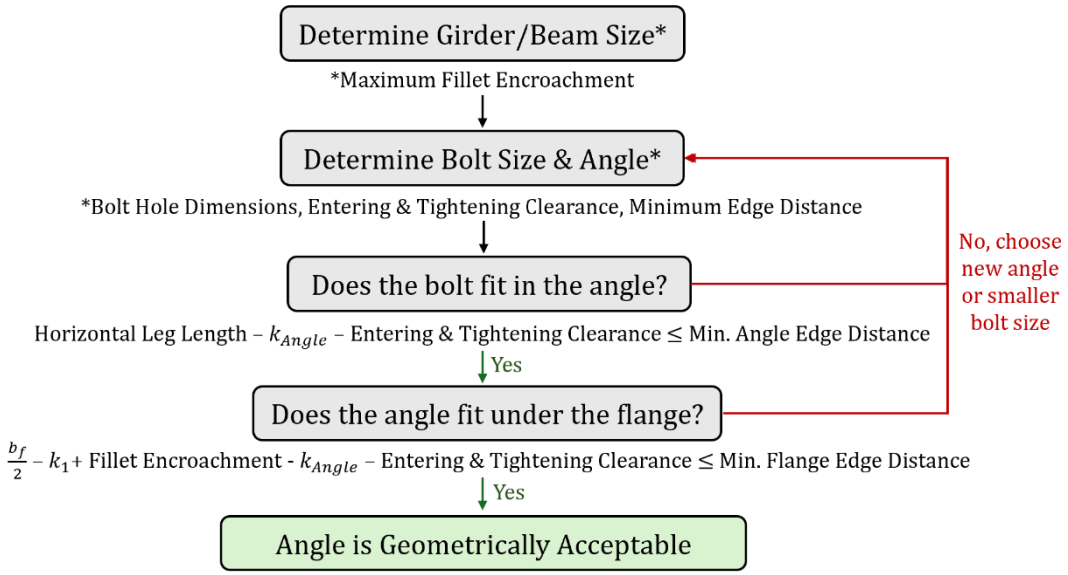

Figure 18: Steps for Geometric Compliance

If possible, the machinery utilized by the fabricator in the automation of hole-punching of the angles should be considered when determining the bolt-hole placement of the drop-in connection. While this automated process was not considered in Figure 18 or preliminary design

due to the limited number needed for testing, it would be beneficial in an industry application due to the large number of angles likely needed. If the design does not allow for the use of automated machinery, the fabricator may manually drill the holes, as was done in this project.

While only considered in beam setback due to beam length under-run or over-run, the allowable dimensional tolerances discussed and listed in ASTM A6 Section 12 were not considered elsewhere in the design (ASTM, 2024). Due to unavoidable variations in the listed geometrical dimensions of hot-rolled shapes, the most extreme allowable tolerances may impact the geometrical constraints when designing a drop-in connection.

In the strength design portion of the preliminary design process, the controlling limit states of weld rupture, angle shear, and transverse bending of the girder/beam flange were considered for the drop-in connection. The most likely of which is the transverse bending of the flange, providing a ductile failure mode. Angle shear may govern if a relatively thin and shallow angle is utilized, and weld rupture may control if the weld is undersized.

3.2.2 Connection Design Summary

The following Table 2 details the full-scale connection design summary. All girder/beam flanges feature a standard bolt hole, and angles feature a short-slotted (oriented long-side transversely) bolt hole to aid in fit-up. All bolts were ASTM F3125 Grade A325. These connections did not utilize the advantage of fillet encroachment and are transversely spaced at the location of the AISC listed k_1 value of the flange. The longest leg of the angle section is always oriented as the vertical leg, allowing for the greatest shear resistance. The bearing length is shown in Figure 19 and is described as the length is which the beam/girder top flange is in bearing on the horizontal angle leg. It should be noted that the design weld sizes are reported in

the table; Appendix C provides the measured weld sizes at varying intervals for each connection. All drawings are found in Appendix A

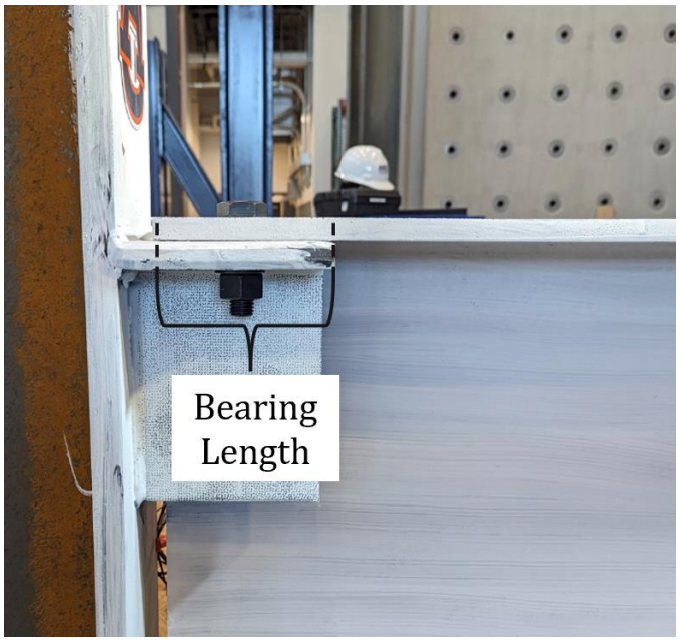

Figure 19: Bearing Length Visual

Table 2: Connection Design Summary

Conn. Type	Conn. Name	Beam Size	Angle/Shear Tab Size	Size and No. of Bolts	Bearing Length (in.)	Weld Position	Vertical Weld Size (in.)	Horizontal Weld Size (in.)
Girder to Column	A	W24x68	L8x4x3/4	Two ¾''	5	2V&2H	13/16	5/16
	B		L8x4x3/4		5	2V&2H	3/8	5/16
	C		L8x4x3/4		3	V&2H	5/16	1/4
	D		L6x4x5/16		5	V&H	5/16	5/16
	E		L8x4x1/2	Two ¾''	5	V&2H	5/16	5/16
	F		3/8x5x12.5	Four 1''	-	2V	5/16	-
	G	W16x36	L6x4x5/16	Two ¾''	3	V&2H	5/16	5/16
	H		L4x3x1/2 (Flipped)		3	2V&2H	5/16	5/16
	I	W24x68	L6x4x5/16	Two ¾''	5	2V&2H	5/16	5/16
	J		L4x3x1/2		3	2V&2H	5/16	5/16
Beam to Column	K		L6x4x5/16	Two ¾''	5	2V&2H	5/16	5/16
	L		L4x3x1/2		5	2V&2H	5/16	5/16

The intent of each connection is explained below:

- Connections A and B evaluated the general behavior of the girder top flange and drop-in connection angles. The angles were oversized to induce a flange bending failure mode.
- Connection C evaluated the effect of a reduced bearing length while maintaining the same angle size as Connections A and B.

- Connection D evaluated the effect of a reduced angle size and weld.
- Connections E and F were the benchmark drop-in connection and shear tab.
- Connection G investigated general behavior for a smaller girder (reduced flange width and thickness) and angle size.
- Connection H evaluated the effect of a mirrored/flipped angle orientation.
- Connection I is a modification of Connection D, in which the weld geometry was improved.
- Connection J investigated the behavior of undersized angles, inducing an angle failure.
- Connections K and L evaluated column web behavior opposite the drop-in connection for a beam-column connection.

3.3 Specimen Fabrication

Detailed drawings used for the fabrication of the girders, connections, columns, and lateral braces were developed. These drawings can be found in Appendix A. All specimen fabrication was performed according to the approved drawings by certified individuals. All unfabricated steel rolled sections and plate were acquired by AISC from Sisken Steel & Supply, including steel from Gerdau, Nucor, SSAB, and Steel Dynamics. The average material properties obtained from mill test reports for the specimens are provided in Table 3. The full mill test reports can be found in Appendix B. All supplementary steel sections not utilized in fabrication were donated to the laboratory, some of which were later used in the final development of Test 6.

Table 3: Average Mill Test Report Results

Shape	Grade	F_y (ksi)	F_u (ksi)	Elongation (%)
W24x68	A572/A992	55.9	72.4	23.7
W16x36	A572/A992	58.0	73.0	26.5
W14x82	A572/A992	55.1	71.1	24.7
L8x4x3/4	A572	54.6	75.3	26.1
L8x4x1/2	A36/572	56.5	73.0	26.0
L6x4x5/16	A36 (Meets A572 Gr.50)	57.9	76.1	25.0
L4x3x1/2	A36/50	55.1	73.5	29.0
3/8" Plate	A572 GR.50	67.0	77.7	31.0

The North Alabama Fabrication Company (NAFCO) donated their time, facility, and personnel to fabricate the specimens. NAFCO developed official shop drawings, which were then reviewed and approved by the research team. During fabrication, the research team was informed of the limitations of the available equipment to punch holes in the desired location on the angle. This limitation resulted in the holes being manually drilled. Fabrication was completed in October 2023 and shipped to the Advanced Structural Engineering Laboratory (ASEL). Figure 20 provides a photo of two fabricated columns with drop-in angle connections at the NAFCO facility and Figure 21 shows a photo of the specimen and supplementary material's arrival at ASEL.

Figure 20: NAFCO Fabrication Photo (Provided by Doug Abernathy)

Figure 21: Specimen and Supplementary Material Arrival at ASEL

3.4 DIC Verification

Before full-scale testing occurred, the DIC software results were verified by performing a tensile test on a specimen with a 2D DIC setup. The specimen was a 12-inch-long steel plate with a cross-section of 2.96 inches by 0.26 inches (cross-sectional area of 0.7696 in^2) that was similarly

prepared for DIC to that described for other specimens, excluding mill scale removal. The test setup is shown in Figure 22.

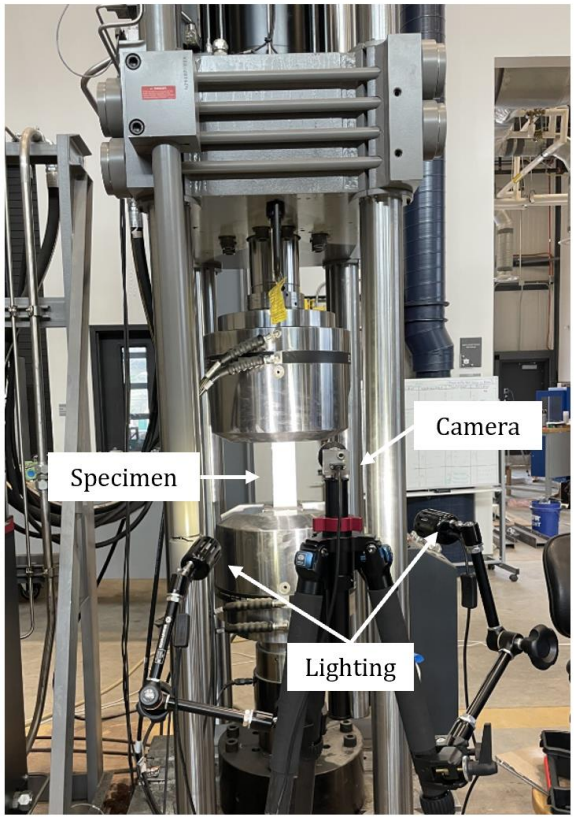

Figure 22: DIC Verification Test

Utilizing the laboratory's Universal Testing Machine (UTM), the specimen was uniformly and gradually extended at a rate of 0.0125 inches per second to a force of 14.5 kips and held for approximately 40 seconds. Figure 23 shows the strain reported via DIC at this load. Utilizing Hooke's Law, a calculated stress of 18.8 ksi, and an assumed Modulus of Elasticity of 29,000 ksi, an approximate strain of 650 microstrains was expected and confirmed on the specimen via DIC.

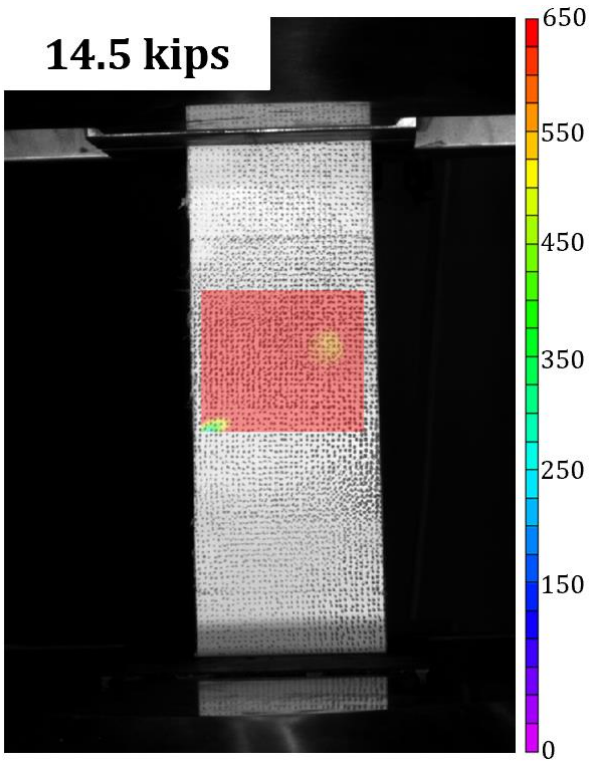

Figure 23: Verified DIC Result (Longitudinal Strain (ε_{yy}) – Engineering)

3.5 Specimen Preparation

To ensure accurate DIC results, specimen preparation was carefully planned and performed according to the following steps and recommendations. Per Correlated Solution's Speckle Kit User Manual (Version 6), the following steps were taken to achieve reliable DIC results (Correlated Solutions, 2023). In general, the areas of interest for DIC analysis of the connection (in varying capacities for each test) included the exterior facing visible angle leg of one angle, the entire width and variable length of the top flange, and the column web located opposite the connection. These dimensions are noted in Chapter 4 and were approximated via finite element modeling performed by Robel Alemayehu, Ph.D.

To prepare the specimen, a thin layer of matte white spray paint was applied in multiple passes to create a uniform background. For all tests, apart from Test 2 (Connections C and D),

the mill scale was carefully removed from the surface of the steel with an angle grinder prior to the application of paint. This removal allowed for optimal bonding of the spray paint to the steel and minimized the likelihood of the paint flaking off due to high strain during testing.

Utilizing the provided speckle kit, shown in Figure 24, a speckle pattern was applied on the white paint with black ink and a stamp/stamp roller, providing a stark contrast between the dots and background. The dot sizes utilized on these specimens ranged from 0.13” to 0.5” and were placed at random to produce confidence in the results. The dot size was chosen with consideration of the area of interest and the camera’s field of view; for example, a larger area of interest required a larger dot size due to the greater field of view. To further achieve the desired 50/50 white/black color, a black fine-tipped marker was utilized to add more speckling, particularly in areas that the stamp/stamp roller was unable to properly reach. Figure 25 and Figure 26 show the progression of an angle and top flange being prepared for DIC use.

Figure 24: Speckle Kit

Figure 25: Angle DIC Preparation Progression

Figure 26: Top Flange DIC Preparation Progression

In some cases, the top flange featured strain gauges and rosettes that were not removed prior to the application of paint and were present during testing. These strain gauges were covered by electrical tape and the wires were routed and taped in such a way to stop movement during testing. The tape was then covered in paint and speckled like the rest of the area of interest; an example is shown in Figure 27. These areas in which the steel was not visible to the camera were not included in post-testing analysis.

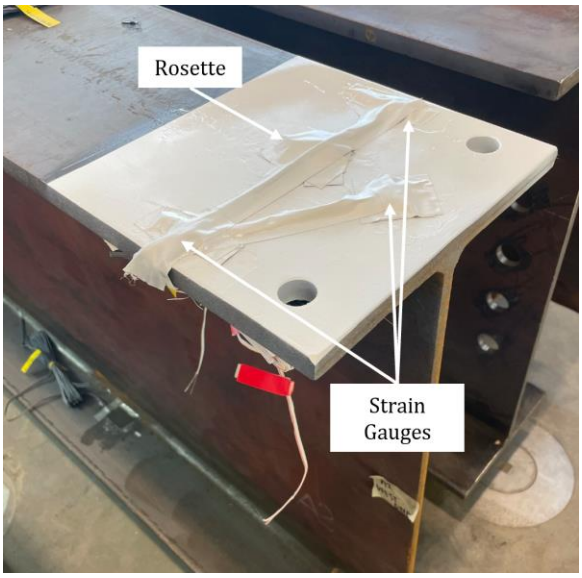

Figure 27: Top Flange with Strain Gauges for DIC

3.6 Testing Setup

All full-scale testing was performed in the ASEL high bay from February to July of 2024.

3.6.1 General Overview

This experimental test setup idealized a realistic application by testing two opposing connections at once with a connecting girder/beam undergoing four-point bending. It utilized W14x82 stub columns with a shop-welded connection on each flange, allowing for the column to be reused in the testing of a different connection and reducing the total number of columns needed for the test program. The general girder-column experimental setup is shown in Figure 28 and is similar for the beam-column setup. Though the true application of this connection is intended for composite construction, this test evaluated the girder without a composite slab. To account for realistic composite slab behavior, the beam span lengths were reduced for testing to provide reasonable combined shear and rotation at the connections. The column center-to-center spacing for the W24x68 and W16x36 were 18’ and 14’, respectively. Calculations of the center-to-center spacing chosen for representative shear and rotation of a composite slab are found in

Appendix D. Also, lateral supports were provided on each side of the girder/beam at three locations to prevent lateral buckling and replicate lateral restraint due to a composite slab for all tests unless noted otherwise. These supports, shown in Figure 29, were located at midspan and five feet from the center line of each stub connection column, set back/shimmed a maximum of half an inch from the flange(s), and lubricated before testing.

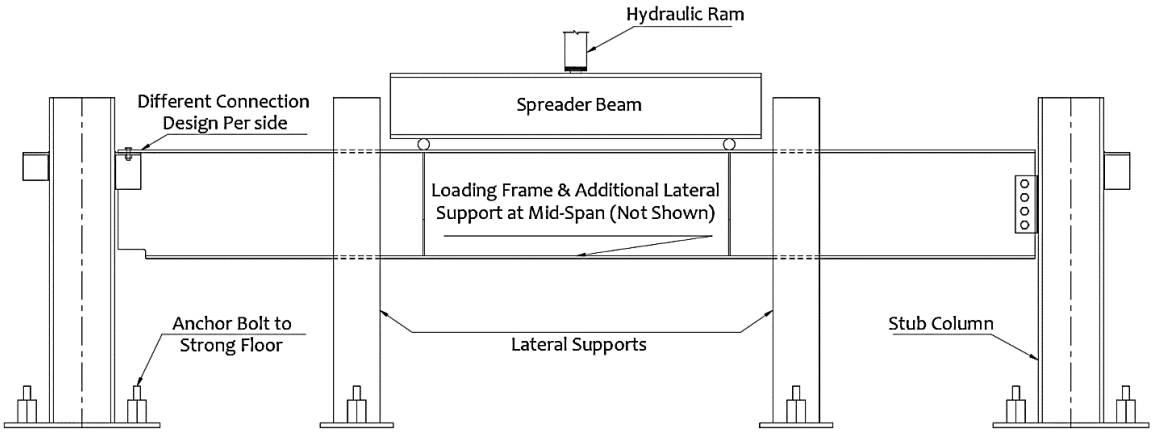

Figure 28: Girder-Column Testing Setup

Figure 29: Lateral Supports

Figure 30 provides a rendering designed by Robel Alemayehu, Ph.D. of the general test setup in the laboratory.

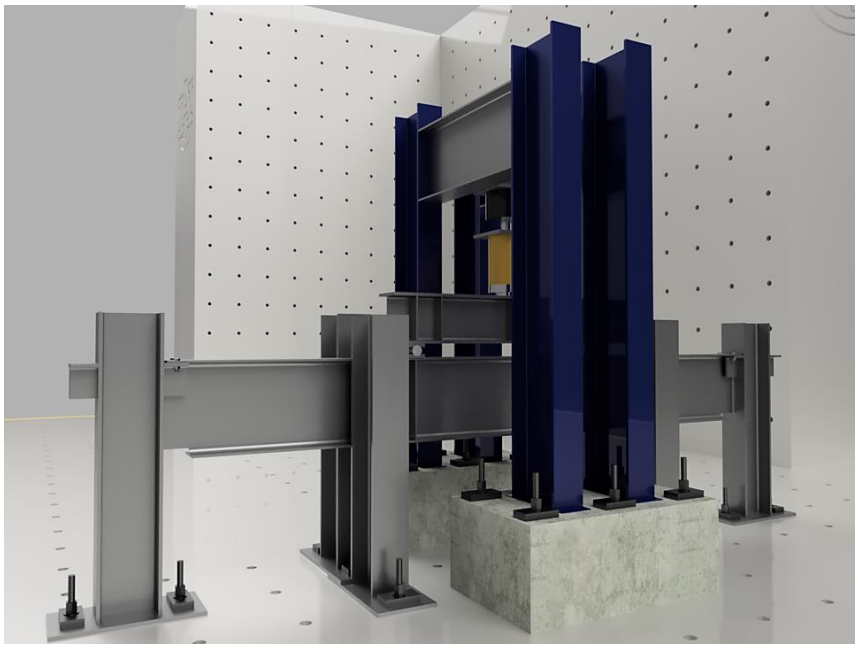

Figure 30: Rendering of Test Setup

An existing double-column load frame was utilized for all tests. A 600-kip capacity Power Team hydraulic ram actuator and 400-kip load cell, featuring a safe over-range of 150%, were mounted on the underside of the load frame headers. Two point-loads were applied at 1/3rd distances of the girder/beam length (directly above the stiffeners) via the connected hydraulic ram and spreader beam contacting the supports. These loading supports, shown in Figure 31, were well lubricated using dry lube immediately before testing to prevent the effects of friction.

Figure 31: Closeup of Point Loads and Lubrication

The loading frame, stub columns, and lateral supports were anchored to the strong floor via pre-tensioned Dywidag bars. Each girder/beam was erected with an overhead crane to realistically evaluate the true construction process of the drop-in connection. All bolts were conservatively tightened to 20% of the minimum required slip-critical bolt pretension found in AISC Table J3.1 using a calibrated wrench. For example, 3/4 in. bolts were tightened to approximately 6 kips, and 1 in. bolts were tightened to approximately 10 kips (AISC, 2022). Some connections utilized bolts that were oriented upside down to allow for a better view of the connection angle to be seen by the DIC cameras; the shear plane of the upside down bolts did not vary from the shear plane intended with an upright bolt, an example of this is shown in Figure 32.

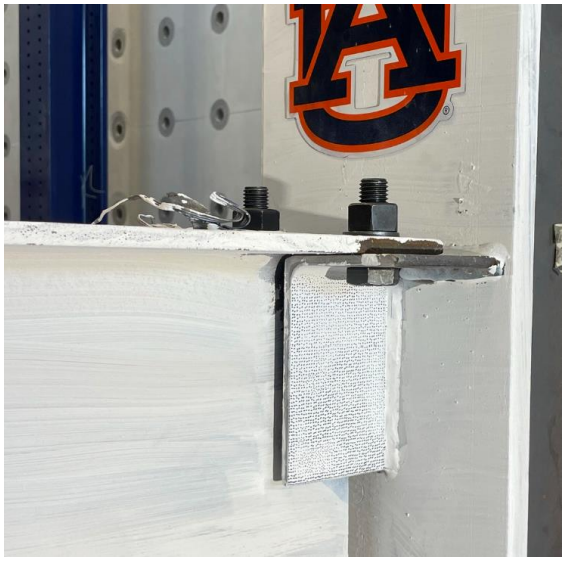

Figure 32: Example of Upside-Down Bolts

Due to top-flange local buckling at the location of the point loads, Cross-Laminated Timber (CLT) blocks were wedged adjacent to the stiffener in later tests. Figure 33 shows an example of the CLT block locations.

Figure 33: CLT Blocks to Prevent Top-Flange Local Buckling

3.6.2 DIC Setup

For all tests noted in this thesis, DIC was utilized in varying capacities to capture the yield lines and deformations in 2D or 3D of various members of the connection. The potential locations/areas of interest (AOI) to be investigated via DIC that were considered for each test were the girder/beam top flange, vertical angle leg, shear tab, and column web. A typical setup includes the following: a computer with VIC-2D and VIC-3D DIC software, a tripod with connected aluminum arm extension, multiple light sources, 12.3 Megapixel camera(s), and appropriate lense(s), and cabling. It is to be noted that two cameras are required for a 3D analysis, while a 2D analysis requires only one camera. Due to a limited number of cameras (four total), tests were limited to the number of connection components that could be captured via DIC. Typical DIC setups are shown in Figure 34 and Figure 35.

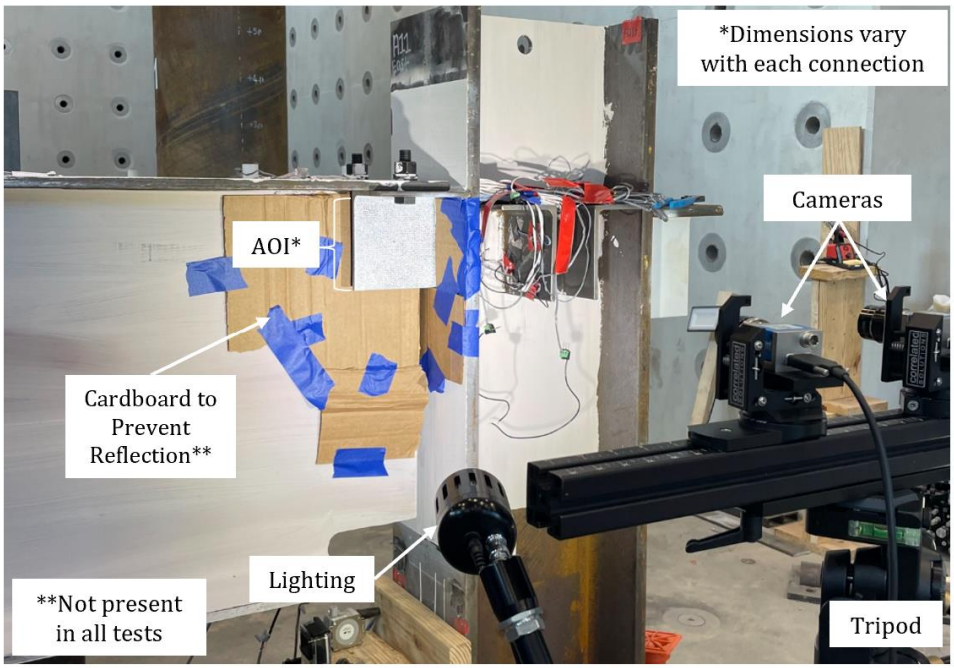

Figure 34: Typical DIC Setup for Angles, Tab, and Column Web

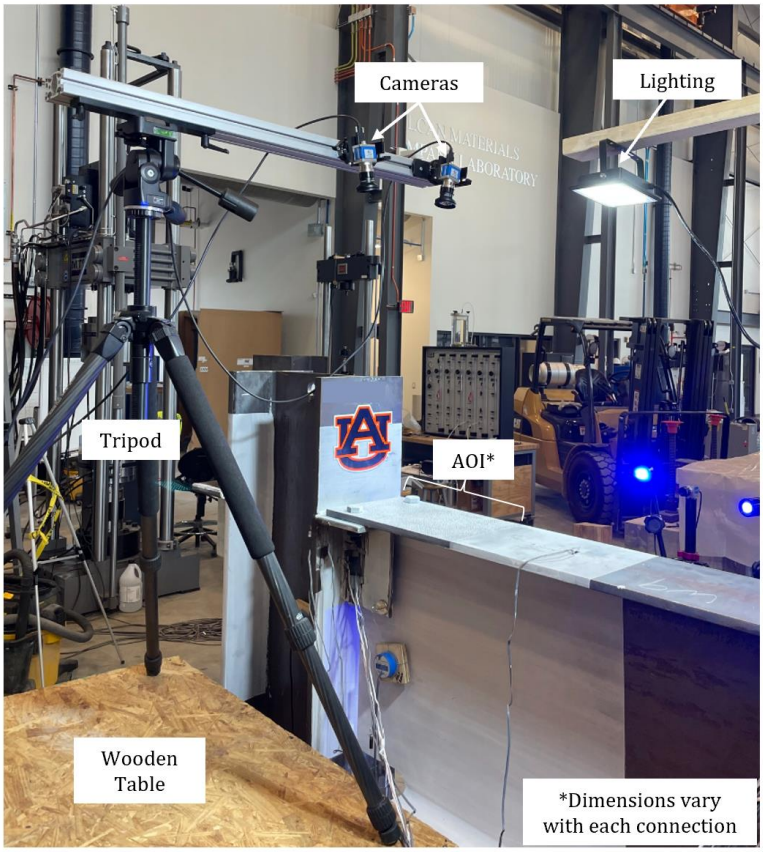

Figure 35: Typical DIC Setup for Girder Top Flange

To begin, the proper lens for each camera was chosen with consideration of the size of the AOI, distance between the camera and the specimen, lighting available, and expected out-of-plane movement. The available lenses were two f2.8/12 mm lenses, two f2.0/28 mm lenses, and two f2.8/50 mm lenses; each of which is shown in Figure 36. If a 3D analysis was being prepared, the same lens was chosen for both cameras focused on the same specimen. After selection, the camera and lens were connected and attached to the tripod.

Figure 36: Cameras and Lenses

For all specimens, the tripod was positioned in such a way that allowed for the attached camera to achieve an optimal view of the specimen. For a 3D analysis, the cameras are angled in such a way that allows for out-of-plane movement to be captured, while a 2D analysis requires that the camera be planar to the specimen. For connection angles, the shear tab, and column webs, the tripod was placed at a similar height and approximately 4 ft. from the AOI. Due to the height of the girder and the limited height of the tripods, two wooden tables measuring approximately 40” and 60” tall, shown in Figure 37, were built to elevate the tripod for proper viewing of the top flange. These tables were placed next to the specimen and the tripod was then placed carefully on top of the tables, with the aluminum arm cantilevering over the girder. Once the cameras were properly positioned, the cameras were connected to the computer and VIC-Snap was opened, displaying the camera’s view and allowing for adjustments to be made.

Figure 37: Built Wooden Tables

Supplementary lighting was provided in the form of multiple LED lamps, which were adjusted to illuminate the specimen for analysis. Proper lighting was critical to minimizing aliasing (wave-like patterns) or incomplete results due to reflection. White and blue LED lights were used in this project; blue light may be noticeable in regular pictures taken but did not influence DIC results. The amount of light entering the camera was able to be fine-tuned by adjusting the aperture setting on each lens to accommodate for the lack of or abundance of light. After observing ideal exposure (lighting) results on VIC-Snap, the focus on the lens was adjusted to properly view the AOI and produce minimal noise.

Immediately before testing, calibration photos were taken with a NIST-certified aluminum calibration board, all options considered are pictured in Figure 38. The calibration spacing was chosen in which all three hollow dot marks on the board were visible to the camera(s). The board was positioned in front of the camera at relatively the same distance as the specimen and rotated at various angles in and out-of-plane with each calibration photo for a 3D-DIC analysis. The board was kept planar to the camera for a 2D-DIC analysis. These images were processed before testing to confirm adequate calibration images and allowed for strain to be

calculated in measurement units rather than pixels for a 2D-DIC analysis. They also provided for stereo-triangulation in a 3D-DIC analysis.

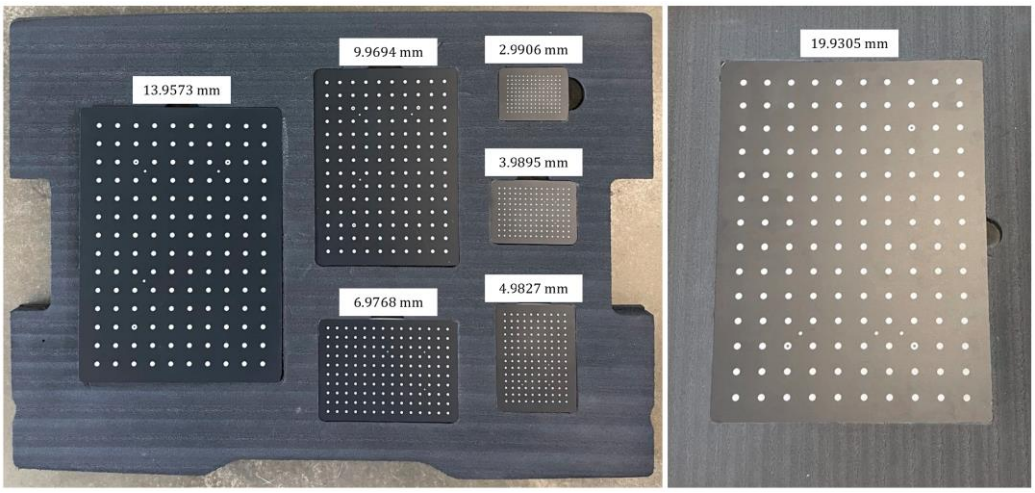

Figure 38: Calibration Boards (Spacing Noted)

3.7 Testing Matrix and Procedure

Six total tests were conducted: five girder-to-column tests and one beam-to-column test. Table 4 below describes the testing matrix. In total, 12 connections were tested, as two different connections were utilized in each test with the full details of each connection provided in Table 2. If a connection failed before the connection on the opposite end of the girder/beam, the test was repeated after retrofitting the failed connection. While a retrofitted/repeated test was performed for all girder-to-column tests, DIC data was determined to be inconsequential in these repeated tests due to already observed strain patterns and are therefore not discussed in this thesis.

Table 4: Testing Matrix and Order

Test	Connections
1	A & B
2	C & D
3	E & F
4	G & H
5	I & J
6	K & L

A Power Team hydraulic pump connected to the actuator was utilized to apply force to the beam/girder at a variable rate. Via VIC-Snap (a Correlated Solutions Software), the DIC cameras captured images and loading data at a rate of 1.0 Hz for the entire duration of the test. Photos were captured immediately before the engagement of the spreader beam and the load points and concluded at their disengagement. Interval force measurements and associated picture numbers were recorded by hand for later use in verifying the force experienced in each picture. During testing, people walked around the specimen to ensure safety and captured images of the specimen under load.

3.8 Post-Testing DIC Analysis

Upon completion of testing, the DIC images were analyzed in VIC-2D and VIC-3D. A reference image of the specimen (taken before loading was applied) was selected. All measured strains and displacements were relative to the reference image. An area of interest that would appropriately capture the connection's deformation was then selected on this image to be analyzed. It is important to note that all areas of interest excluded any strain gauges, bolts, and areas of improper speckling. Therefore, the final strain profile may not be complete in the figures

shown. An example is provided in Figure 39 where strain gauges and bolts were excluded from the AOI shown in red.

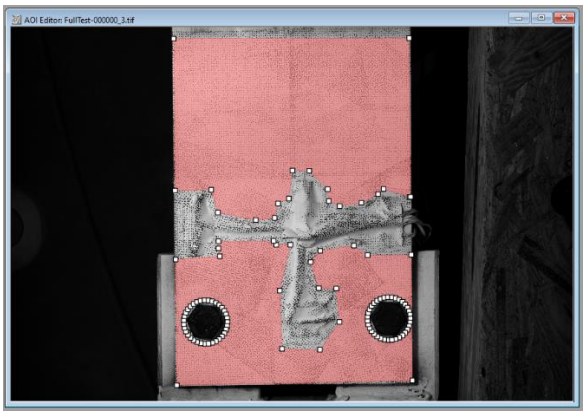

Figure 39: Selected AOI Excluding Strain Gauges

As well, a step and subset size were chosen according to the speckle pattern and size; both were automatically set by the system to produce accurate results while also accounting for spatial resolution. Before running the analysis in VIC-2D or VIC-3D, options to adjust the factory-set interpolation spline, subset weight, correlation criterion equation, etc. were presented. All initial factory settings were retained. Post-processing options included selecting a tensor type; engineering strain was chosen, but various other tensors were also available to be used. The analysis then ran, and strain data was produced.

Chapter 4: Execution of Testing Program

4.1 Introduction

This chapter describes the execution and results of the testing matrix previously discussed in this thesis. As variations of the DIC system were utilized for various connection elements, the summary table of areas investigated is shown below in Table 5. The dimensions of the areas of interest for each specimen are noted in its respective subsection; these areas were determined through prior FEA modeling performed by Robel Alemayehu, Ph.D., which predicted the most likely area to view plastic deformations.

Table 5: Connection DIC AOI

Test	Connection	2D or 3D		
		Girder Top Flange	Angle/Plate	Column Web
1	A	2D	-	-
	B	3D	2D	-
2	C	2D	2D	-
	D	2D	2D	-
3	E	3D	2D	-
	F	-	2D	-
4	G	-	2D	-
	H	3D	2D	-
5	I	-	3D	-
	J	-	3D	-
6	K	-	-	3D
	L	-	-	2D

All transverse (ε_{xx}), longitudinal (ε_{yy}), and shear (ε_{xy}) strains presented in this thesis were calculated using the engineering strain tensor programmed in Correlated Solution's VIC-2D and VIC-3D software (Correlated Solutions, 2022). This shear strain (ε_{xy}) is described as half the value of the engineering shear strain (γ_{xy}). The Von Mises strains (ε_v) were calculated utilizing equation 4.1, provided by Correlated Solutions in the DIC post-processing software. As the DIC system only calculates surface strain, this equation uses a principal plane strain formation (Correlated Solutions, 2020b).

$$\varepsilon_v = \frac{2}{3}\sqrt{\varepsilon_1^2 - \varepsilon_1\varepsilon_2 + \varepsilon_2^2} \qquad 4.1$$

Where:

ε_1= x-axis principal strain

ε_2 = y-axis principal strain

As well, due to the discussion of yield lines in this chapter, a summary table of each steel section's theoretical strain at yield is noted in Table 6.

Table 6: Steel Section Yield Strains According to Mill Report

Steel Section	Theoretical Tensile Strain at Yield (microstrain)	Theoretical Shear Strain at Yield (microstrain)
W24x68	1930	1470
W16x36	2000	1520
W14x82	1900	1445
L8x4x3/4	1880	1430
L8x4x1/2	1950	1480
L6x4x5/16	2000	1520
L4x3x1/2	1900	1445
3/8” thick plate	2310	1755

These yielding tensile strains (utilized for comparison to all shown strains) were calculated via Hooke’s Law. The average tensile yield stress (f_y) provided in Table 3 and an assumed Modulus of Elasticity (E) of 29,000 ksi were used in this calculation to determine the above values. The engineering yield shear strain (γ_{xy}) was calculated with an assumed shear yield stress of $\frac{1}{\sqrt{3}} f_y$ and an assumed shear modulus (G) of 11,000 ksi. This engineering strain value was then divided by two to produce the above shear strains at yield for each steel section. These values are beneficial when viewing the 2D and 3D strain profiles when noting plastic and elastic deformation. While a positive or negative transverse or longitudinal strain indicates tension or compression, it is to be noted that for all shear strain profiles produced, a positive or negative value indicates the angular change.

The shear reactions experienced in testing are compared to the current AISC equation G3-1 shown in equation 4.2 below (AISC, 2022). Because the full cross-sectional strain profile cannot be determined via DIC, the strain at the surface will be discussed but cannot be directly compared to the above equation. This equation determines the nominal shear strength of a single-angle leg assuming complete shear yielding of the cross-section. In addition, this expression accounts for shear buckling, but does not apply in the discussed testing as all angles have a shear buckling value equal to one.

$$V_n = 0.6F_y btC_{v2} \tag{4.2}$$

Where:

V_n = nominal shear strength

F_y = tensile yield stress

b = depth of the leg resisting the shear force

t = thickness of the angle leg

C_{v2} = web shear buckling coefficient

For clarity, the transverse and longitudinal orientations are shown in Figure 40. For a beam/girder, longitudinal refers to the direction parallel to the beam/girder span and transverse refers to the direction perpendicular to the span. For the column web, longitudinal refers to the vertical direction and transverse refers to the horizontal direction when looking at the web.

a. **b.**

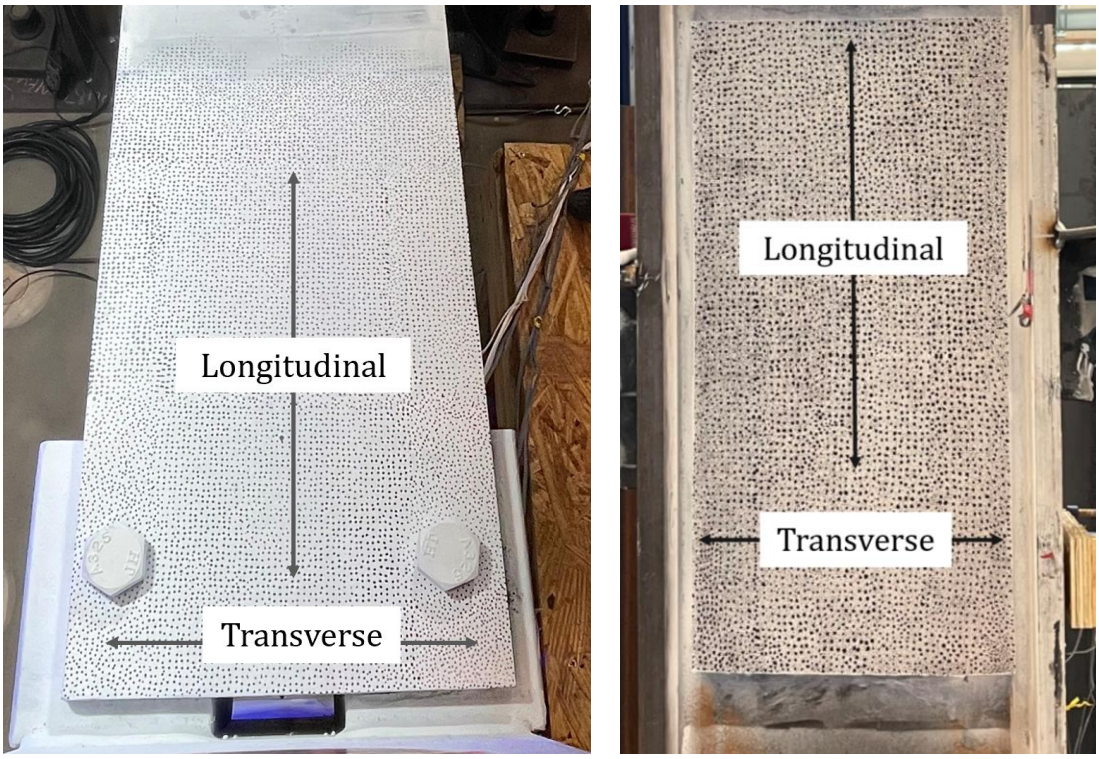

Figure 40: Longitudinal and Transverse Directions (a) Flange and (b) Column Web

4.2 Test 1

Test 1 utilized a W24x68 girder to test the girder-to-column connections, A and B, both of which were made of L8x4x3/4 angles with a bearing length of five inches. Using all four available DIC cameras, images of Connection A's girder top flange and Connection B's girder top flange and angle were captured for DIC analysis. Connections A and B are pictured in Figure 41 before testing; Connection B is encased in blue light due to DIC lighting.

a. **b.**

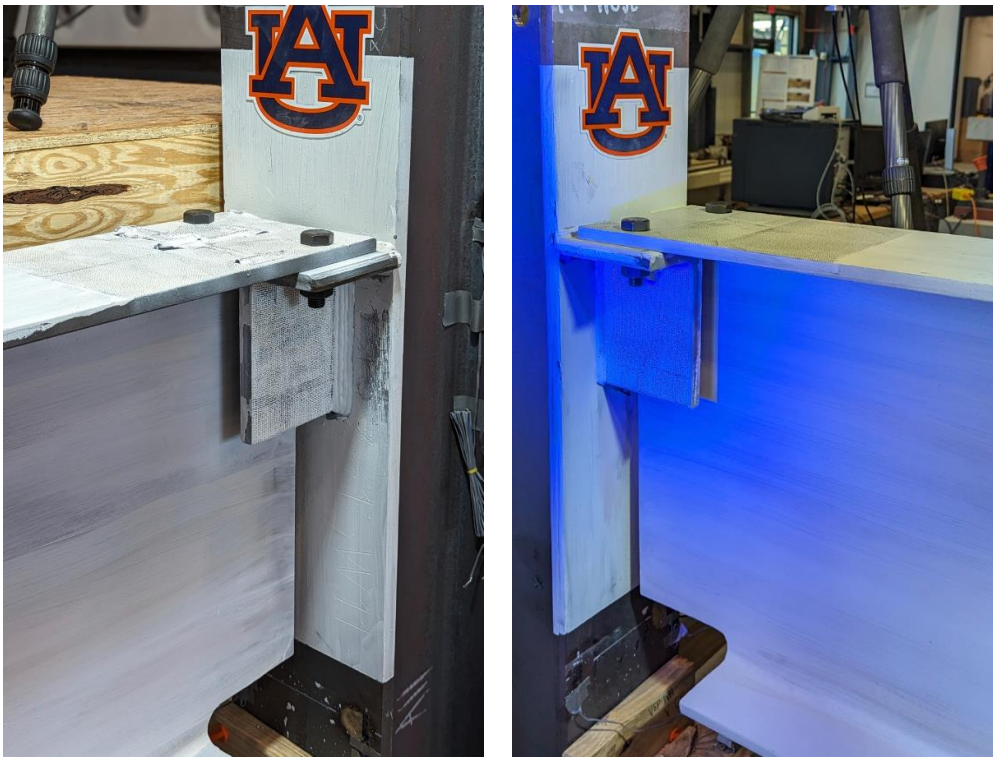

Figure 41: Test 1 Before Testing (a) Connection A and (b) Connection B

Test 1 achieved a maximum force of approximately 280 kips on the test girder, equating to a maximum shear of 140 kips at each connection, well above the connections' factored design strength of 78 kips. Testing was concluded due to instability of the spreader beam and girder, caused by lateral torsional buckling (LTB) and local buckling of the web and flange near the loading points; CLT stiffeners had not been utilized adjacent to the steel stiffeners. The plasticly-deformed girder and rotated spreader beam are shown in Figure 42. A relative rotation of 0.019 radians was achieved for Connection A and a relative rotation of 0.016 radians for Connection B; it is noted that these are not the absolute maximum rotations achieved for these connections as another round of testing was performed that resulted in connection failure; that subsequent test is not discussed in length in this thesis.

a. **b.**

Figure 42: Test 1 Deformed Girder (a) Spreader Beam Instability due to LTB of Girder and (b) Local Buckling of Flange and Web Near Loading Points

While little noticeable visual plastic deformation occurred in Connections A and B during testing, as shown in Figure 43, surface strains determined via DIC shine a light on the behavior of each connection.

a. **b.**

Figure 43: Test 1 After Testing (a) Connection A and (b) Connection B

4.2.1 Connection A

To investigate Connection A's top flange, an approximate area of 117 square inches (13 inches longitudinally by the width of the girder top flange) was prepared closest to the column face. Upon completion of the test, the captured images of Connection A were analyzed in VIC-2D. It is noted that due to the attached strain gauges on Connection A's top flange obstructing the camera's view of the underlying steel, the associated wires and tape were excluded from the defined AOI in the VIC-2D analysis. This area is seen in the middle and lower portions of the flange and remains white with black speckling in all progression images. Steel strain cannot be concluded in these areas and should be understood when looking at Connection A top flange figures. Also, due to out-of-plane movement during testing and monocular vision of the DIC system (see Chapter 2 for further explanation), a clear compression bias has formed beyond the bearing length of the angles as the girder moved away from the sensor. While this area towards midspan is not suitable for conclusive evidence about strain magnitude, the flange area bearing on the angles stayed in relative original planar view, producing reliable data.

Figure 44 visualizes the girder's strain field progression, in microstrain units, with (a) Von Mises strains (ε_v), (b) transverse strains (ε_{xx}), and (c) longitudinal strains (ε_{yy}) for a connection shear (or reaction) of 40, 60, 80, 100, and 140 kips.

a.

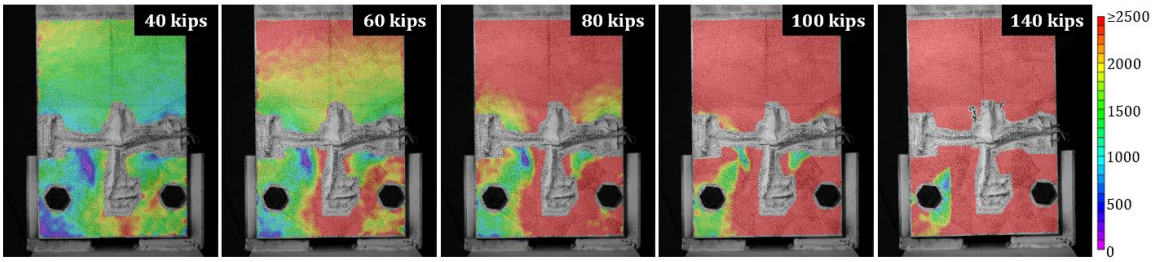

b.

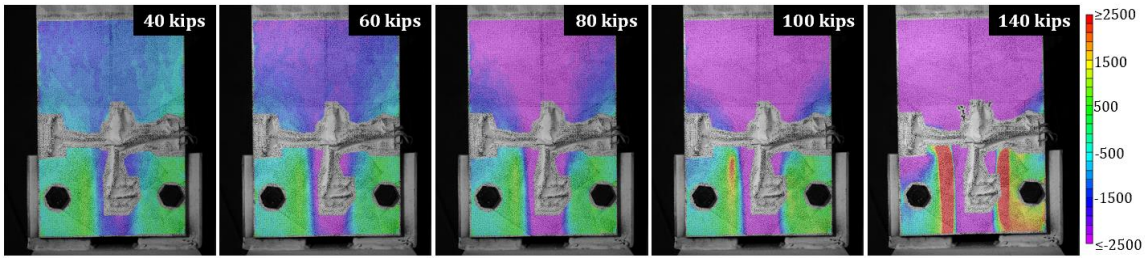

c.

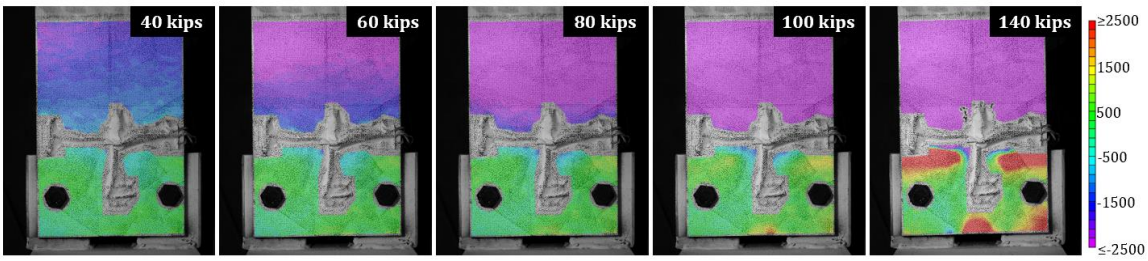

Figure 44: Connection A (Test 1) 2D DIC Flange Deformation Progression (a) Von Mises Strain (ε_v) (b) Transverse Strain (ε_{xx}) – Engineering, and (c) Longitudinal Strain (ε_{yy}) – Engineering

Figure 44 is oriented in such a way that the midspan of the girder is in the upper direction of the progression photo and the stub column/connection angles are in the lower portion of the photo. Shown by both Von Mises and transverse strains, a wide initial yield line begins to form on the centerline of the flange closest to the face of the column, in the region unsupported by the connection angles at a shear of 40 kips. It then gradually moves towards the midspan of the beam, eventually passing the transverse edge of the angles. Further insight and according to

Figure 44 (b), the region between these initial yield lines is in compression. Though the magnitude of these yield lines cannot be concluded beyond the bearing length, the flaking of the speckle pattern, due to the deformation of the underlying steel, suggests that they extend approximately 2.5 inches beyond the supported region. This observation is further shown in Figure 45 in which the end of the bearing length and continuation of the yield lines (seen via flaking of paint) are noted. At a shear of 100 kips, a secondary set of yield lines are seen forming along the interior angle edges. Initially, the area at the left-hand angle edge farthest from the column exhibits yielding, followed by complete yielding over both angle's interior edges at the maximum shear. These secondary yield lines encase an area of tension as the flange bends about the interior edge of each angle.

Referencing Figure 44 (c), longitudinal strains are seen forming at the location of the transverse edge of the underlying angle at a shear of 100 kips, this is the same time in which transverse yield lines begin to show plastic deformation about the interior angle edge; this region has reached complete yield at the maximum shear of 140 kips. This late yield line formation about the transverse angle edge encases an area of tension and suggests greater in-plane rotational development at higher shears as the flange begins to deform about the transverse edge of the angle. Again, a rotation of 0.019 radians was achieved for this connection during this test sequence. Though not visible to the human eye, the surface of this girder flange went mostly plastic by the end of testing, as seen in the Von Mises strain progression.

Figure 45: Connection A (Test 1) Yield Line Length According to Flaking of Paint

To further investigate the initial failure mode of flange bending about the interior longitudinal edges of the angles, a transverse cross-sectional cut was made approximately midway between the transverse edge of the angles and the bolt centerline at various shear forces, as shown in Figure 46.

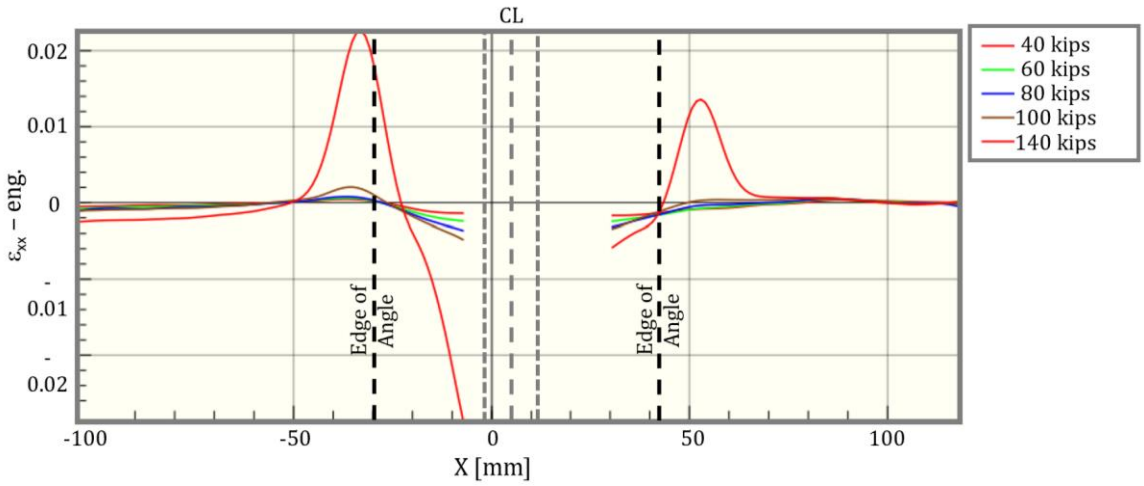

Figure 46: Connection A (Test 1) DIC Flange Section Cut Transverse Strain (ε_{xx}) Profile

The theoretical centerline (CL) of the flange (with the edges of the flange web noted on each side) and the edge of the right-hand and left-hand angles (as seen from plan view with the midspan of the girder into the plane) are noted for reference in Figure 46. Maximum tensile strains of 0.023 and 0.014 are located approximately 0.12 in. (3 mm.) left of the left-hand angle and 0.38 in (9.6 mm) right of the right-hand angle. From the available data, a maximum compressive strain of 0.028 is revealed 0.34 in. (8.6 mm) left of the web edge, likely in or near the actual fillet of this girder. Conclusively, three (likely four, had the strain gauges not been present) plastic hinges formed across the width of the girder flange during this test. Again, due to LTB of the girder, these results are not symmetric.

4.2.2 Connection B

The investigation of Connection B's behavior included the analysis of the girder's top flange and the vertical angle leg via DIC. For the girder, an approximate area of 117 square inches (13 inches longitudinally by the width of the girder top flange) was prepared closest to the column face, and a rough area of 46 square inches (entire visible vertical angle face) was

prepared for the angle. The captured images of Connection B's top flange were analyzed in VIC-3D and the angle was analyzed in VIC-2D.

Figure 47 displays the girder's 2D strain field during testing, in microstrain units, with (a) Von Mises strains (ε_v), (b) transverse strains (ε_{xx}), and (c) longitudinal strains (ε_{xx}) for a connection shear of 40, 60, 80, 100, and 140 kips. It is noted that small areas of incomplete data seen in the lower middle portion of the flange are due to preliminary flaking of the spray paint on top of the flange beginning at a shear of 80 kips.

a.

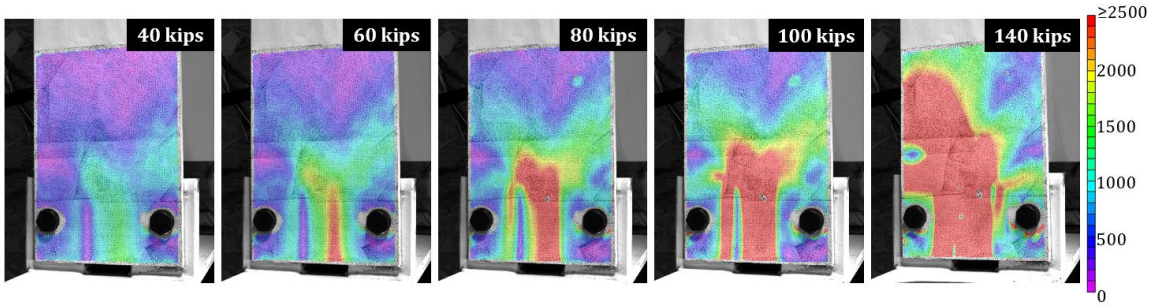

b.

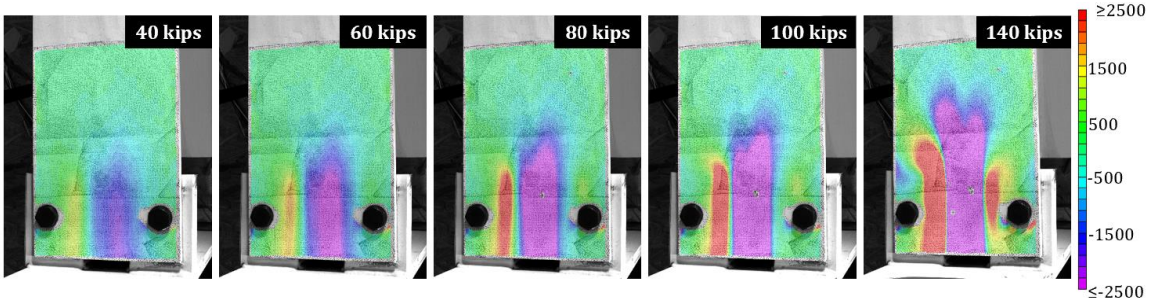

c.

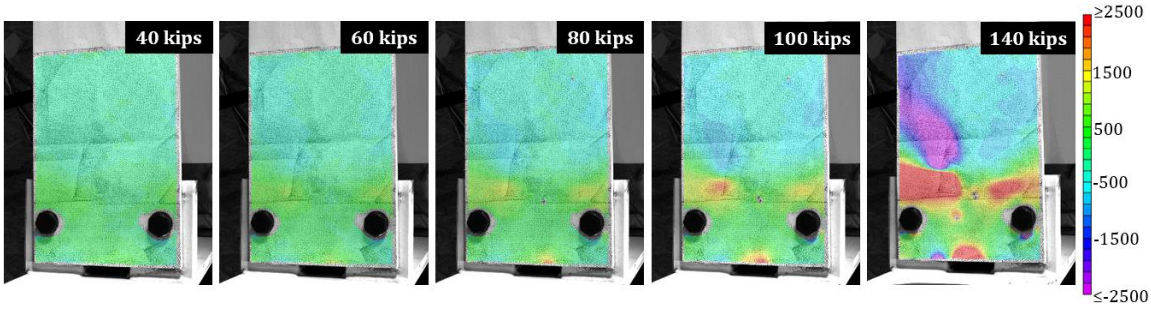

Figure 47: Connection B (Test 1) 2D DIC Flange Deformation Progression (a) Von Mises Strain (ε_v), (b) Transverse Strain (ε_{xx}) – Engineering, and (c) Longitudinal Strain (ε_{yy}) – Engineering

Figure 47 is oriented in such a way that the midspan of the girder is in the upper direction of each progression photo and the stub column/connection angles are in the lower portion of each image. In parts (a) and (b), at a shear of 40 kips, a prominent strain field approaching yield and indicating a region of compression is seen having formed on the longitudinal centerline of the flange closest to the face of the column, between the regions supported by the angles. Through

the progression, it gradually moves towards the midspan of the beam, eventually spreading out at an angle once passing the transverse edge of the connection angles. These yield lines continued for an approximate distance of five inches beyond the edges of the angles. According to Figure 47 (b), the region encased between these initial yield lines is in compression. As well, at a shear of 40 kips, a strain line approaching yield and encasing an area of tension, appears along the interior longitudinal left-hand angle edge and progresses towards midspan, branching out at an angle similar to, but shallower, than that of the initial yield lines. Eventually, a latent yield line like that of the previously described has fully formed along the right-hand angle's longitudinal interior edge at the maximum shear of 140 kips.

Starting to be revealed at a shear of 80 kips, longitudinal strains are seen encroaching the yield limit along the transverse edges of the angles. Shown in Figure 47(c), this area is in tension as the flange begins to deform about the transverse edge of the angles, resulting in an increase of in-plane rotation; again, a rotation of 0.016 radians was achieved in this test. While the strains shown are not equivalent about the longitudinal centerline of the flange, these strains could likely be concluded as such had LTB not occurred in testing. Overall, the strain fields presented for Connection B are comparable to Connection A in their magnitude and formation; both flange surfaces were plastically deformed by the end of testing.

To further describe the deformations and strains that occurred in Connection B, Table 7 (noted in units of microstrain) visualizes the flange in a 3D space in which the displacement in the z-direction is amplified by 25% compared to the X and Y axes. The Z-axis is relative to the initial position of the flange immediately before testing (in which z equaled zero) and becomes negative as the specimen deformed away from the camera and towards the ground. The X-axis ranges from -4.75 in. to 4.75 in., in which 0 in. is located at the longitudinal centerline of the

flange; a positive X-value reflects part of the flange that is to the right of the centerline and over the right-hand angle (in reference to the plan view seen in Figure 47) and vice-versa. The Y-axis ranges from -6.5 in. to 6.5 in., the largest value of 6.5 in. represents the part of the flange closest to midspan, while the smallest value of -6.5 in. represents the part of the flange closest to the stub column. Figure 48 shows a reference to orient the viewer for the 3D figures shown in Table 7.

Figure 48: Connection B 3D Reference

In addition to the results discussed for the 2D strain progression; at a maximum shear of 140 kips, the flange is shown with a shallow deformation along the longitudinal centerline between the two connection angles. In the region in which the flange is no longer bearing on the angles (Y-coordinates of -1.5 in. and greater), the flange is seen deforming in the negative Z-direction with a maximum deformation of approximately 0.4 inches located at the far left-hand side of the flange.

Table 7: Connection B (Test 1) 3D DIC Flange Deformation Progression

	Von Mises Strain (ε_v)	Transverse Strain (ε_{xx}) - Engineering	Longitudinal Strain (ε_{yy}) - Engineering
Load (kips)	≥2500 2000 1500 1000 500 0	≥2500 1500 500 -500 -1500 ≤-2500	
40	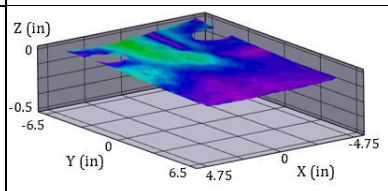	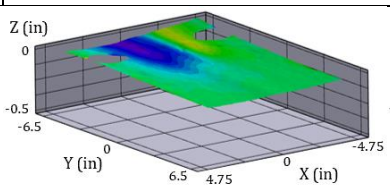	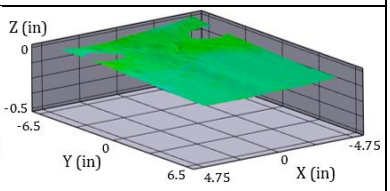
60	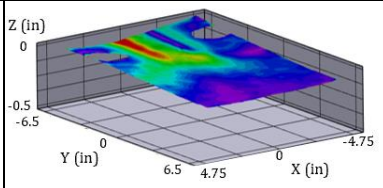	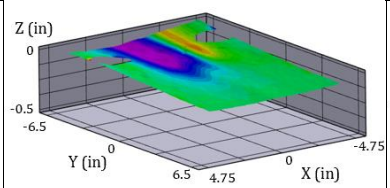	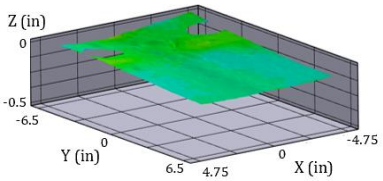
80	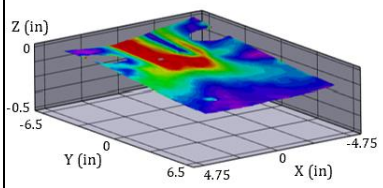	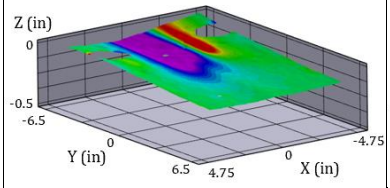	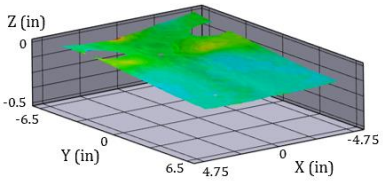
100	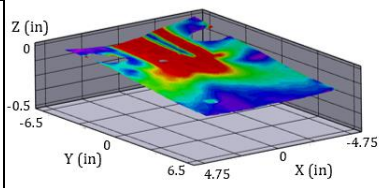	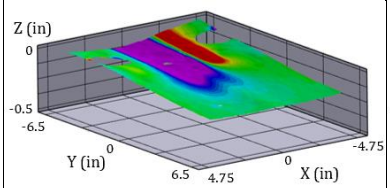	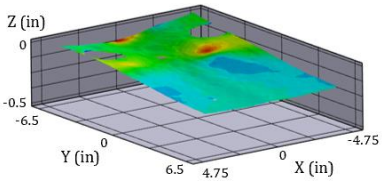
140	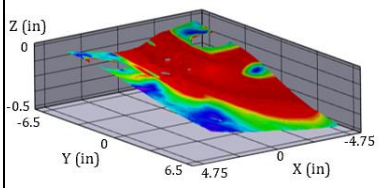	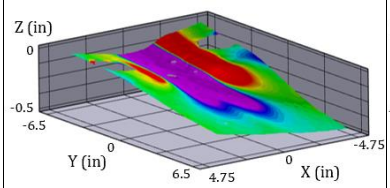	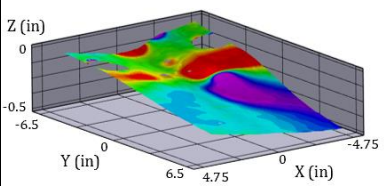

In further investigation of the initial failure mode, a transverse cross-sectional cut, like that of Connection A, was made approximately halfway between the transverse edge of the

angles and the bolt centerline at the same shear reactions as previously listed. This is shown in Figure 49.

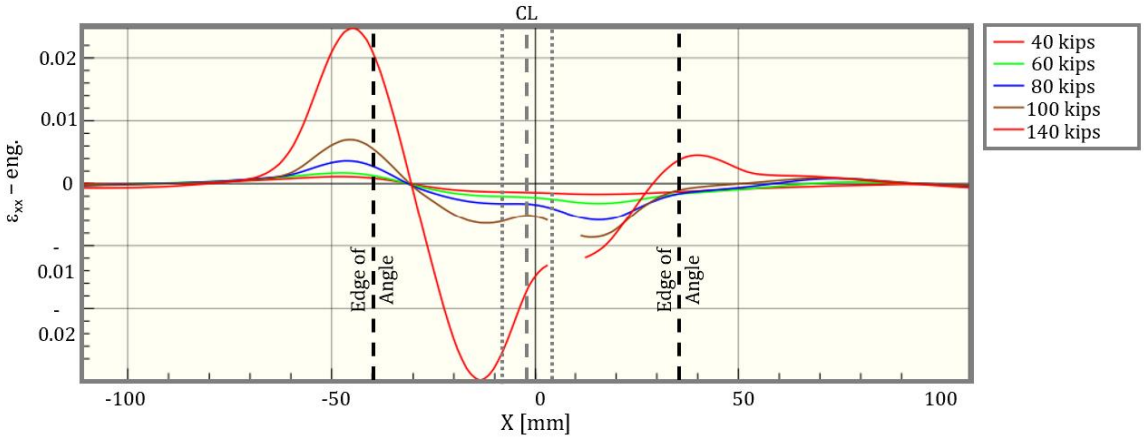

Figure 49: Connection B (Test 1) DIC Flange Section Cut Transverse Strain (ε_{xx}) Profile

The theoretical centerline (CL) of the flange (with the edges of the flange web noted on each side) and the edge of the right-hand and left-hand angles (as seen from plan view with the midspan of the girder into the plane) are noted for reference in Figure 49. Two plastic hinges developed in this flange, one of which occurred near or at the longitudinal edge of the left-hand angle and another that occurred near the left edge of the web in the fillet zone. Specifically, an absolute maximum tensile strain of 0.025 and maximum compressive strain of 0.03 developed approximately 0.2 in. (5.0 mm) left of the left-hand angle and 0.22 in. (5.7 mm) left of the left web edge, respectively. Again, these results are not symmetrical due to LTB of the girder.

Figure 50 shows the Connection B vertical angle leg strain formation, in microstrain units, in (a) Von Mises strain (ε_v) and (b) shear strain (ε_{xy}) for a connection shear of 40, 60, 80, 100, and 140 kips. The upper right-hand area (free end) of the angle begins to yield and extends across the angle to the left lower corner (attached to the column), displaying a complex strain

field and areas of plastic deformation. It is noted that a small region in both (a) and (b) at 140 kips does not display data due to lighting variances encountered during testing.

a.

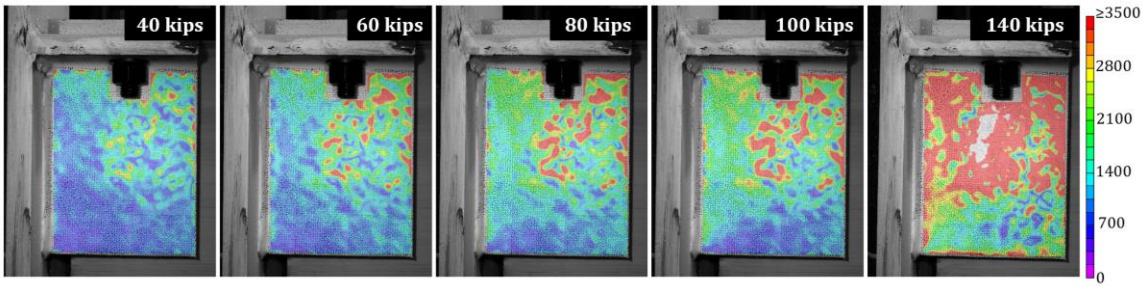

b.

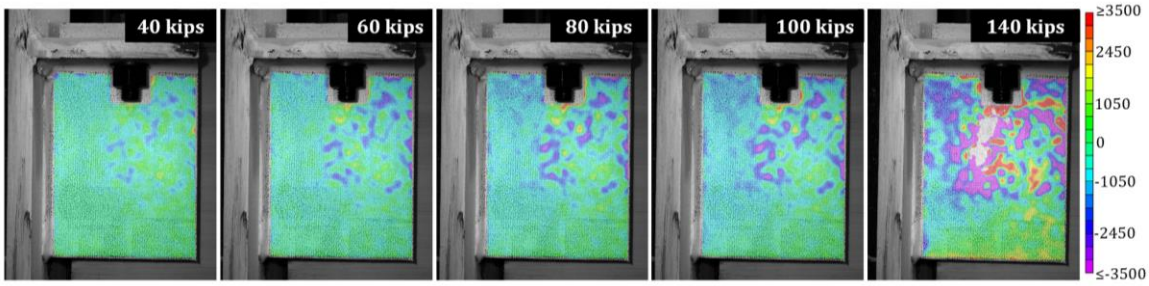

Figure 50: Connection B (Test 1) DIC Angle Deformation Progression (a) Von Mises Strain (ε_v) and (b) Shear Strain (ε_{xy}) – Engineering

Utilizing equation 4.2 and the noted average yield stress for this angle section, a nominal shear strength of approximately 195 kips would be predicted for a singular L8x4x3/4 angle and 390 kips for both connection angles. According to Figure 50 (a) and (b), the upper portion of the angle has exceeded the predicted yield shear strain, but full failure of the angle was not reached in this test.

4.3 Test 2

Test 2 consisted of girder-to-column connections, C and D, the former of which was made of L8x4x3/4 angles, same as connections A and B, but with a smaller bearing length of 3.0 inches, and the latter which utilized shallower and thinner L6x4x5/16 angles with a bearing

length of 5.0 inches (same bearing length as connections A and B). A limited weld size was provided for Connection D and was the controlling limit state according to preliminary design. A W24x68 girder was utilized for this test. Using all available DIC cameras, images of both connection C and D's girder top flange and angle legs were captured for 2D-DIC analysis. Connections C and D are pictured in Figure 51 before testing.

a. **b.**

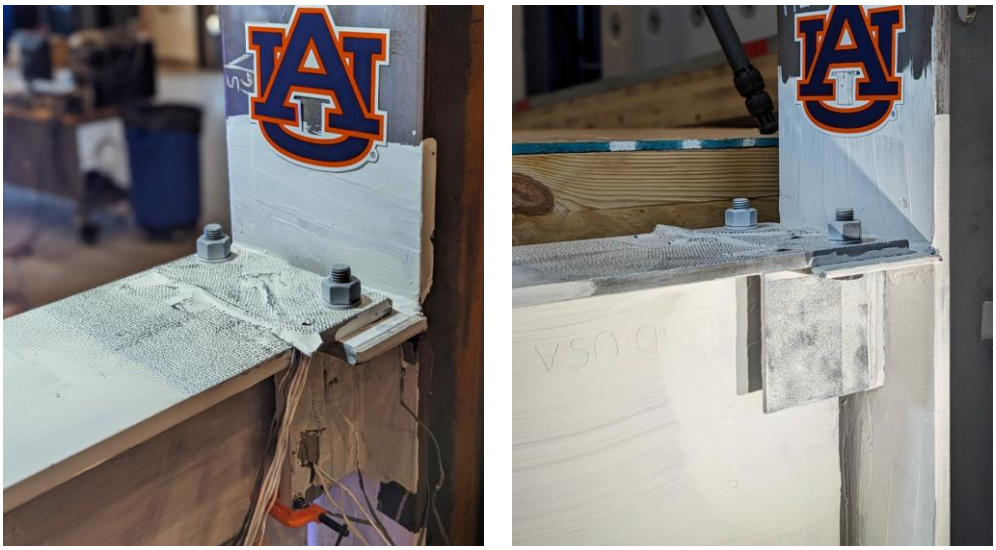

Figure 51: Test 2 Before Testing (a) Connection C and (b) Connection D

Test 2 reached a maximum force of approximately 258 kips on the test girder, equating to a maximum shear of 129 kips at each connection. The test was immediately concluded due to a brittle failure of the horizontal and vertical welds (of one angle) on Connection D. The connection shear at this time was well above the design capacity of each connection. The connections after testing are shown in Figure 52. While little plastic deformation is visibly seen in Connection C, Connection D had plastically buckled near or at the time of weld failure. At weld failure, Connection D reached a relative rotation of 0.01 radians and Connection C rotated 0.015 radians. While not discussed in this thesis, further testing was conducted with Connection D and a retrofitted side to successfully fail the connection.

a. **b.**

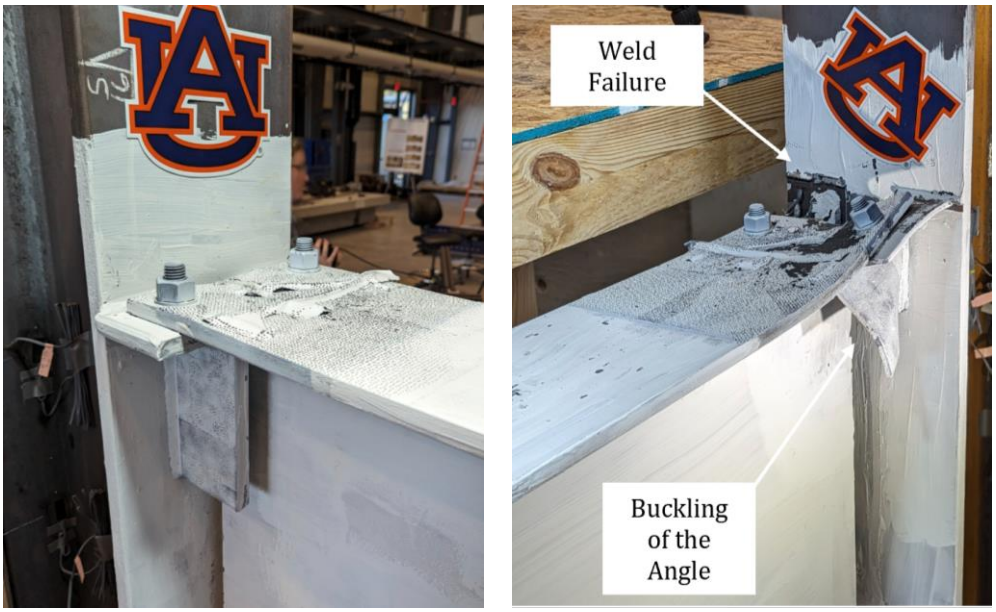

Figure 52: Test 2 After Testing (a) Connection C and (b) Connection D

4.3.1 Connection C

An approximate area of 81 square inches (9.0 inches longitudinally by the width of the girder top flange) was prepared closest to the column face to investigate Connection C's girder top flange. A rough area of 30 square inches (entire visible vertical angle face) was prepared for the angle. Once Test 2 was concluded, both sets of images were analyzed in VIC-2D.

Figure 53 exhibits the girder's yield line formation, in units of microstrain, with (a) Von Mises strains (ε_v) and (b) transverse strains (ε_{xx}) for a connection shear (or reaction) of 25, 30, 35, 40, and 125 kips. Figure 53 is oriented in such a way that the midspan of the girder is in the upper direction of the progression photo and the stub column/connection angles are in the lower portion of the photo.

a.

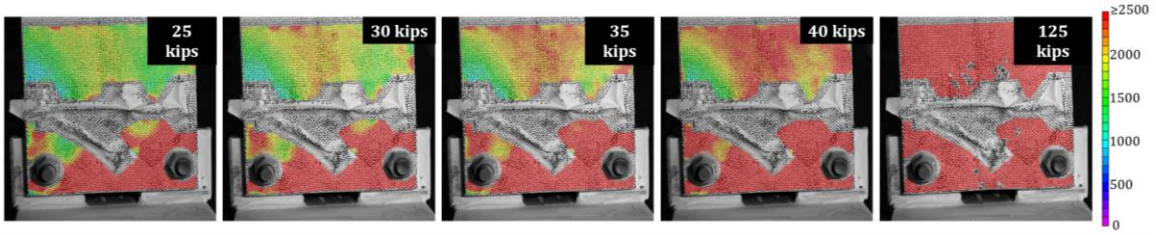

b.

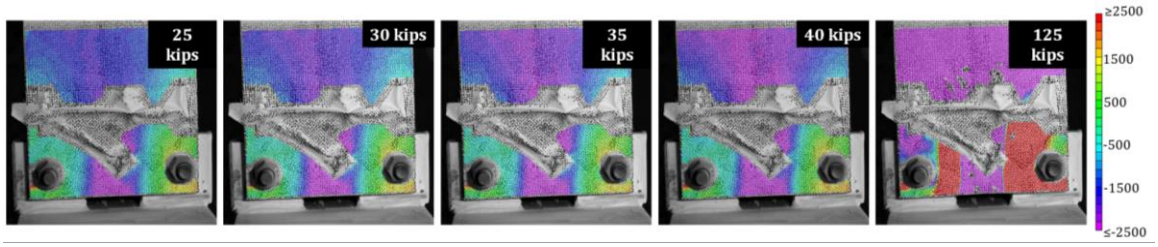

Figure 53: Connection C (Test 2) DIC Flange Deformation Progression (a) Von Mises Strain (ε_v) and (b) Transverse Strain (ε_{xx}) – Engineering

In both strain tensors at a shear of 25 kips, large areas of yielding (in compression) are seen beginning to form on the longitudinal centerline of the flange closest to the face of the column and gradually move towards the midspan of the beam, like that of previously discussed girders. Also, at the maximum shear of 125 kips, tensile yield lines are prominent along the interior longitudinal edges of the angles, corresponding to the observations shown in previous connections. At the conclusion of this test, the flange surface had completely yielded, as shown in the Von Mises strain progression.

Longitudinal strains (ε_{yy}) were not included in this figure due to insignificant data observed, likely due to the placement of the strain gauges in areas where large magnitudes of longitudinal strain would likely have occurred. These areas where the strain gauges were located were covered with tape and excluded from the defined area of interest in the VIC-2D analysis.

This area is seen in the middle and lower portions of the flange and remains white with black speckling in all progression images.

Like that of Connection A, the area of the flange beyond the bearing length (towards midspan) cannot be referenced to provide any reliable data because of the girder's movement away from the visual sensor; as discussed in Chapter 2, a singular camera cannot interpret this out-of-plane movement properly and perceives it as compression, creating a compression bias in this region. Though this area towards midspan is not suitable for conclusive evidence pertaining to strain magnitudes and exact yield line progression distance, the flaking of paint shown (at the maximum shear) beyond the bearing length provides insight into the probable length of the yield lines. As the underlying steel surface deformed, the spray paint began to flake off, revealing the extent of the yield lines. Through this inference, it can be concluded that the yield lines extended approximately three to four inches beyond the bearing length of three inches.

To further investigate the transverse strain observed in Connection C's girder top flange, a transverse cross-sectional cut was made approximately midway between the transverse edge of the angles and the bolt centerline at various shear forces, as shown in Figure 54.

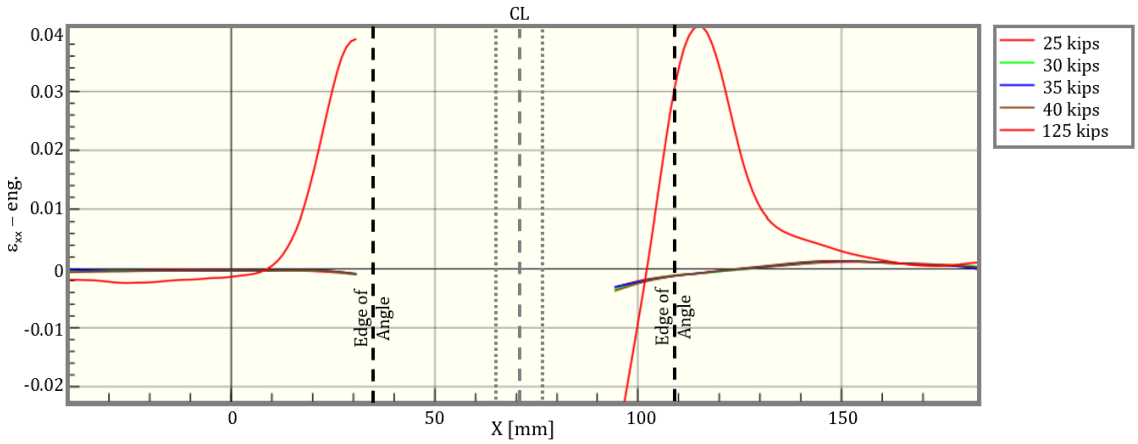

Figure 54: Connection C (Test 2) DIC Flange Section Cut Transverse Strain (ε_{xx}) Profile

The theoretical centerline (CL) of the flange (with the edges of the flange web shown on each side) and the edge of the right-hand and left-hand angles (as seen from plan view with the midspan of the girder into the plane) are noted for reference in Figure 54. While large portions of strain data are not visible due to the strain gauges, two plastic hinges are apparent near the longitudinal edges of the angles; another plastic hinge is found near the web edge, likely in the fillet zone. Precisely, two tensile strains of 0.04 and 0.038, at a connection shear of 125 kips, are located approximately 0.47 in. (12 mm) and 0.18 in. (4.6 mm) to the right and left of their respective angle's edge. A maximum compressive strain of 0.02 is located approximately 0.79 in. (20 mm) left of the right-hand web edge.

In Figure 55, the strain field formation of Connection C's vertical angle leg, in microstrain units, is shown in (a) Von Mises strain (ε_v) and (b) shear strain (ε_{xy}) for a connection shear of 25, 30, 35, 40, and maximum of 125 kips.

a.

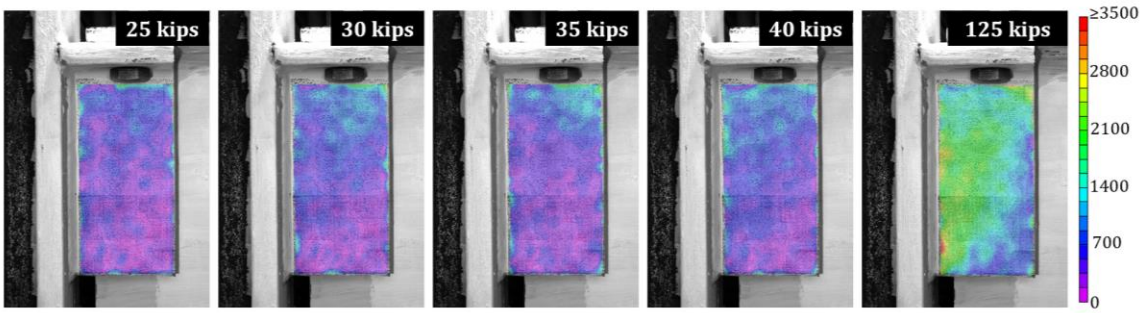

b.

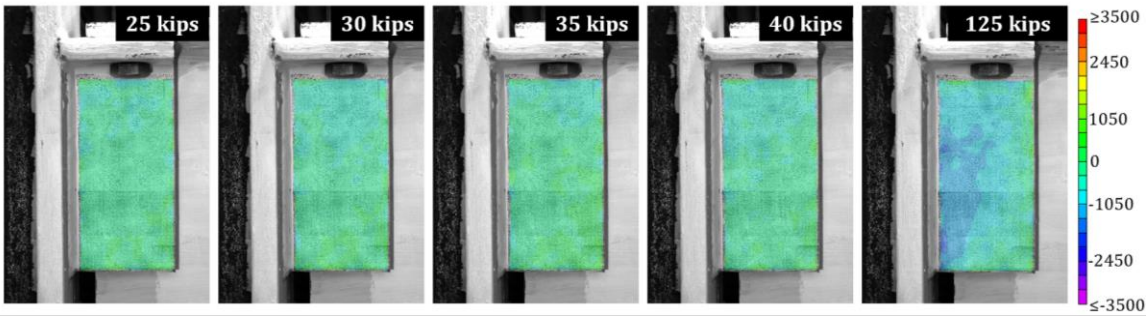

Figure 55: Connection C (Test 2) DIC Angle Deformation Progression (a) Von Mises Strain (ε_v) and (b) Shear Strain (ε_{xy}) – Engineering

As the angle is stocky compared to its bearing length, the lower left-hand area (fixed to the column) of the angle does not show signs of surface yielding until a connection shear of 125 kips is reached. This area extends diagonally across the angle to the upper right-hand corner (free end), resulting in small amounts of plastic deformation. Like that of Connection B, a large nominal shear strength of approximately 195 kips would be predicted for a singular L8x4x3/4 angle and 390 kips for both connection angles, according to equation 4.2. As displayed in Figure 55 (b) and ignoring stress concentrations near the weld, a majority of the angle remains approximately equal to the yield prediction. However, complete angle failure of this connection was no observed.

4.3.2 Connection D

Identical to the analysis of Connection C, Connection D's behavior was investigated via 2D-DIC of both the girder's top flange and the vertical angle leg. For the girder, an approximate area of 126 square inches (14 inches longitudinally by the width of the girder top flange) was prepared closest to the column face; a rough area of 34 square inches (entire visible vertical angle) was prepared for the angle.

Figure 56 displays the girder's strain formation, in units of microstrain, with (a) Von Mises strain (ε_v) and (b) transverse strains (ε_{xx}) for a connection shear of 25, 30, 35, 40, and 125 kips. Progression photos are oriented in such a way that the midspan of the girder is in the upper direction of each photo and the stub column/connection angles are in the lower portion of the photo.

a.

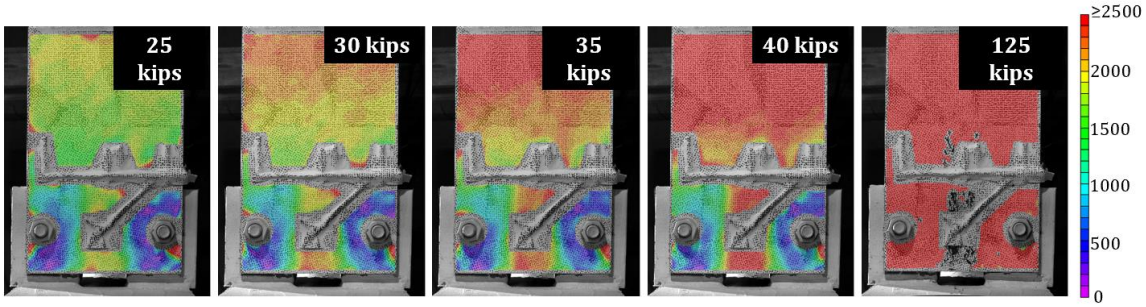

b.

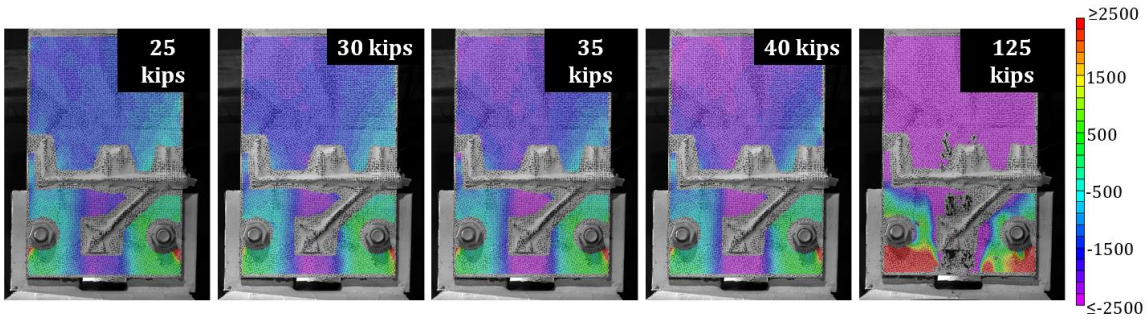

Figure 56: Connection D (Test 2) DIC Flange Deformation Progression (a) Von Mises Strain (ε_v) and (b) Transverse Strain (ε_{xx}) – Engineering

Prominently shown at a shear of 30 kips, is a wide strain field along the longitudinal centerline of the flange showing plastic deformation. According to Figure 56(b), this unsupported region between the angles has yielded in compression. While this initial yield line is akin to previously discussed connections, the exclusion of yield lines along the interior longitudinal edges of the angles proves contrary to those seen in previous connections that utilized stiffer angles. Longitudinal strain (ε_{yy}) formation was not included in this figure due to little beneficial data in terms of connection behavior due to the location of the strain gauges.

Similar to connections A and C, conclusive strain magnitudes beyond the edges of the angles cannot be determined due to out-of-plane movement of the area beyond the bearing length. The monocular vision of the 2D-DIC system cannot capture this movement so a clear

compression bias was formed and is evident throughout progression images. While this area towards midspan is not suitable for conclusive evidence pertaining to strain magnitude, the flaking of the speckle pattern, shown at the maximum shear, can provide insight into the length and progression of the yield lines. Due to yielding at the steel's surface, the paint flakes off, revealing areas of deformation. With this deduction, it can be assumed that the yield lines extend approximately three to four inches beyond the bearing length of five inches.

In further investigation of the discussed primary failure mode, a transverse cross-sectional cut of Connection D's girder top flange is presented in Figure 57. The cut was made approximately halfway between the transverse edge of the angles and the bolt centerline at various shear forces. The theoretical centerline (CL) of the flange (with the edges of the flange web noted on each side) and the edge of the right-hand and left-hand angles (as seen from plan view with the midspan of the girder into the plane) are shown. Unlike that seen previously in stiffer deeper connections, very little tensile strain is observed. The maximum compressive strain provided is 0.01 and is located 19 mm (0.75 in.) left of the web edge. If flaking had not occurred

at the centerline late in testing, perhaps a compressive strain of greater magnitude would have been revealed closer to the web, similar to that seen in previous connections.

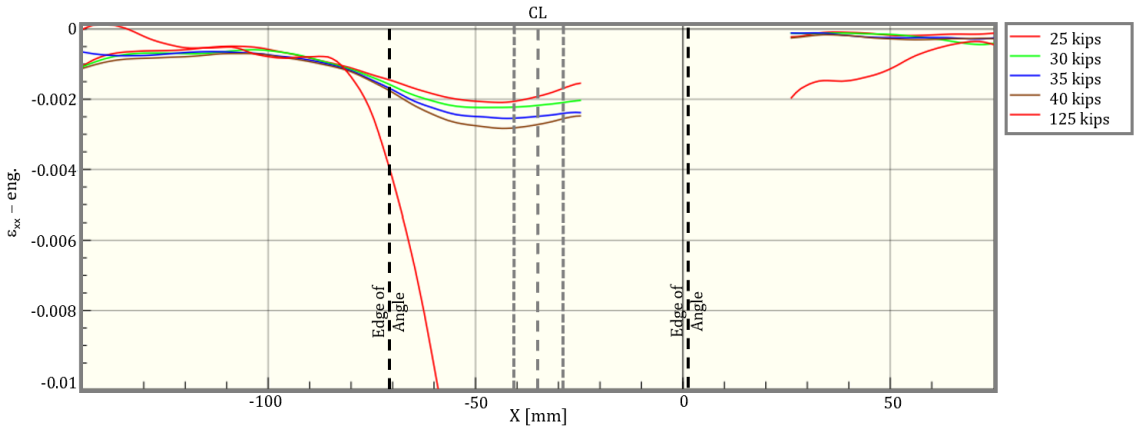

Figure 57: Connection D (Test 2) DIC Flange Section Cut Transverse Strain (ε_{xx}) Profile

The strain field formation of Connection D's vertical angle leg is shown, in microstrain units, in Figure 58 (a) Von Mises strain (ε_v) and (b) shear strain (ε_{xy}) for a connection shear of 25, 30, 35, 40, and maximum of 125 kips. The upper right-hand area (attached to the column) of the angle begins to yield and extends along and down the angle to the lower right-hand corner (fixed end). As would be expected, the highest shear strain occurred closest to the column face and actual connection interface. At the highest shear, a majority of the angle has yielded according to the Von Mises strain. It is noted that this angle's weld did not fail but experienced buckling at the time of its counterpart's weld failure.

a.

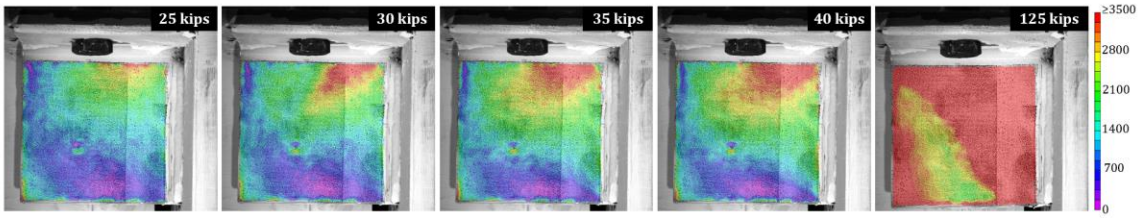

b.

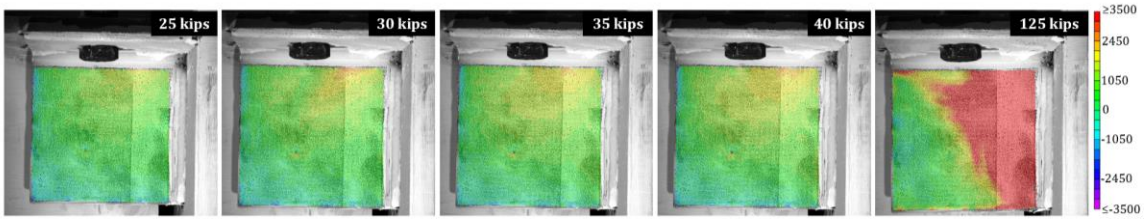

Figure 58: Connection D (Test 2) DIC Angle Deformation Progression (a) Von Mises Strain (ε_v) and (b) Shear Strain (ε_{xy}) – Engineering

A nominal shear strength of approximately 65 kips would be predicted for a singular L6x4x5/16 angle and a total nominal shear strength of 130 kips for both connection angles, according to equation 4.2. According to Figure 50 (a) and (b), the upper portion of the angle has exceeded the predicted yield shear strain. From the surface strains shown and the knowledge that angle buckling occurred at the end of testing (though it is unknown if buckling of the angle occurred before or after weld failure), the current AISC shear strength can be considered reasonable in determination of the nominal strength for this angle.

4.4 Test 3

Test 3 served as the benchmark test to compare a typical industry shear tab and a proposed drop-in connection of similar capacity (based on preliminary design). It consisted of connections E and F, utilizing a connecting W24x68 girder. Connection E was composed of L8x4x1/2 angles (same geometry but ¼ inch thinner than connections A, B, and C) and a bearing length of 5.0 inches. Connection F was a conventional shear tab with a plate size of 3/8x5x12.5

and four 1.0 in. bolts. All four available cameras were used to capture Connection E's vertical leg angle and girder top flange, as well as the Connection F shear tab. Connections E and F are presented in Figure 59 before testing.

a. **b.**

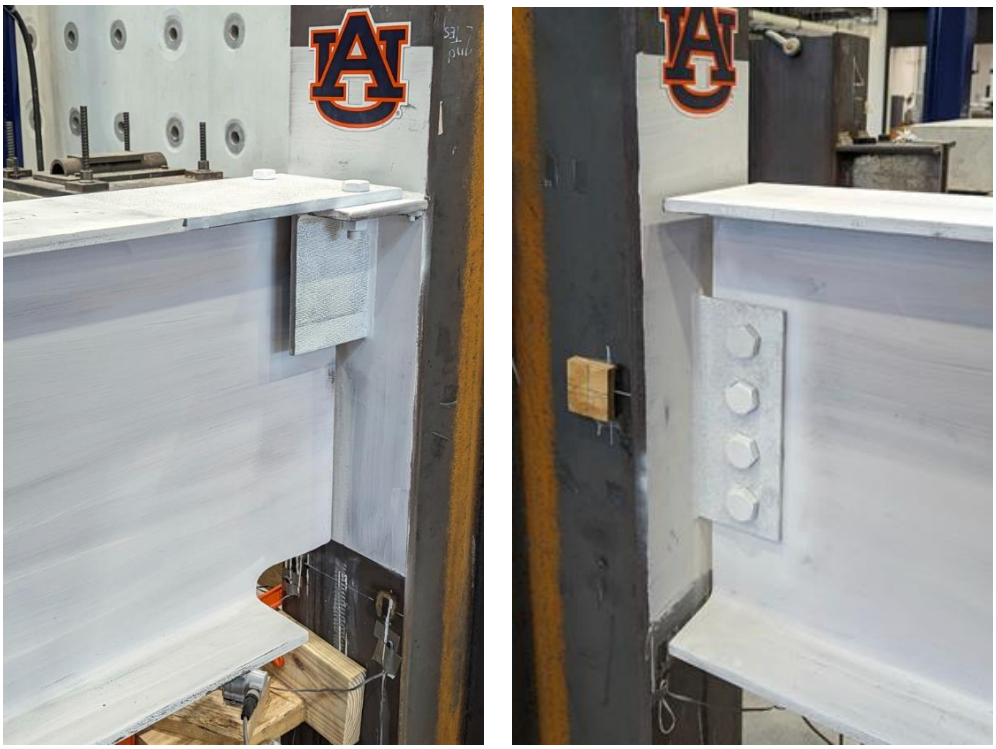

Figure 59: Test 3 Before Testing (a) Connection E and (b) Connection F

To reduce the likelihood of LTB of the girder occurring during testing, the lateral supports were shimmed to a maximum of ¼ in. away from the flange, compared to the previously established ½ in. Test 3 achieved a maximum force of approximately 299 kips on the test girder, equating to a maximum shear of 149.5 kips at each connection, almost double the designed shear capacity of 78 kips. The test was concluded due to instability of the spreader beam, like that seen in Test 1. Connection E achieved a relative rotation of 0.027 radians and the shear tab, Connection F, rotated a comparable 0.030 radians. The connections after testing are shown in Figure 60. The girder web or flange at each connection is seen almost touching the

column face, further showing the rotation experienced during this test. Though not discussed in this thesis, further testing of these connections was performed and resulted in greater rotations at failure.

a. **b.**

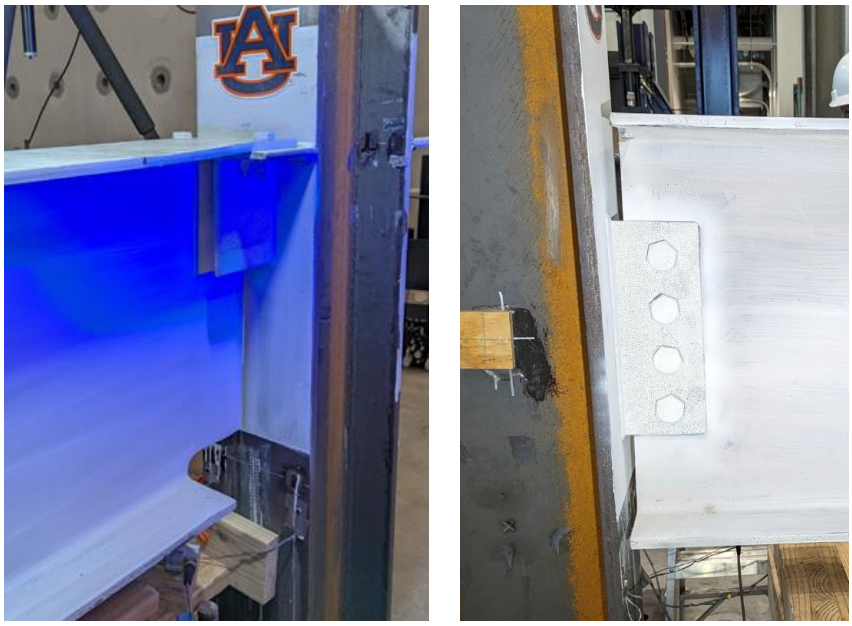

Figure 60: Test 3 After Testing (a) Connection E and (b) Connection F

4.4.1 Connection E

To capture Connection E's behavior, an approximate area of 126 square inches (14 inches longitudinally by width of the girder top flange) of the girder top flange was prepared closest to the column face. As well, a rough area of 46 square inches (entire visible vertical angle face) was prepared for the angle.

Figure 61 shows the progression of the girder's strain field, in microstrain units, with (a) Von Mises strains (ε_v), (b) transverse strains (ε_{xx}), and (c) longitudinal strains (ε_{yy}) for a connection shear of 40, 60, 80, 100, and 145 kips. The photos below are oriented in such a way that the midspan of the girder is in the upper direction and the stub column/connection angles are in the lower portion of the photo. It is noted that due to a glare created by excessive lighting,

Connection E's top flange DIC results display a small area of incomplete data. This area is seen in the upper left-hand portion of the flange in all progression images and should be noted when viewing the following figures.

a.

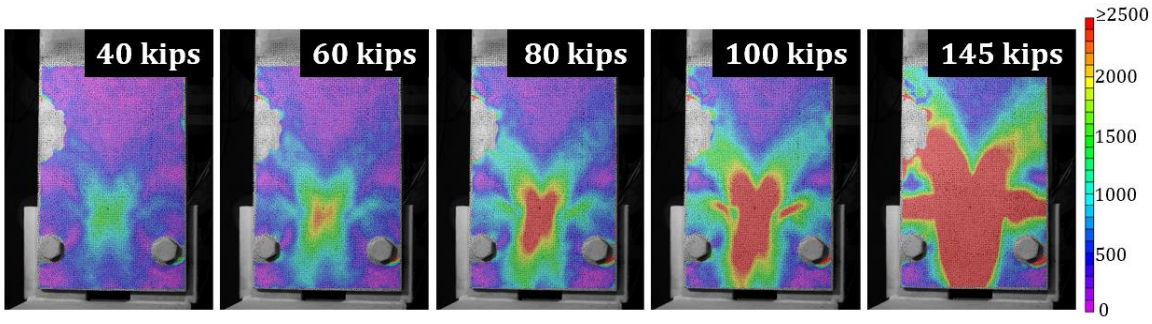

b.

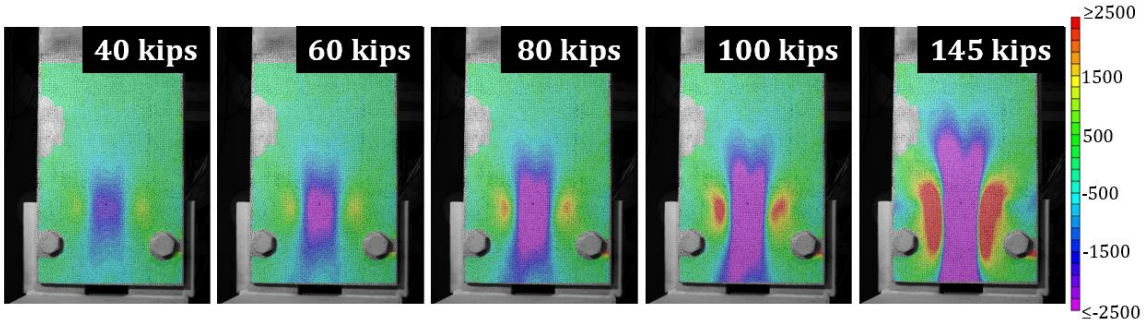

c.

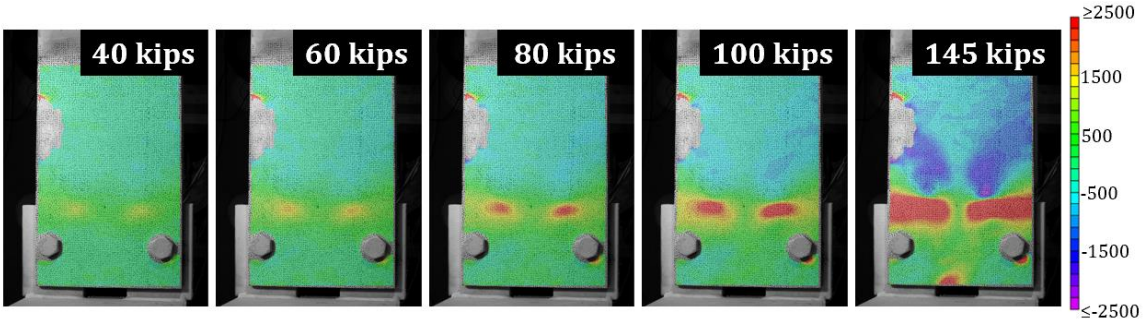

Figure 61: Connection E (Test 3) 2D DIC Flange Deformation Progression (a) Von Mises Strain (ε_v), (b) Transverse Strain (ε_{xx}) – Engineering, and (c) Longitudinal Strain (ε_{yy}) – Engineering

Referring to parts (a) and (b), initial yield lines are observed forming at the intersection between the longitudinal centerline of the flange and the transverse edge of the angles, spreading towards the column face and midspan of the beam. The starting location of transverse yielding is contrary to previous connection flanges in which the transverse yield lines began closest to the column face, nevertheless, the yield line eventually progresses towards the face of the column and midspan in a manner most like Connection B. As well, this distance beyond the bearing length is approximately four to five inches, comparable to that confirmed by DIC for Connection B which utilized an identical bearing length of five inches. Most clearly seen in Figure 61(b), secondary yield lines begin to form on the interior corners of the connection angles at a shear of 80 kips, continuing along the longitudinal interior edge of the angle towards the column and past the angle's transverse edge towards midspan. Once again, the starting point of these secondary yield lines is akin to those observed in Connection A, but variant to connections B and C. However, the final formation along the interior longitudinal edge of the angles is rather identical for all those (besides Connection D that did not experience tensile yielding) previously discussed. The region between the initial yield lines is in compression and the secondary yield lines encase an area in tension.

While visible in all progressive shear forces, the longitudinal strains are seen approaching the yield limit at 80 kips along the transverse edge of the angles. Referencing Figure 61(c), this area is in tension; these yield lines continue along the transverse angle edge creating a plastic hinge in which the flange rotates about. Again, a rotation of 0.027 radians was achieved during this test, likely of which occurred due to the yielding and subsequent loss of stiffness at the end of the bearing length. A secondary set of yield lines past the bearing length and away from the connection are also seen forming at a shear of 145 kips and encase an area of compression. In

total, four transverse and two longitudinal plastic hinges appeared to have formed during this test.

To adequately capture Connection E's behavior, Table 8, noted in units of microstrain, reveals the flange's strains and deformations in a 3D space in which the displacement in the z-direction is exaggerated by 25% comparative to the X and Y axes. The Z-axis is relative to the initial position of the flange immediately before testing (z equal to 0) and becomes negative as the specimen moves further from the camera. The X-axis ranges from -4.75 in. to 4.75 in., in which 0 in. is located at the longitudinal centerline of the flange; a positive X-value reflects part of the flange that is to the right of the centerline and over the right-hand angle (in reference to the plan view seen in Figure 61) and vice-versa. The Y-axis ranges from -7 in. to 7 in., the largest value of 7 in. represents the part of the flange closest to midspan, while the smallest value of -7 in. represents the part of the flange closest to the stub column/connection angles. A reference image is shown in Figure 62 to orient the viewer properly.

Figure 62: Connection E 3D Reference

Supplementary to the results discussed for the previously shown strain progression; at a maximum shear of 140 kips, the flange is seen greatly deformed in the Z-direction with the greatest deformation located at the end closest to midspan. This maximum deformation of approximately 0.25 inches is likely exaggerated due to the hinging of the flange about the transverse angle edges. As well, the small deformation in the area between the longitudinal angle edges is seen due to the multiple hinges formed about the interior longitudinal edge of each angle.

Table 8: Connection E (Test 3) 3D DIC Flange Deformation Progression

	Von Mises Strain (ε_v)	Transverse Strain (ε_{xx}) - Engineering	Longitudinal Strain (ε_{yy}) - Engineering
Load (kips)	≥2500 2000 1500 1000 500 0	≥2500 1500 500 -500 -1500 ≤-2500	
40	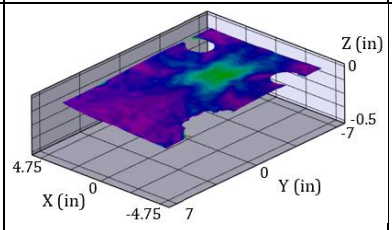	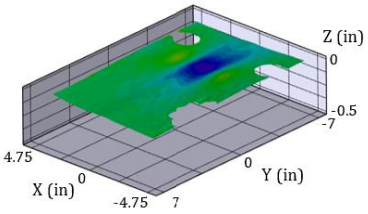	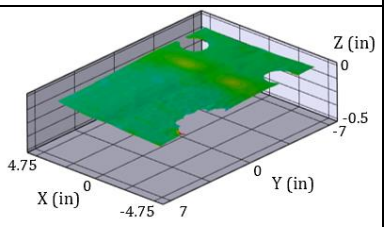
60	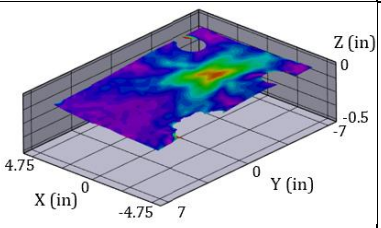	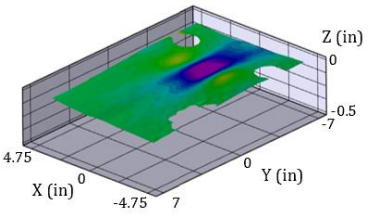	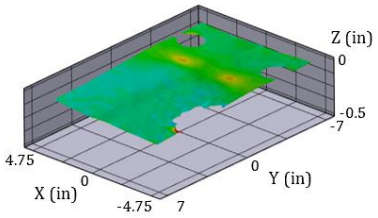
80	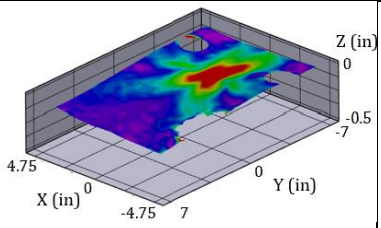	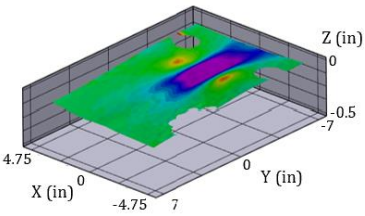	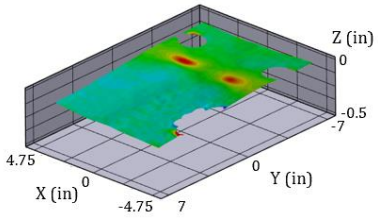
100	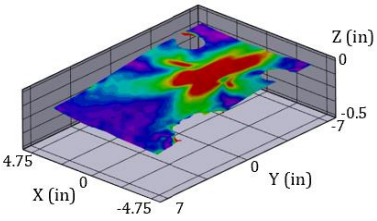	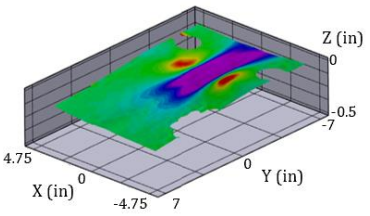	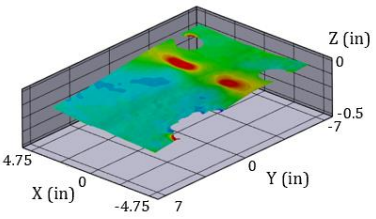
140	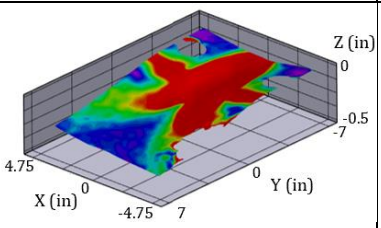	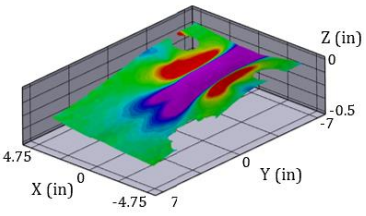	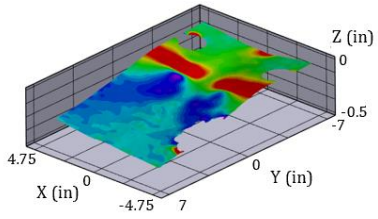

For further analysis of the initial failure mode of transverse bending, a transverse cross-sectional cut of Connection E's girder top flange made approximately midway between the transverse edge of the connection angles and the bolt centerline at various shear forces is shown in Figure 63.

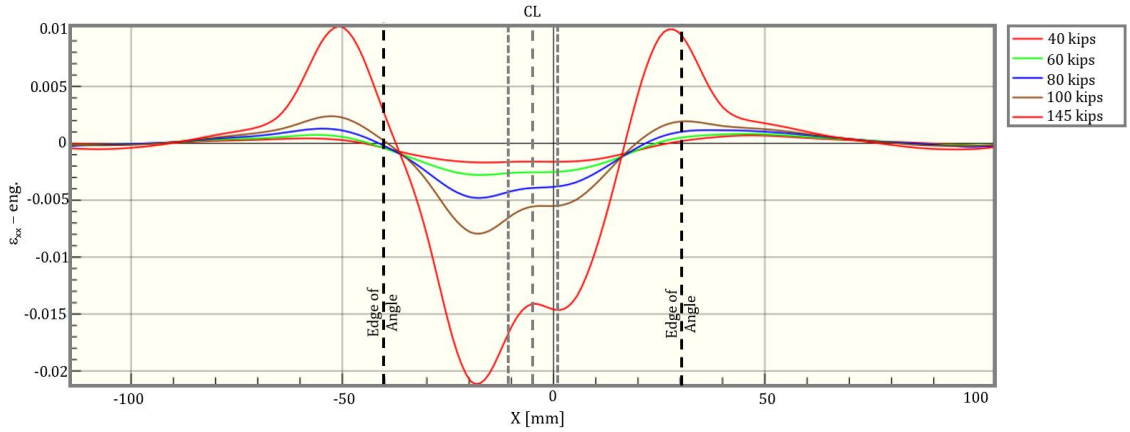

Figure 63: Connection E (Test 3) DIC Flange Section Cut Transverse Strain (ε_{xx}) Profile

The theoretical centerline (CL) of the flange (with the edges of the flange web noted on each side) and the edge of the right-hand and left-hand angles (as seen from plan view with the midspan of the girder into the plane) are noted for reference in Figure 63. Analogous to previously discussed cross-sectional plots, two maximum tensile strains are located near the longitudinal interior edges of each angle and two compressive strains are found close to the beam's web, likely in the fillet zone. Specifically occurring at a connection shear of 145 kips, two tensile strains of 0.01 formed approximately 0.38 in. (9.7 mm) left of the left-hand angle edge and 0.14 in. (3.5 mm) left of the right-hand angle edge. As well, compressive strains of a greater magnitude, 0.02 and 0.015, are located approximately 0.31 in. (8 mm) left of the web

edge and 0.05 in. (1.5 mm) right of the web edge, respectively. The shift to the left for the right-hand side is likely due to instability of the spreader beam.

Figure 64 shows the Connection E vertical angle leg strain formation in (a) Von Mises strain (ε_v) and (b) shear strain (ε_{xy}) for a connection shear of 40, 60, 80, 100, and 145 kips.

a.

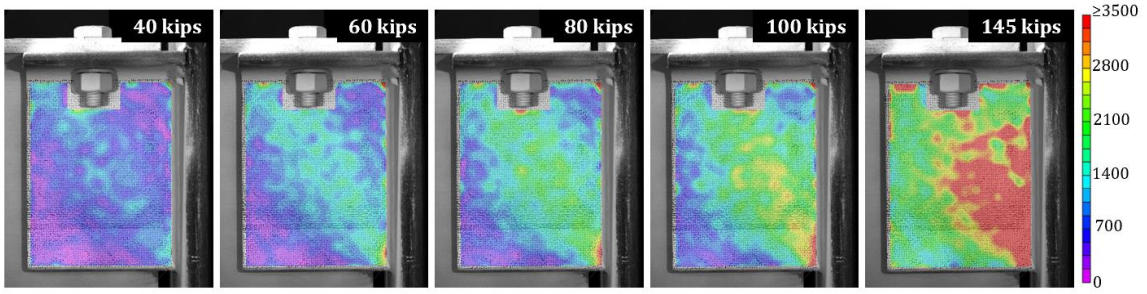

b.

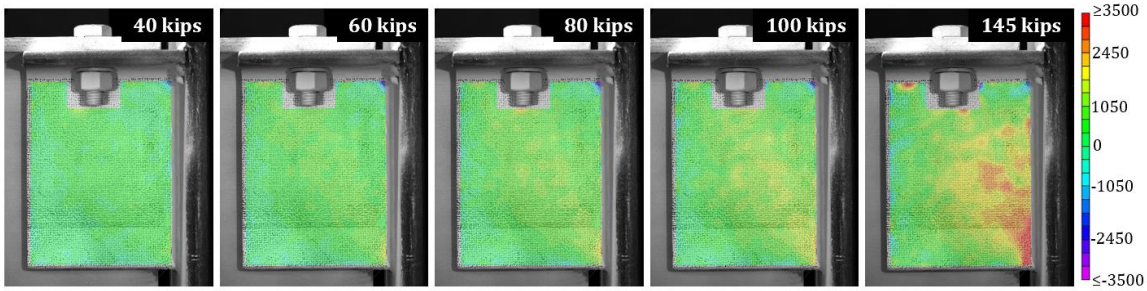

Figure 64: Connection E (Test 3) DIC Angle Deformation Progression (a) Von Mises Strain (ε_v) and (b) Shear Strain (ε_{xy}) – Engineering

Most prominently seen starting at a shear of 80 kips in Figure 64(a), the lower right-hand area (fixed to the column) of the angle begins to yield and extends diagonally across to the upper left-hand corner (free end) of the angle. This pattern is similar to the strain field progression seen in Connection C where yielding begins closest to the fixed end and propagates out at an angle towards the free end. Shown in Figure 64 (a) and (b), a large majority of the angle has reached or exceeded the predicted yield shear strain. Utilizing equation 4.2 with the noted average yield stress for this angle, a nominal shear strength of approximately 135 kips would be predicted for a

singular L8x4x3/4 angle and a nominal strength of 270 kips for both connection angles. This prediction cannot be confirmed or denied for this angle as testing did not display an angle failure mode.

4.4.2 Connection F

The entire visible steel plate face (approximately 58 square inches) of Connection F was prepared for 2D-DIC analysis. Figure 65 displays the Connection F shear tab strain development in (a) Von Mises strain (ε_v) and (b) shear strain (ε_{xy}) for a connection shear of 40, 60, 80, 100, and a maximum of 145 kips.

a.

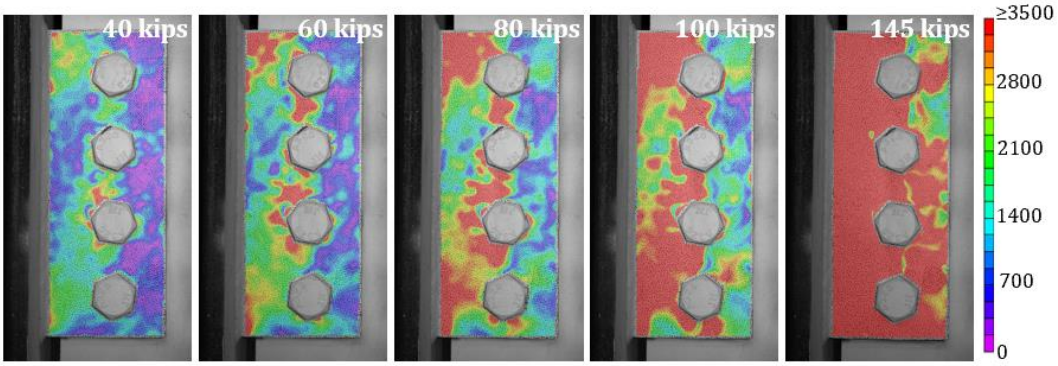

b.

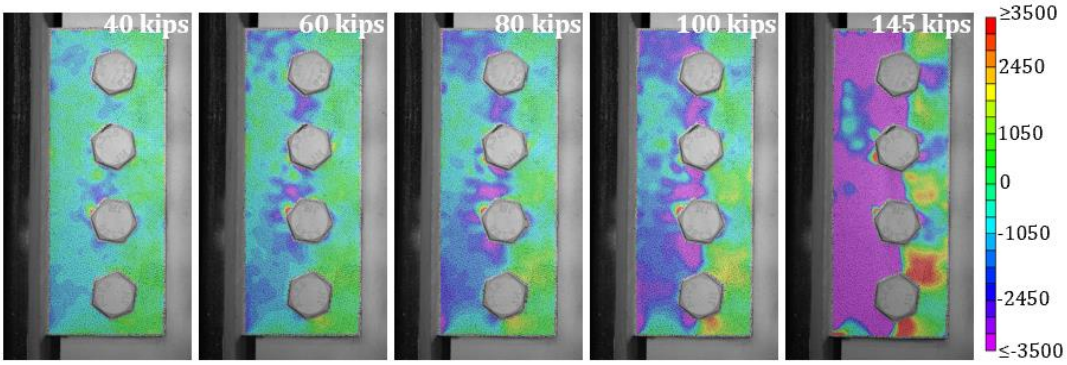

Figure 65: Connection F (Test 3) DIC Shear Tab Deformation Progression (a) Von Mises Strain (ε_v) and (b) Shear Strain (ε_{xy}) – Engineering

It is observed that the area between the bolt and weld line (left-hand side) uniformly yielded in shear through the progression of the test. This failure of the plate was not surprising as it has been observed in testing of shear plates for many years (Astaneh et al., 1989). It can be assumed that the yielding shown greatly contributed to the achieved rotation of 0.03 radians during this test.

4.5 Test 4

Test 4 was comprised of two girder-to-column connections, Connections G and H, utilizing a smaller W16x36 girder. Connection G was composed of L6x4x5/16 angles with a bearing length of three inches, like that of Connection D but with a shorter bearing length. Connection H consisted of L4x3x1/2 angles that were oriented with the vertical leg closest to the exterior of the column (flipped or mirrored compared to all other connections described in this thesis) and featured a bearing length of three inches. These connections, unlike the previously discussed, were designed for a lower factored shear of 52 kips. Pertaining to DIC, Connection G and H angles were captured in 2D with one camera allocated to each, and Connection H girder top flange was captured in 3D, as significant out-of-plane deformation was expected, utilizing the two remaining cameras.

a. **b.**

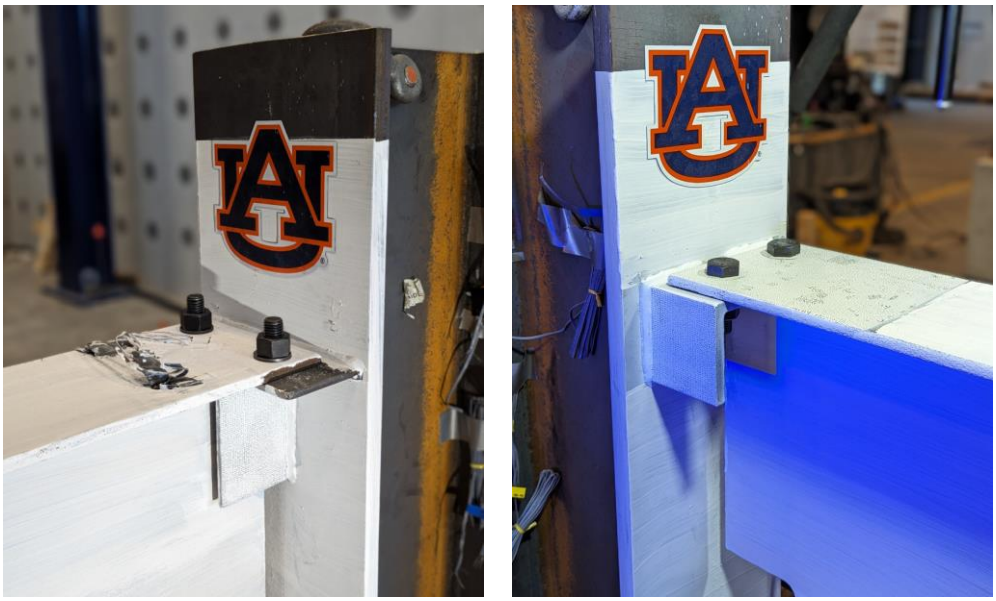

Figure 66: Test 4 Before Testing (a) Connection G and (b) Connection H

Test 4 attained a maximum load of 113.5 kips on the girder, with a connection shear of 56.75 kips. Testing concluded after design shear was reached due to significant deformation of the flange and horizontal angle legs of Connection H, as shown in Figure 67. Relative rotations of 0.018 and 0.01 radians were achieved for Connection G and Connection H, respectively. Though not discussed in this thesis, Connection G was later retested to failure with a retrofitted opposing end.

a. **b.**

Figure 67: Test 4 After Testing (a) Connection G and (b) Connection H

4.5.1 Connection G

An approximate area of 22 square inches (entire visible vertical angle face) was prepared to evaluate the Connection G angle. Figure 68 visualizes the Connection G vertical angle leg strain formation in (a) Von Mises strain (ε_v) and (b) shear strain (ε_{xy}) for a connection shear of 25, 30, 35, 40, and 55 kips. Akin to connections C and E, strain fields begin to appear at the lower right-hand area (attached to the column) and upper left-hand area (free end) of the angle. This test sequence shows areas of plastic deformation at the surface, but further strength was achievable. Again, a successive test, not discussed in this thesis, was performed on this connection to evaluate behavior at failure.

a.

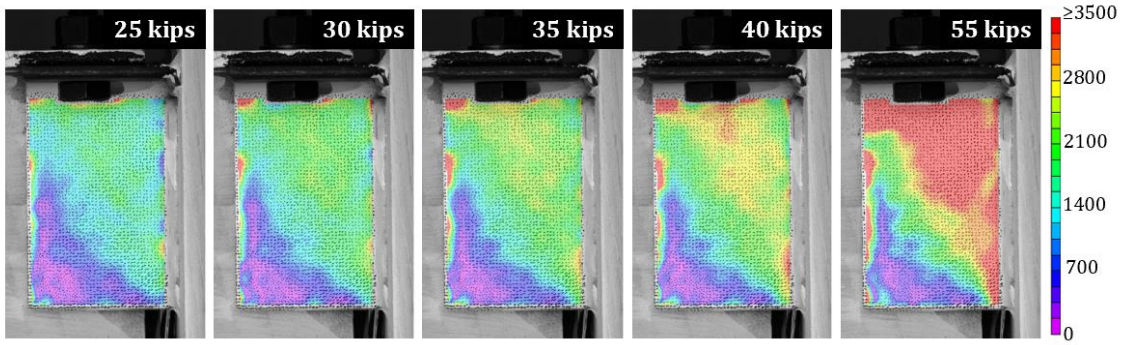

b.

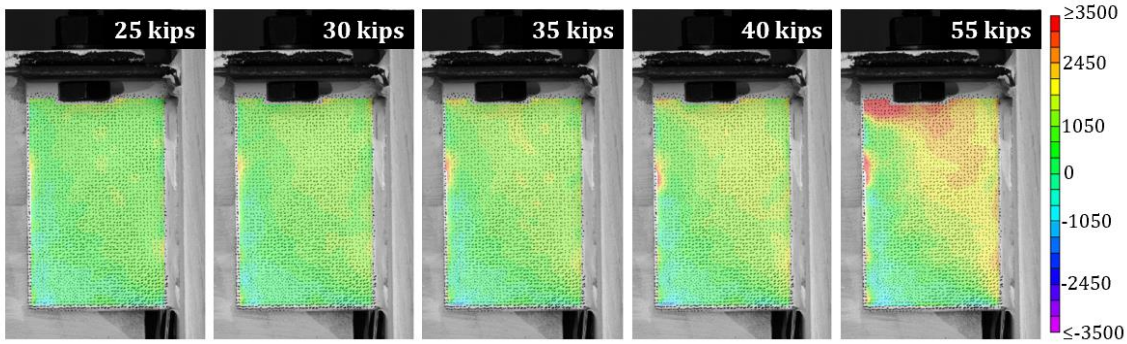

Figure 68: Connection G (Test 4) DIC Angle Deformation Progression (a) Von Mises Strain (ε_v) and (b) Shear Strain (ε_{xy}) – Engineering

Like that seen in connections C and E, the strain field is most prominently seen in the top right-hand portion nearest to the column face (fixed-end). According to Figure 68 (b), this portion has exceeded the predicted yield shear strain. Utilizing equation 4.2 with the noted average yield stress for this angle section, a nominal shear strength of approximately 65 kips would be predicted for a singular angle and a nominal strength of 130 kips for both connection angles. This angle did not fail during testing and therefore the ultimate capacity of the angle alone cannot be determined.

4.5.2 Connection H

For Connection H, an approximate area of 63 square inches (9 inches longitudinally by the width of the girder top flange) was prepared closest to the column face for the girder top flange and a rough area of 15 square inches (entire visible vertical angle face) was prepared for the angle. Figure 69 shows the girder's strain formation, in microstrain units, with (a) Von Mises strain (ε_v), (b) transverse strains (ε_{xx}), and (c) longitudinal strains (ε_{yy}) for a connection shear of 25, 30, 35, 40, and 55 kips.

a.

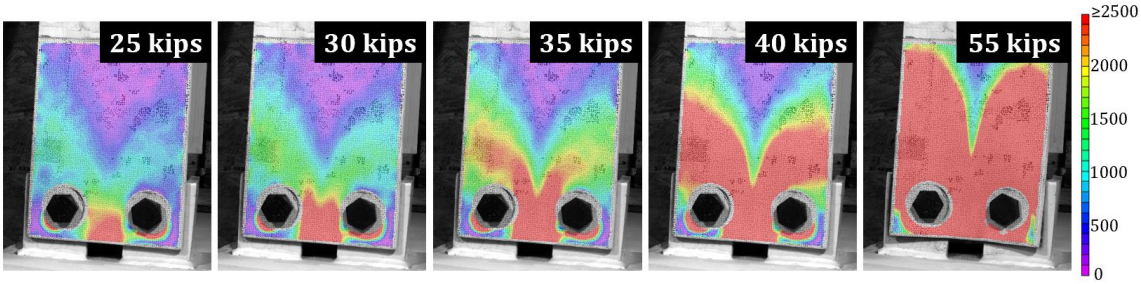

b.

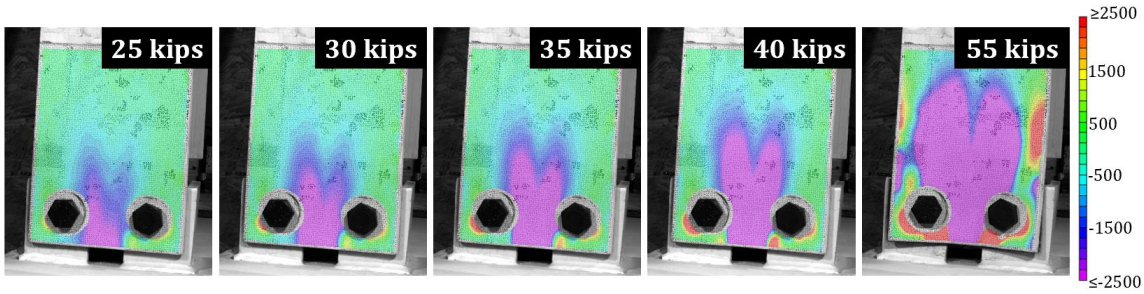

c.

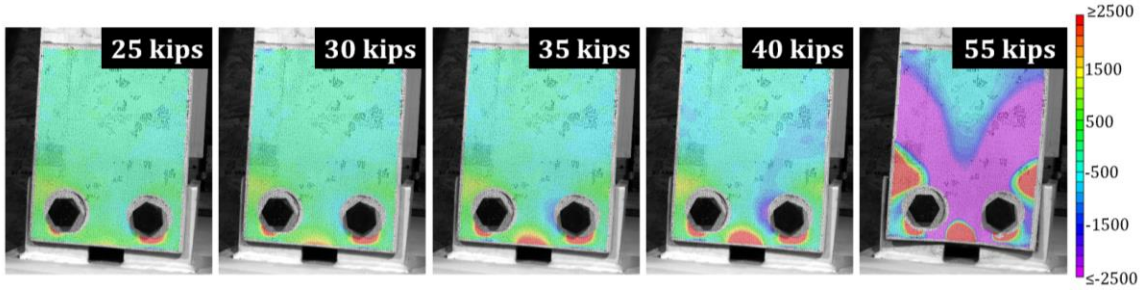

Figure 69: Connection H (Test 4) 2D-DIC Flange Deformation Progression (a) Von Mises Strain (ε_v), (b) Transverse Strain (ε_{xx}) – Engineering, and (c) Longitudinal Strain (ε_{yy}) – Engineering

In Figure 69 (a) and (b) at a low shear of 25 kips, the area closest to the column face and unsupported by the angles begins to show a significant compressive strain field indicating plastic deformation, similar to the starting location of yielding shown in connections B and C. Akin to the previous connections, these yield lines progress towards midspan as shear increases,

however, in a dissimilar pattern, due to the horizontal angle leg deformation, the yield lines begin to spread out into two distinct separate paths, eventually encasing a larger area in compression.

At a shear of 55 kips, the longitudinal yield line pattern has suddenly formed. The yield lines closest to the exterior edges of the connection angles (nearest the stiffer vertical angle leg) encase an area of tension in which a plastic hinge has formed, allowing for the flange to partially rotate about the transverse edge of the angles. Instead of rotating about a stiff transverse angle edge, the flexible horizontal angle leg deformed along with the flange and vice versa, causing less of a rotation (0.01 radians) and more of a "sinking" vertical translation compared to connections featured with angles that were regularly oriented.

To aid in the visualization of Connection H's behavior and vertical movement, Table 9, reported in units of microstrain, reveals the flange's strains and deformations in a 3D space. The Z-axis is relative to the initial position of the flange immediately before testing and becomes negative as the specimen moves further from the camera. The displacement in the Z-direction is exaggerated by 25% compared to the X and Y axes, to better identify the deformations. The X-axis ranges from -3.75 in. to 3.75 in., in which 0 in. is located at the longitudinal centerline of the flange; a positive X-value reflects part of the flange that is to the right of the centerline and over the right-hand angle (in reference to the plan view seen in Figure 69) and vice-versa. The Y-axis ranges from -4.5 in. to 4.5 in., the largest value of 4.5 in. represents the part of the flange closest to midspan, while the smallest value of -4.5 in. represents the part of the flange closest to the stub column/connection angles. A reference image is shown in Figure 70 to orient the viewer properly.

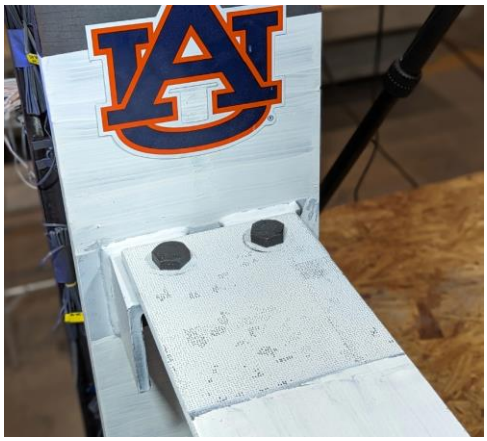

Figure 70: Connection H 3D Reference

In addition to the results discussed for the strain progression of Connection H; at a maximum shear of 55 kips, the flange is seen greatly deformed in the negative Z-direction with an approximate deformation of 0.7 inches located in the region closest to midspan. This maximum deformation is due to the sandwiching of the flange about its longitudinal centerline and vertical movement following the bending of the horizontal legs. As well, the area closest to the stub column has a 0.2 in. deformation in the positive Z-direction as the flange edges hinged upwards towards the stiff vertical angle legs.

Table 9: Connection H (Test 4) 3D DIC Flange Deformation Progression

	Von Mises Strain (ε_v)	Transverse Strain (ε_{xx}) - Engineering	Longitudinal Strain (ε_{yy}) - Engineering
Load (kips)	≥2500 2000 1500 1000 500 0	≥2500 1500 500 -500 -1500 ≤-2500	
25	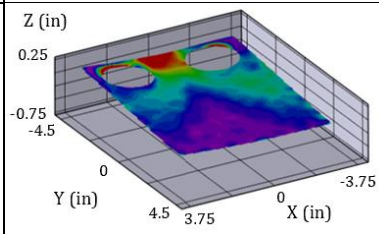	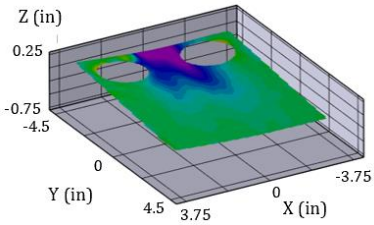	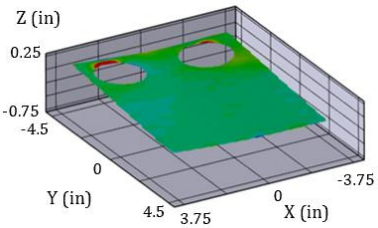
30	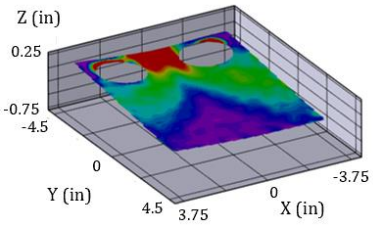	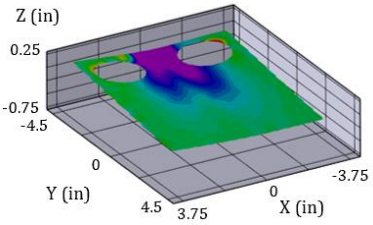	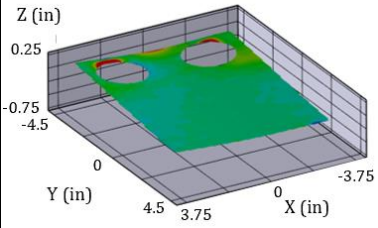
35	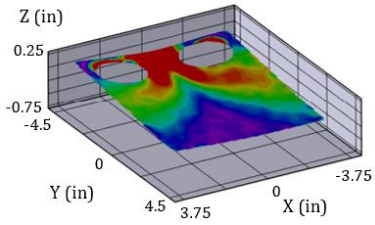	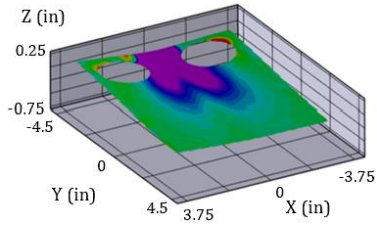	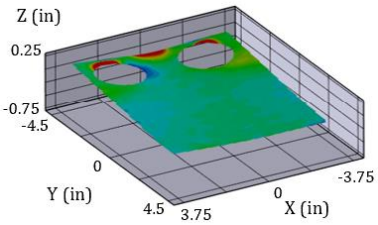
40	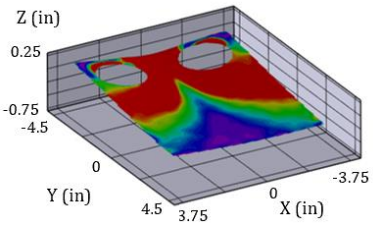	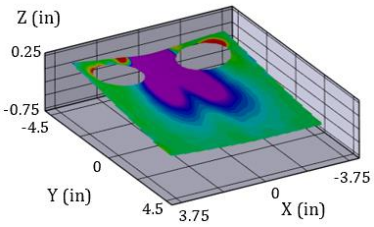	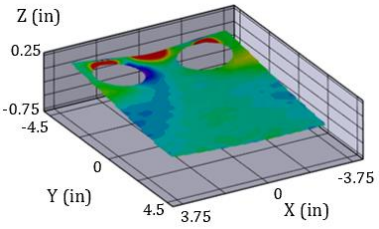
55	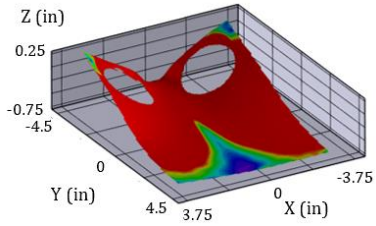	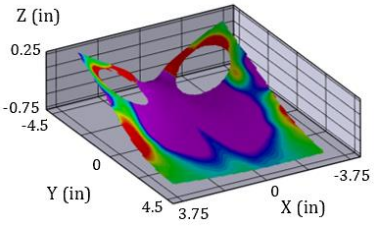	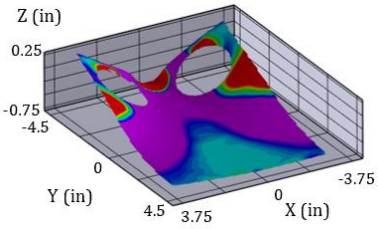

In further investigation of the failure mode of transverse yielding, a transverse cross-sectional cut of Connection H's girder top flange was made approximately at the transverse edge of the angle and is shown in Figure 71.

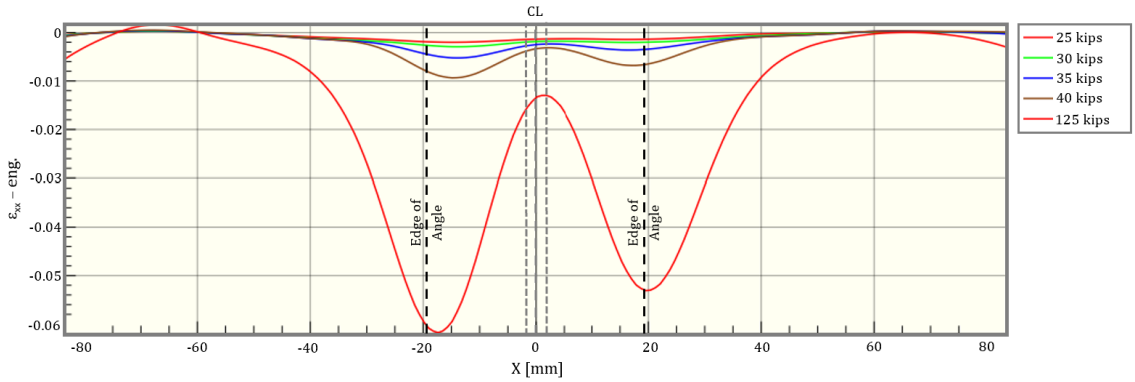

Figure 71: Connection H (Test 4) DIC Flange Section Cut Transverse Strain (ε_{xx}) Profile

It is noted that the transverse cut was not made midway between the transverse edge of the angle and the bolt line, like that in previous plots, due to large areas of unprocessed data located around the bolts, as seen in Figure 69. The theoretical centerline of the flange (with the edges of the flange web noted on each side) and interior edge of the right-hand and left-hand angles (as seen from plan view with the midspan of the girder into the plane) are noted on the figure for reference. As shown in the strain progression profile, no transverse tensile strains are noted along the flange cross-section; this is a noticeable contrast against other angles that are oriented differently. Specifically, large compressive strains of 0.06 and 0.05 are located approximately 1.5 mm (0.06 in.) right of the left-hand angle's edge and 0.6 mm (0.02 in.) right of the right-hand angle's edge.

In Figure 72, the Connection H vertical angle leg strain formation in (a) Von Mises strain (ε_v) and (b) shear strain (ε_{xy}) for a connection shear of 25, 30, 35, 40, and maximum of 55 kips is shown. The upper portion of the angle begins to yield before a shear of 25 kips and throughout

Test 4, it extends towards the lower portion of the angle, eventually resulting in a majority of the angle leg's surface yielding at the maximum shear. This angle's shear strain progression is in stark contrast to all other connections, likely due to their orientation.

a.

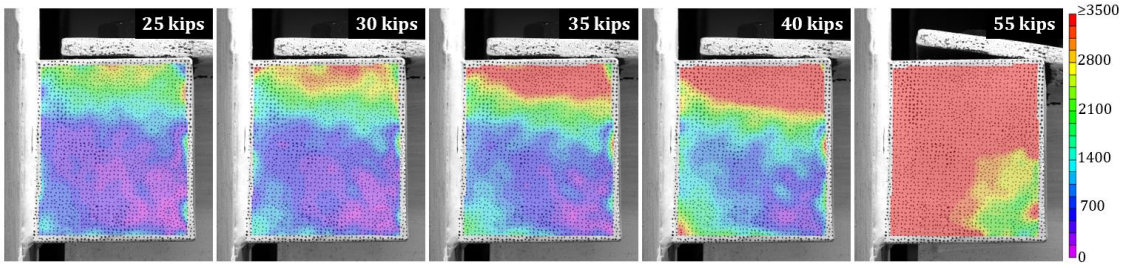

b.

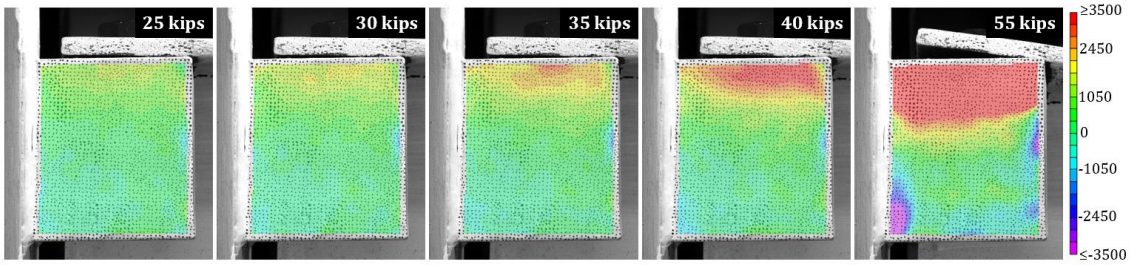

Figure 72: Connection H (Test 4) DIC Angle Deformation Progression (a) Von Mises Strain (ε_v) and (b) Shear Strain (ε_{xy}) – Engineering

Utilizing equation 4.2 and the noted average yield stress for this angle section, a nominal shear strength of approximately 66 kips would be predicted for a singular L4x3x1/2 angle and 132 kips for both connection angles. As the vertical angle leg did not fail during this test, this strength prediction cannot be verified.

4.6 Test 5

Test 5 involved two girder-to-column connections, I and J, connected with a W24x68 girder. The former mentioned connection was L6x4x5/16 angles with a bearing length of 5.0 inches, the same as Connection D but with an improved weld pattern. The latter was made of

L4x3x1/2 angles with a bearing length of three inches. Both connections were made relatively small and under-designed to induce an angle failure mode prior to a flange bending failure. Also, this test did not include lateral supports, as shown in Figure 73, to allow for the assessment of the torsional rigidity of the connection. Using all available DIC cameras, images of both Connection I and J's vertical angle legs were captured for DIC analysis in 3D. Connections I and J are pictured in Figure 74 before testing. Connection J is encased in blue light due to DIC lighting.

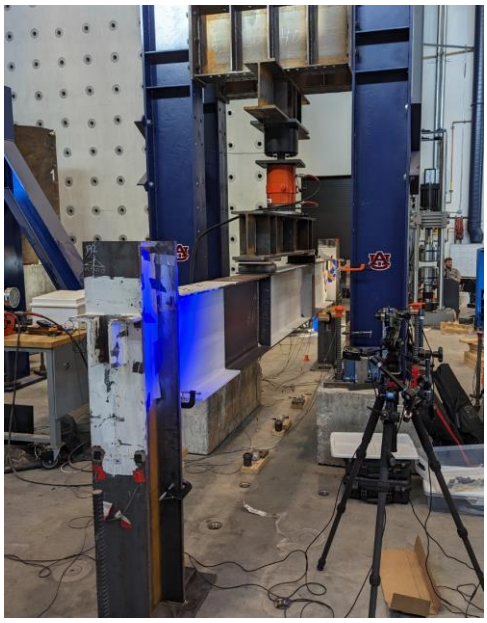

Figure 73: Test 5 Setup Without Lateral Supports

a. **b.**

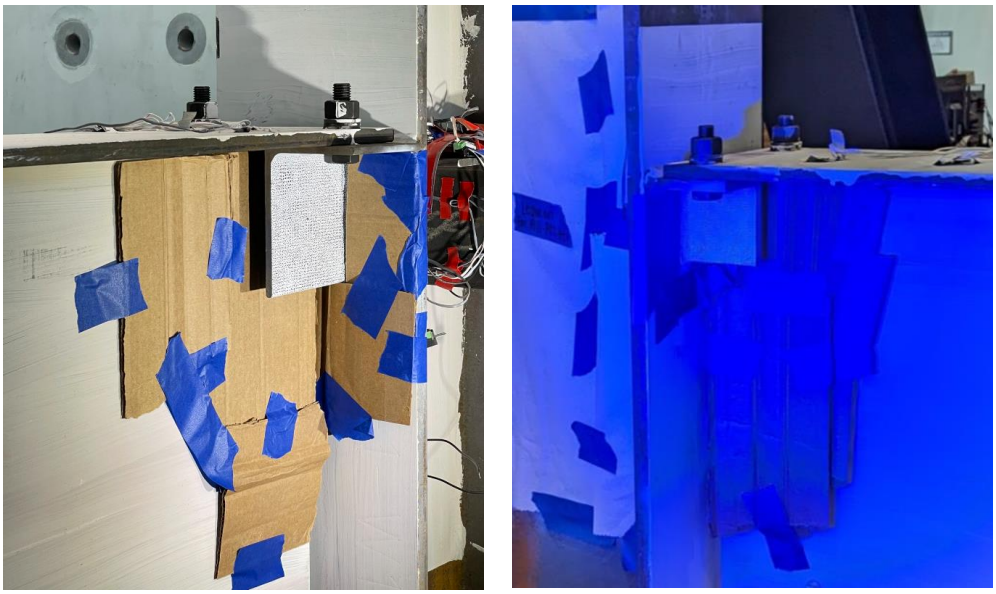

Figure 74: Test 5 Before Testing (a) Connection I and (b) Connection J

Test 5 achieved a maximum load of approximately 230 kips on the girder, resulting in an approximate connection shear of 115 kips. Relative rotations of 0.0009 and 0.006 radians were achieved for connections I and J, respectively. The girder was loaded to its theoretical nominal moment capacity (approximately 600 kip-ft) and held at that loading as the connections were assessed (AISC, 2022). The load was then taken off the specimen; no lateral displacement of the girder occurred at this loading as seen in Figure 75.

Figure 75: Test 5 Girder at Theoretical Nominal Moment Capacity

Little to no noticeable deformations of the connections occurred at the conclusion of testing, as seen in Figure 76. The flaking seen on top of the flanges is that of whitewash (mixture of lime and water) that had previously been applied.

a. **b.**

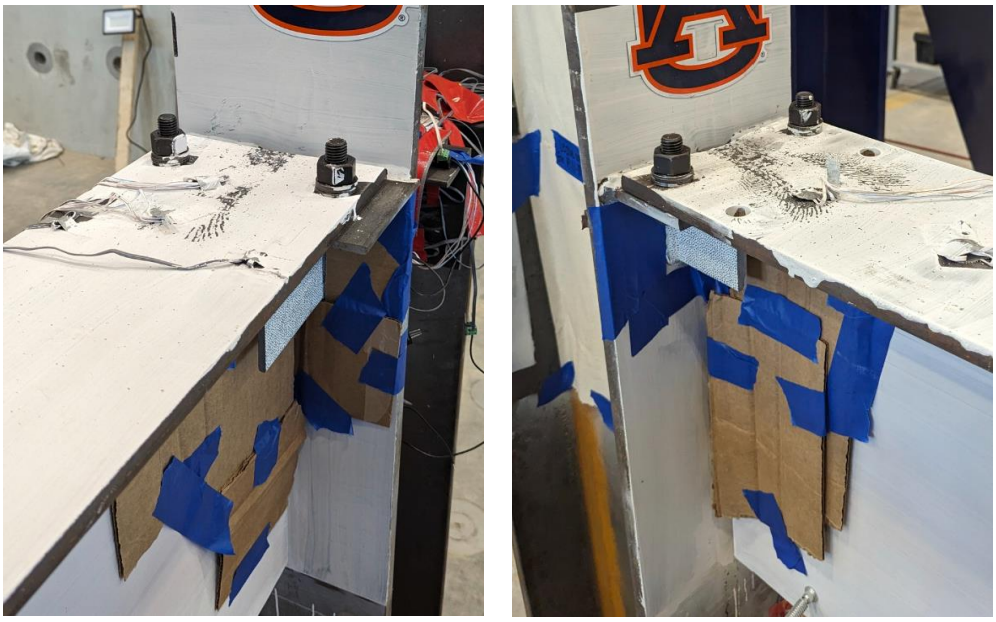

Figure 76: Test 5 After Testing (a) Connection I and (b) Connection J

4.6.1 Connection I

For Connection I, an approximate area of 30 square inches (entire visible vertical angle face) was prepared to evaluate the vertical angle leg. Figure 77 shows the Connection I vertical angle leg strain formation, in microstrain units, in (a) Von Mises strain (ε_v) and (b) shear strain (ε_{xy}) for a connection shear of 40, 60, 80, 100, and 110 kips. Yielding is seen starting before a shear of 40 kips, in which the upper right-hand corner (attached to the column), lower right-hand corner (attached to the column), and upper left-hand (free end) of the angle begin to yield. At a shear of 60 kips, these yield lines connect, resulting in complete yielding of the upper right-hand area at the maximum shear. As connections C and I utilize the same bearing length and angle section, their final strain field patterns are relatively the same.

a.

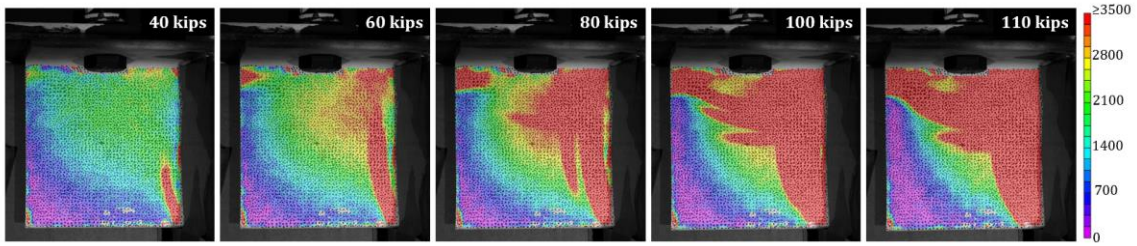

b.

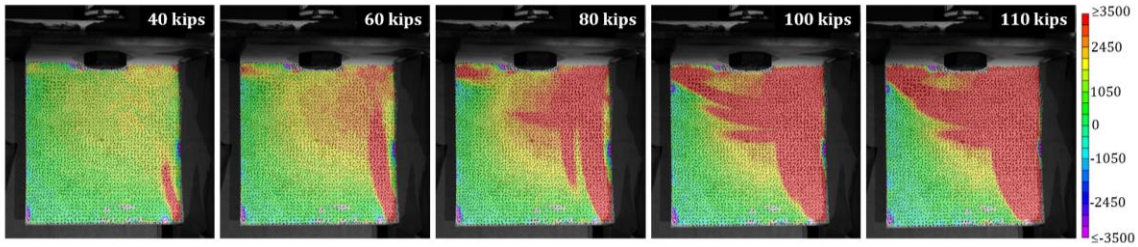

Figure 77: Connection I (Test 5) DIC Angle Deformation Progression (a) Von Mises Strain (ε_v) and (b) Shear Strain (ε_{xy}) – Engineering

Utilizing equation 4.2 and the noted average yield stress for this angle section, a nominal shear strength of approximately 65 kips would be predicted for a singular angle and 130 kips for both connection angles. It is noted that though the angles did not fail in this test sequence, a retrofitted test did produce failure of this angle at a shear greater than that predicted by equation 4.2.

4.6.2 Connection J

An approximate area of 15 square inches (entire visible vertical angle face) was investigated via DIC for Connection J. Shown in Figure 78, the strain field formation of the vertical angle leg, in units of microstrain, is visualized in (a) Von Mises strain (ε_v) and (b) shear strain (ε_{xy}) for a connection shear of 40, 60, 80, 100, and 110 kips. Similar to connections C and I, the upper and lower left-hand area (attached to the column) and upper-right-hand area (free

end) of the angle begin to yield before a shear of 40 kips. Eventually, at maximum shear, the upper left-hand diagonal of the angle is completely yielded.

a.

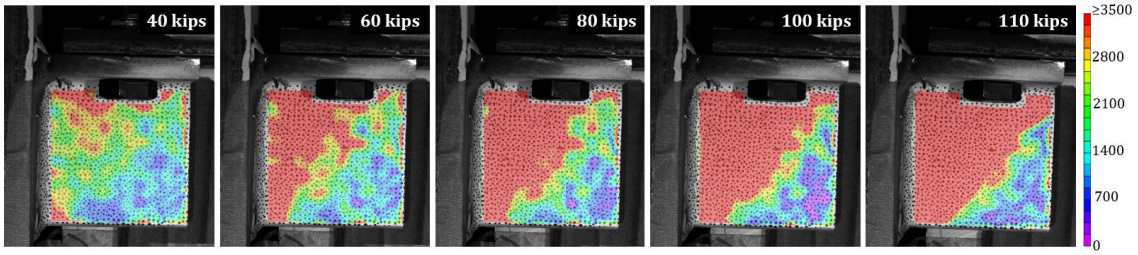

b.

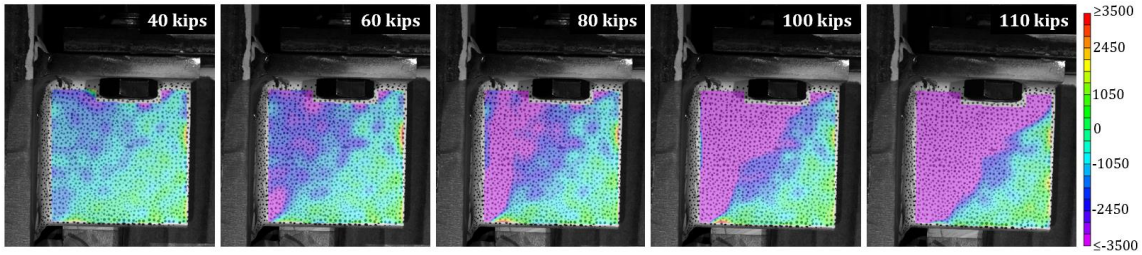

Figure 78: Connection J (Test 5) DIC Angle Deformation Progression (a) Von Mises Strain (ε_v) and (b) Shear Strain (ε_{xy}) – Engineering

Utilizing equation 4.2 and the noted average yield stress for this angle section, a nominal shear strength of approximately 66 kips would be predicted for a singular L4x3x1/2 angle and 132 kips for both connection angles. Though failure of the angles did not occur in this test cycle, later testing approximately met this strength for the angle set.

4.7 Test 6

Test 6 served as the solo evaluator of beam-column drop-in connections. The connections were made from the remaining donated angle and beam sections. Connection K utilized 6x4x5/16 angles with a bearing length of 5.0 inches, the same geometry and bearing length as Connection D. Connection L used L4x3x1/2 angle with a bearing length of five inches. Each

connection was welded to one side of a W14x82 stub column web, like that which would be utilized at the exterior beam of a building; this column featured a web thickness of 0.51 inches. While oversized for a typical beam-to-column connection, a W24x68 section was utilized due to immediate availability for testing. It is noted that due to the insufficient weld size provided by the fabricator for Connection L, an additional weld was added in-house to achieve the specified weld size.

As the failure modes of these connection angles and flanges were already well observed in previous tests, the column web of each connection was of greatest interest. The opposing column web of both connections was imaged for DIC analysis, utilizing all DIC cameras. It is to be noted that Connection K was analyzed via 3D DIC utilizing two cameras. However, while Connection L was observed in testing with two cameras, due to variations in the angle of the cameras, it was unable to be analyzed via the VIC-3D software. Connection L was instead processed via 2D DIC utilizing one camera's deformed images. The beam top flange and column web (where DIC imaging was not utilized) of each connection were covered in whitewash (a mixture of lime and water). Yielding the underlying steel would cause the whitewash to flake off, revealing the strain field pattern. Both connections are pictured in Figure 79 and Figure 80 before testing. Connection K is encased in blue light due to DIC lighting.

a. **b.**

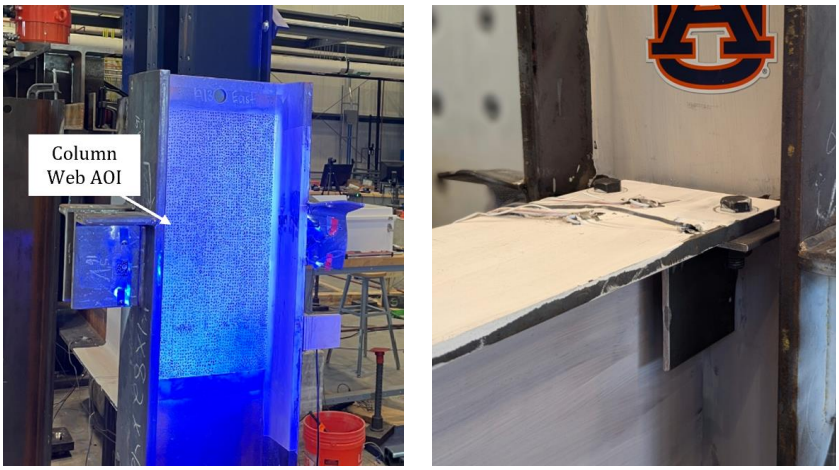

Figure 79: Connection K (Test 6) Before Testing (a) Column Web and (b) Connection Flange and Angles

a.

b.

c.

Figure 80: Connection L (Test 6) Before Testing (a) Column Web, (b) Connection Flange, and (c) Connection Angle

Test 6 achieved a maximum load of 248.5 kips on the beam, resulting in a connection shear of 124.25 kips, well above the design load of 39 kips. Testing was concluded due to rupture of the beam top flange in Connection L and significant deformation of the angles and column webs. At conclusion of the test, Connection K reached a relative rotation of 0.02 radians; Connection L did not display accurate results for the rotation achieved. Due to the importance of viewing the regular images in accompaniment of the strain profiles, the post-testing images of the column webs and connections are presented in their appropriate subsection.

4.7.1 Connection K

To analyze Connection K's column web behavior, an approximate area of 260 square inches (24 inches longitudinally by the width of the column web) of the column web was prepared directly behind the connection angles. Pictured in Figure 81, Connection K's beam top flange (in a similar fashion shown in previous testing) and column web plastically deformed during testing. While the column web deformation is difficult to see due to the speckling pattern, the general deformation is outlined in red in Figure 81(a); the top and bottom of the connection angles are also referenced for the viewer. Figure 81(a) and (c) may be used in reference to each other as the tape measure begins at the top of the column in each photo and allows the viewer to orient oneself to the deformation's location.

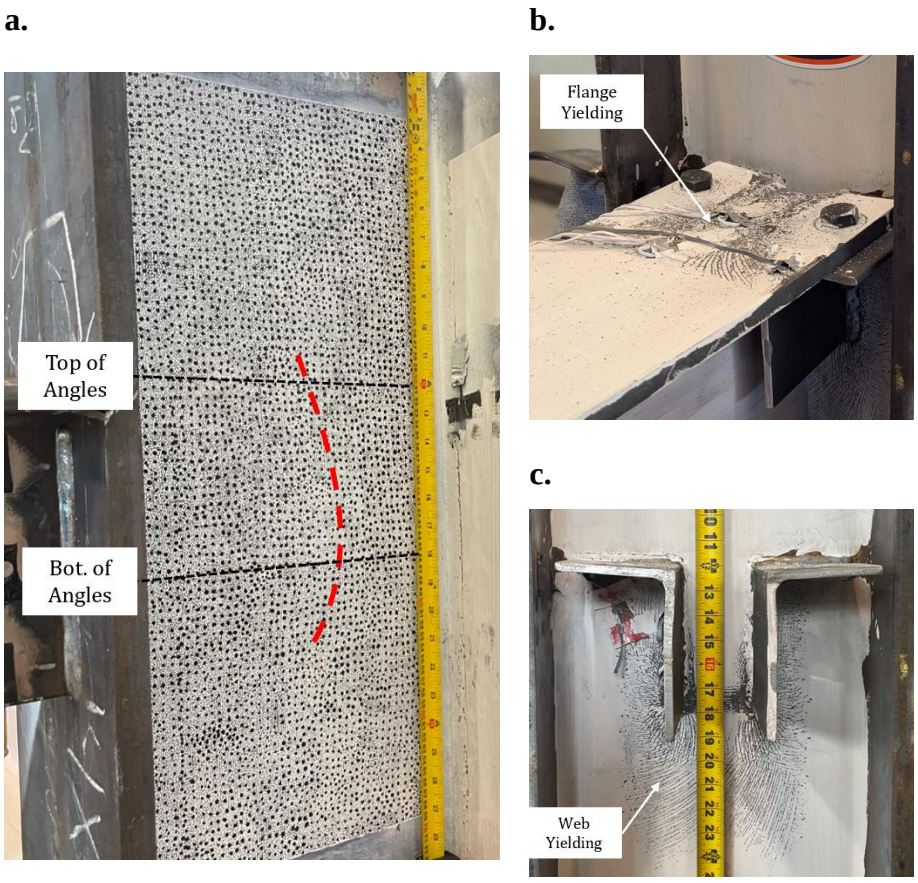

Figure 81: Connection K (Test 6) After Testing (a) Column Web, (b) Connection Flange, and (c) Connection Angles

Figure 82 shows the strain field formation for Connection K's column web, in units of microstrain, in (a) Von Mises strain(ε_v) , (b) transverse strain (ε_{xx}), and (c) longitudinal strain (ε_{yy}) for a connection shear of 40, 60, 80, 100, and 120 kips. It is noted that areas of unprocessed data in the following figure are due to lighting discrepancies during the test and steel strain in these locations cannot be concluded via DIC. These areas are seen in the form of black and white speckled patches along the longitudinal centerline of the column web.

In reference to Figure 82 (a), yielding is seen starting at a shear of 60 kips at the approximate location of the bottom of the connection angle. These yield lines then spread in a butterfly shape, eventually encasing the entire surrounding area of the connection angle at the

maximum shear, denoting plastic deformation. As the shear increases and therefore rotation of the connection, the tops of the angles begin to move towards the midspan of the beam, while the bottom of the angles push into the column web. It is observed in both Figure 82(b) and (c), that the location corresponding to the bottom of the angle is greatly increasing in tensile strain as connection shear increases, creating a bulging area out of the plane of the web (towards the camera/viewer). As well, the strains at the location corresponding to the top of the connection angles are yielding in compression, resulting in a collapsed area into the plane of the web (away from the camera/viewer).

a.

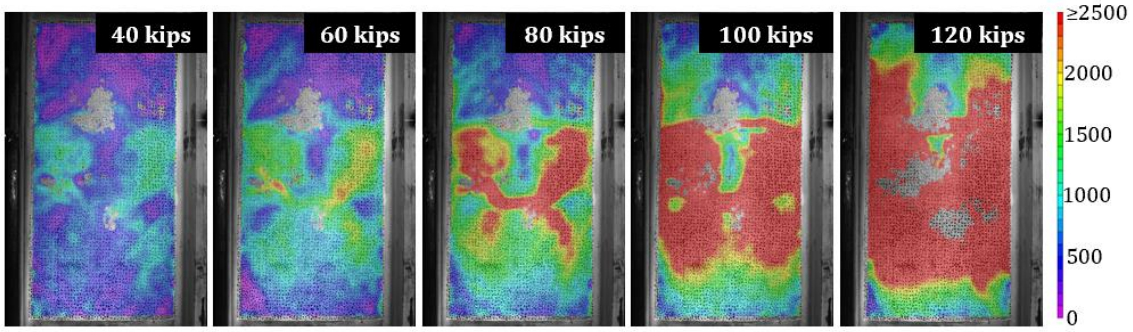

b.

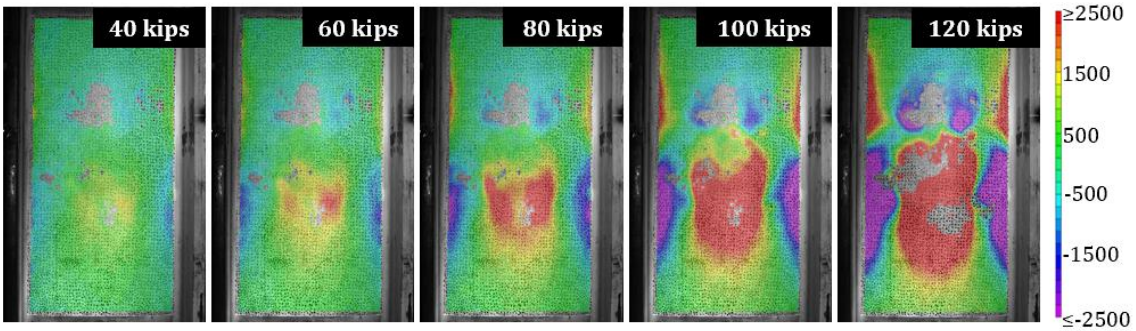

c.

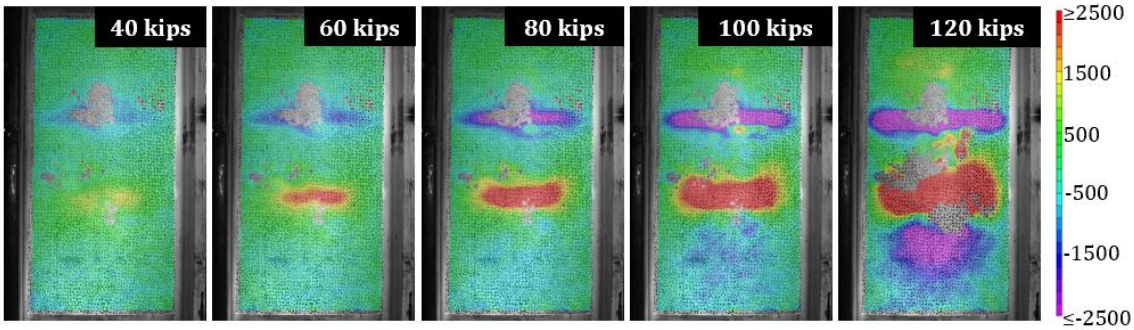

Figure 82: Connection K (Test 6) 2D DIC Column Web Deformation Progression (a) Von Mises Strain (ε_v), (b) Transverse Strain (ε_{xx}) – Engineering, and (c) Longitudinal Strain (ε_{yy}) – Engineering

4.7.2 Connection L

An approximate area of 245 square inches (22.5 inches longitudinally by width of the column web) of the column web was prepared directly behind the connection angles. As noted

above, due to the monocular vision of the 2D-DIC analysis, the large deformations in the column web created compression and tension biases leading to unreliable magnitudes of strain. However, the formation of the strain fields shown may be considered reliable due to small amounts of deformation at lower connection shears.

As shown in Figure 83(b), Connection L's beam top flange plastically deformed in a similar manner experienced in previous testing; however, the top flange fractured unlike in previous tests. As well, the connection angles buckled as seen in Figure 83(b). Like the deformations shown in Connection K, the column web drastically deformed during testing. The general deformation is outlined in red in Figure 81(a) and the top and bottom of the connection angles are referenced. Figure 81(a) and (c) may be used in reference to each other as the tape measure begins at the top of the column and allows the viewer to orient oneself to the deformation's location.

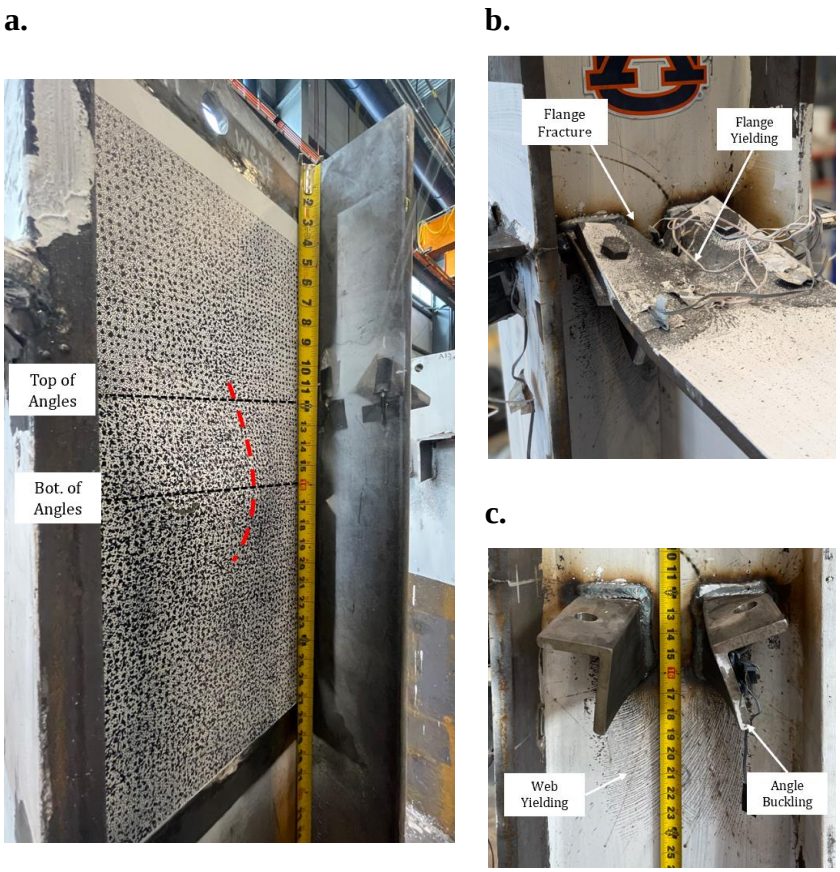

Figure 83: Connection L (Test 6) After Testing (a) Column Web, (b) Connection Flange, and (c) Connection Angles

Figure 82 visualizes the strain field progression for Connection L's column web, in units of microstrain, in (a) Von Mises strain (ε_v), (b) transverse strain (ε_{xx}), and (c) longitudinal strain (ε_{yy}) for a connection shear of 40, 60, 80, 100, and 120 kips. Referring to Figure 84(a), yielding begins before a shear of 40 kips at the approximate location of where the column web and top of the angle are connected. This onset of yielding occurs at a lower shear than that of Connection K. These yield lines then begin to spread around the angle until the entire web surface has yielded at the maximum shear. Figure 84(b) and (c) show large portions of the column web being in compression, leading to a collapse of the web into the plane (away from the camera/viewer). However, the location corresponding to the bottom of the angle is in tension, creating an out-of-

plane bulging (towards the camera/viewer) area. It is to be noted that this region is much smaller in area than that of Connection L but is significantly more pronounced.

a.

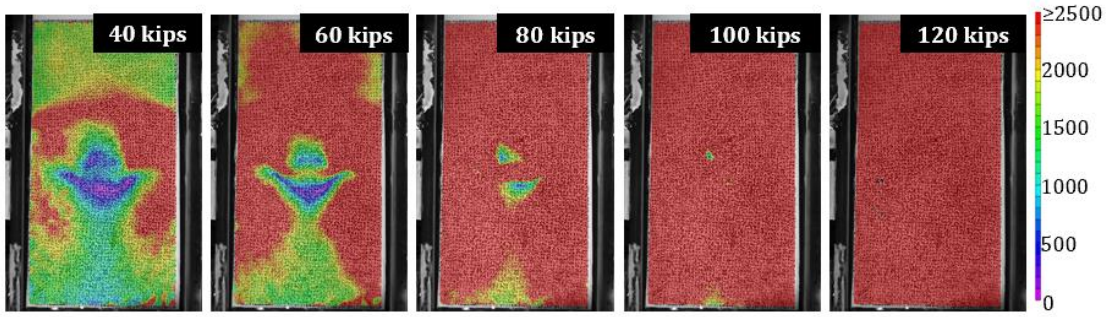

b.

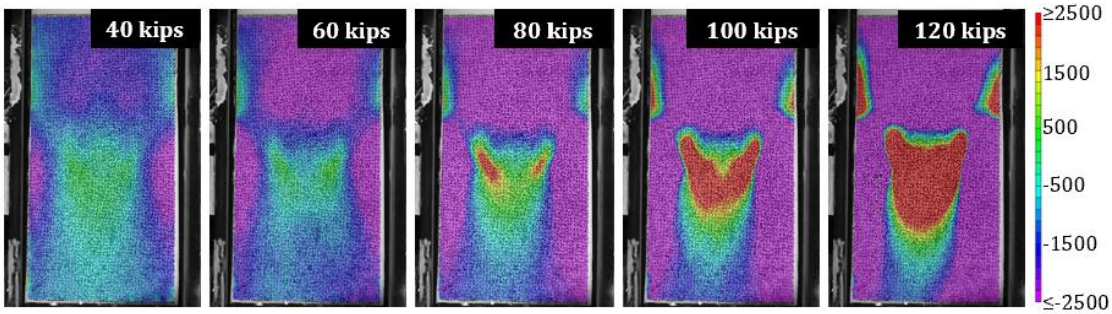

c.

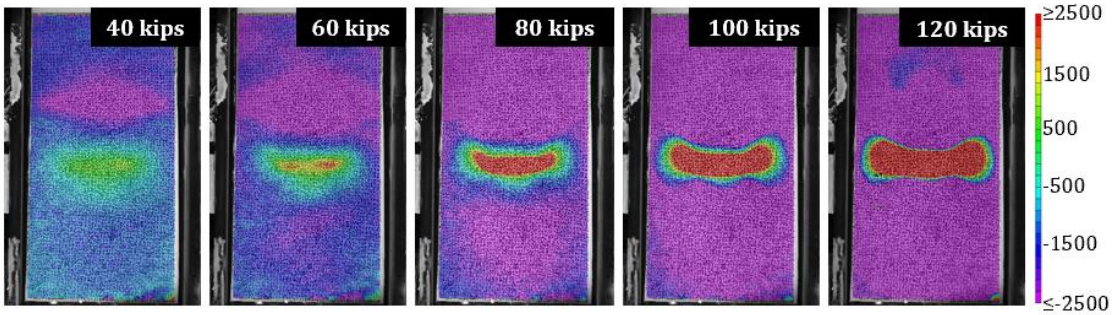

Figure 84: Connection L (Test 6) 2D DIC Column Web Deformation Progression (a) Von Mises Strain (ε_v), (b) Transverse Strain (ε_{xx}) – Engineering, and (c) Longitudinal Strain (ε_{yy}) – Engineering

4.8 Discussion and Comparison

A total of six full-scale tests (five girder-to-column and one beam-to-column) were performed to evaluate 11 drop-in connections and one shear tab connection. Two realistic girder/beam sections, four varying angle sections, two angle orientations, and two bearing lengths were utilized. All tests assessed the girder/beam top flange, vertical angle leg, and/or the column web in varying capacities with DIC, allowing for analysis of the strain fields produced in the loading of these connections. The primary failure mode in these tests was transverse flange bending, with a secondary failure mode of longitudinal flange bending at levels of high shear. Angle shear and angle buckling occurred in some of the tests but occurred after the onset of yielding in the flange. For beam-to-column connections, plastic deformation of the column web was also a subsequent failure mode.

4.8.1 Behavior of Girder/Beam Top Flange

A comparison was performed for all the girder/beam top flanges evaluated with DIC. One of the first findings was that transverse yielding of the top girder/beam flange was observed before yielding in the other elements in all tests. Another finding was with regard to a mirrored/flipped orientation of the connection angles (utilized in Connection H). This orientation decreased the shear capacity of the overall connection and induced transverse yielding at lower shears compared to non-mirrored/flipped connections. Significant plastic deformation was observed in the flange. Therefore, this orientation of the connection angles is not recommended for implementation in the field due to its low capacity and inability to achieve a sufficient rotation of 0.03 radians.

Figure 85 presents all girder top flanges (that were analyzed with DIC) for connections with the original (non-mirrored/flipped) orientation of angles at the maximum shear experienced

during testing. The connection and maximum connection shear experienced are referenced at the top left corner of each image. All displayed flanges prominently featured a large region of plastic deformation due to yielding in compression at the centerline of the flange above the web and fillet zone. As well, all (except for Connection D) showed distinct areas of tension at (or within a negligible distance from) the interior longitudinal edge of each connection angle. The connection angle sizes or bearing lengths of these connections did not significantly influence the location of the transverse yield lines. However, the distance of the primary yield line (encasing an area of compression) beyond the bearing length varied across the connections. If an area of tensile yielding occurred (as in all besides Connection D), it extended just beyond the bearing length of the flange.

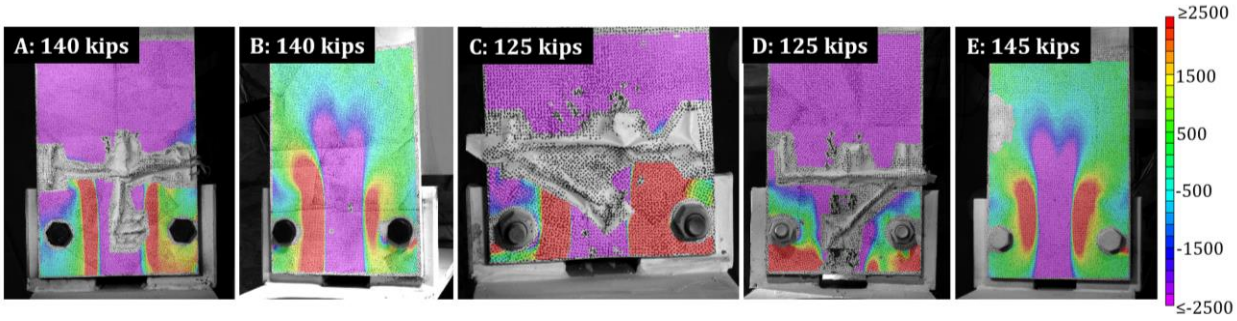

Figure 85: Transverse Yield Lines on Girder Top Flanges at Maximum Shear

Figure 86 presents the maximum transverse compressions (shown in red) and maximum transverse tensions (shown in green), for all Connections A through E. All strains were taken at a cross-sectional cut midway between the transverse bolt centerline and the transverse edge of the angles. The upper bound AISC maximum fillet (k_1 minus half the thickness of the web) and measured fillet for the W24x68 girder are noted. Figure 87 shows how the actual k_1 zone of 0.65 inches was determined by dividing a fillet edge-to-edge distance of 1.3 inches by two on a

W24x68 girder. The angles in the figure are placed at the AISC k_1 value, as was done in full-scale testing.

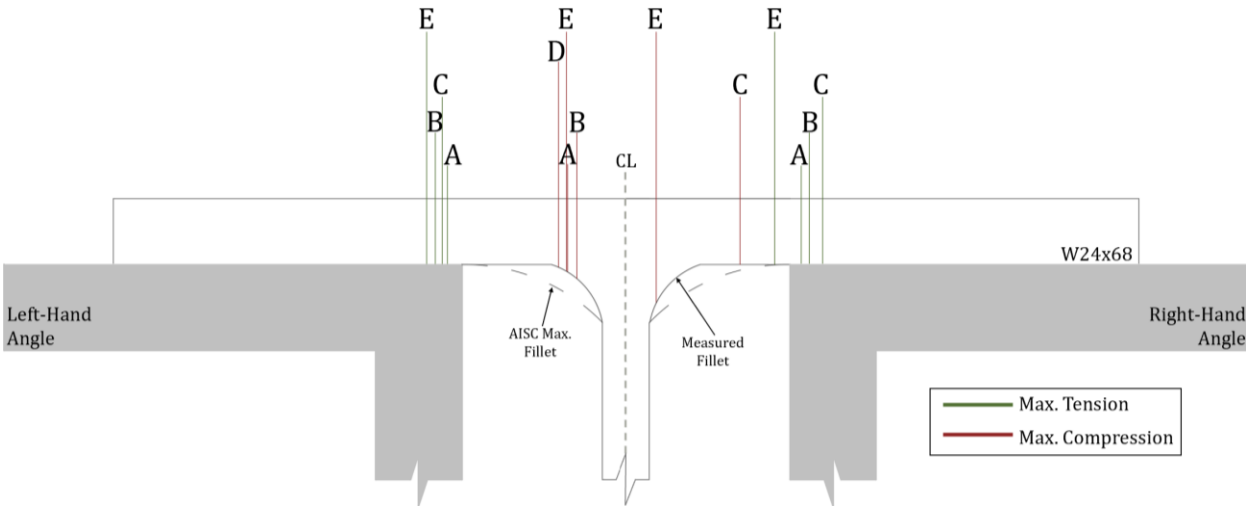

Figure 86: Max. Tension and Compression Maximum Strains on Girder Top Flange

Figure 87: Measured Fillet Size (edge-to-edge) of W24x68 Girder

According to Figure 86, it can be concluded that for this array of flange and angle geometries, the maximum transverse tensile strains for a given connection will be located at or

near the interior longitudinal edge of the vertical angle leg (given that the angle is sufficiently stiff compared to the flange). With this assumption, a designer would have direct knowledge of the probable location of this tensile strain upon determining the angles' placement relative to the girder/beam centerline.

The location of the maximum transverse compression strain is variable according to the actual size of the girder's fillet, as it is likely to occur near the edge of the fillet due to its smaller size. A smaller fillet would likely cause the maximum compression strain to be closer to the centerline of the girder, and therefore, further from the maximum tension (and vice versa). As well, due to the variance in fillet size on each side of the girder web, this location may slightly differ on each side of the flange's centerline. Table 10 lists the distances measured between the maximum transverse tension and compression strains, as shown in Figure 86.

Table 10: Distances Between Maximum Tension and Compression Strain in the Top Flange

Connection	Distance Between Max. Tension and Max. Compression	Percentage of Listed AISC K1 Value
A	1.05 in.	73%
B	1.24 in.	86%
C	0.72 in.	50%
E	1.22 in.	85%
	1.04 in.	72%
Average		**73%**

A significant finding from the study was the distance between the maximum transverse tension and compression ranged from approximately 50 percent to 86 percent of the listed k_1 for the tested W24x68 girders. An approximate value of 75 percent of the listed k_1 is recommended

when doing yield line analysis for the design of drop-in connections similar to those tested. Note that this value was utilized in the AISC study (Drop-In Top Flange Connection), where yield line analysis was performed to develop a flange bending design equation.

The longitudinal yield lines at maximum shear for all connections featuring non-mirrored/flipped angles with applicable DIC results are shown in Figure 88. Longitudinal yielding of the girder top flange was observed at levels of high shear and was the secondary mode of failure for the flange, after transverse yielding. In all shown flanges, plastic hinges extend across the flange area directly above the transverse edge of the connection angles, allowing for a ductile failure in which rotation would disproportionately increase at levels of high shear, compared to rotation noted at levels of low shear.

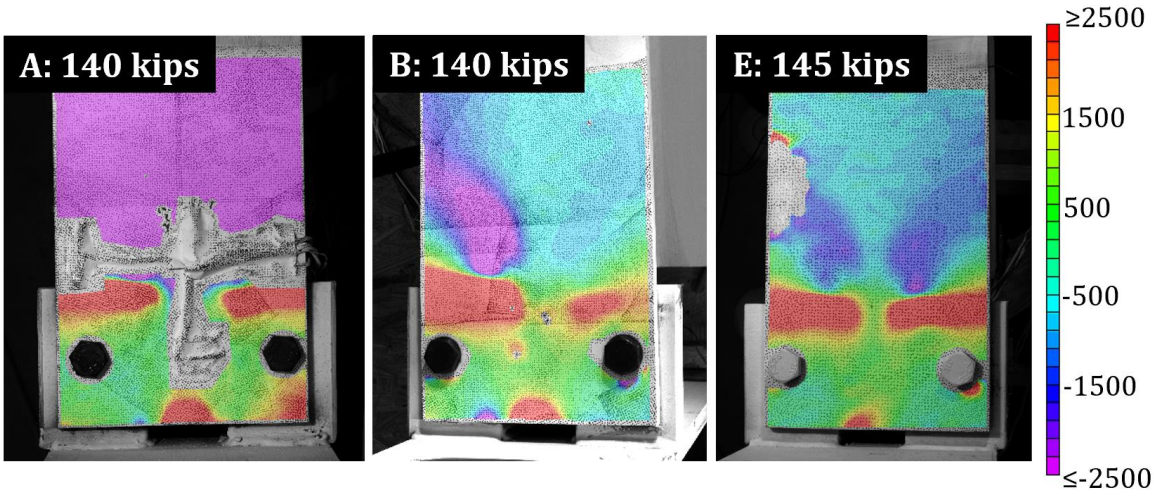

Figure 88: Longitudinal Yield Lines on Girder Top Flanges at Maximum Connection Shear

4.8.2 Behavior of Connection Angles

A comparison was performed for all connection angles evaluated with DIC. One of the first findings was that while plastic deformation of the connection angles' surface did occur in testing, it was not the first element to go into the plastic range. However, the angles were tested

to failure in several of the cases. Also, note that the connection angles for the beam-to-column cases were not analyzed via DIC (due to the column flanges obstructing the view of a potential DIC camera). For these tests, the angles plastically deformed more than other tests discussed, excluding Connection C which experienced angle buckling.

Another finding was that the orientation of the connection angles greatly impacted the overall capacity of the connection. Mirrored/flipped orientation of the connection angles (utilized in Connection H) initiated yielding and vertical displacement of the weaker horizontal angle leg, resulting in significant plastic deformation in the girder flange at lower shears. Again, this orientation of the connection angles is not recommended for utilization in the field due to the decrease in capacity and inadequate rotation needed for a simple connection. For all properly oriented angles, the shear strain profile extended (at an angle) from the lowest portion of the fixed region where the weld was located to the free end. All angles experienced some magnitude of plastic deformation at the surface. As would be assumed, a stockier angle with a greater vertical leg length to bearing length ratio (VL/BL) experienced lower amounts of plastic deformation at similar shears than an angle with a lower VL/BL ratio.

Though DIC cannot definitively determine the shear strain throughout the cross-section of the vertical angle leg, by comparing the current AISC Specification (2022) shear strength equation for a single-angle leg to the observed capacities, the AISC expression provided reasonable results for the cases where the angles were loaded to near failure. As is suggested by the current equation and observed in testing (connections C and E), a thicker angle and therefore a greater shear area will not experience the onset of yielding as early as a thinner angle. The angles tested varied the bearing length, vertical leg length, and vertical leg thickness. However, in all cases, the aspect ratio VL/BL was such that negligible flexural demand was applied.

4.8.3 Behavior of Column Web in Beam-to-Column Connections

A comparison was performed for the two columns webs evaluated with DIC. This was not the main focus of the study but was included for completeness. One observation was that significant plastic deformation of the web in a "one-sided" beam-to-column connection occurred at high connection shear and must be considered in the design, especially when the web is thin. Because the tested connections were loaded on one side of the web, it is possible that a column web that features connections on both sides will not undergo the plastic deformation seen in testing.

In general, both column webs experienced the following pattern of plastic deformation: collapse of the web that occurred at the location of the top of the connection angles as they were pulled towards midspan along with the beam's compression flange via the bolted connection; bulging of the web that occurred at the bottom of the connection angles as they rotated away from the beam's midspan. Further yield line analysis, like that proposed in Ellifritt and Sputo's 1999 study for stiffened seated connections to column webs would be beneficial to properly equate the web's strength for a beam-to-column connection (Ellifritt & Sputo, 1999).

Chapter 5: Summary, Conclusions, and Recommendations

5.1 Summary

The primary objective of this research was to aid in the development of a simplified design process for the implementation of a steel drop-in shear connection in the residential and commercial steel frame sectors. Contributions to this objective include the following:

- identification of geometric limitations and a standardized process to be considered for proper fit-up in the field
- discussion of plastic deformations shown in the testing of the girder top flange and vertical angle leg
- yield line locations of the girder top flange for use in yield line analysis and eventual flange bending design equation
- discussion of shear strain experienced at the surface of the vertical angle leg during testing
- comparison of the connection shear experienced by the angle to the calculated nominal shear strength provided by the current AISC Specification
- discussion of the plastic deformation in a column web due to a drop-in beam-to-column connection.

Prior to testing, current industry connections, practices, and geometric constraints were assessed and considered. A testing matrix and setup were then created to properly assess multiple girder-to-column connections and two beam-to-column connections utilizing Digital Image Correlation (DIC). Full-scale testing was performed on 12 separate connections, 11 of which were drop-in connections. Two wide-flange sections, W24x68 and W16x36, were utilized to

connect the opposing connections. In total, for a girder-to-column connection, six girder top flange sections, eight drop-in connection vertical angles, and one shear tab were assessed via DIC. Four angle sections and two bearing lengths were utilized for the formation of the connections. For a smaller beam-to-column connection, two W14X82 column webs were assessed via DIC.

5.2 Conclusions and Recommendations

Through preliminary recommendations made by the industry panel and consideration of current practices in both the fabrication and erection process, the following conclusions were determined regarding the geometric design of the drop-in connection.

- Geometric compatibility must be considered before strength design to ensure proper fit-up when utilized in the field. A standard preliminary geometry check is presented in Chapter 3. The following will determine the geometric compatibility of this connection and should be considered:
    - bolt size, bolt-hole dimensions, required edge distance, and entering and tightening clearance
    - beam flange width, top flange fillet size, allowable encroachment of the connection angles into the top flange fillet zone
    - length of horizontal angle leg and angle fillet size
    - fabrication machinery
- A beam with a relatively small flange width (less than six inches) will produce few, if any, possible bolt and angle combinations that satisfy geometric constraints. However, a majority of girders/beams regularly used in the residential and commercial building sector have proven geometrically compatible for the utilization of drop-in connections.

- It is recommended that the geometric constraints in regard to common fabrication machinery be further investigated to allow for automatic hole-punching in a full-scale utilization of this connection, rather than hand drilling each angle.

Several conclusions and recommendations for girder-to-column drop-in connections were determined from strain fields produced utilizing DIC:

- Connection angles should be oriented such that the vertical leg of each angle is as close to the girder web as possible to provide adequate shear capacity, minimize plastic deformation of the girder top flange, and provide sufficient rotation of the simple connection.
- For all connection angles tested to failure, the current design equation provided by the AISC Specification (2023) for single-angle leg shear strength, in which the cross section is assumed to have fully yielded, was considered adequate to determine the angle's strength. It is recommended that further testing of various angle geometries and bearing lengths be done to determine the limitations of this established equation for a drop-in connection.
- The two associated limit states observed in testing for the girder top flange of the drop-in connection were transverse and longitudinal flange bending. In all cases, transverse bending of the girder's top flange was initiated before longitudinal flange bending and was considered the primary failure mode.
- In all cases in which sufficiently stiff connection angles were utilized, the girder top flange developed four plastic hinges due to transverse bending. Yield line analysis is recommended for further development of a drop-in connection design. The following

geometric location recommendations for the maximum strains were established from those observed in testing.

- Two yield lines formed at the location of the interior longitudinal angle edges and encased an area that yielded in tension (for the top surface). The other two formed at or near the actual fillet of the girder in which the top of the flange had yielded in compression. An example of these plastic hinges on a girder flange is shown in Figure 89, in which the green lines indicate the hinges (maximum tension) formed at the location of the connection angle interior edges, and the red lines indicate the hinges (maximum compression) formed at or near the fillet ends.

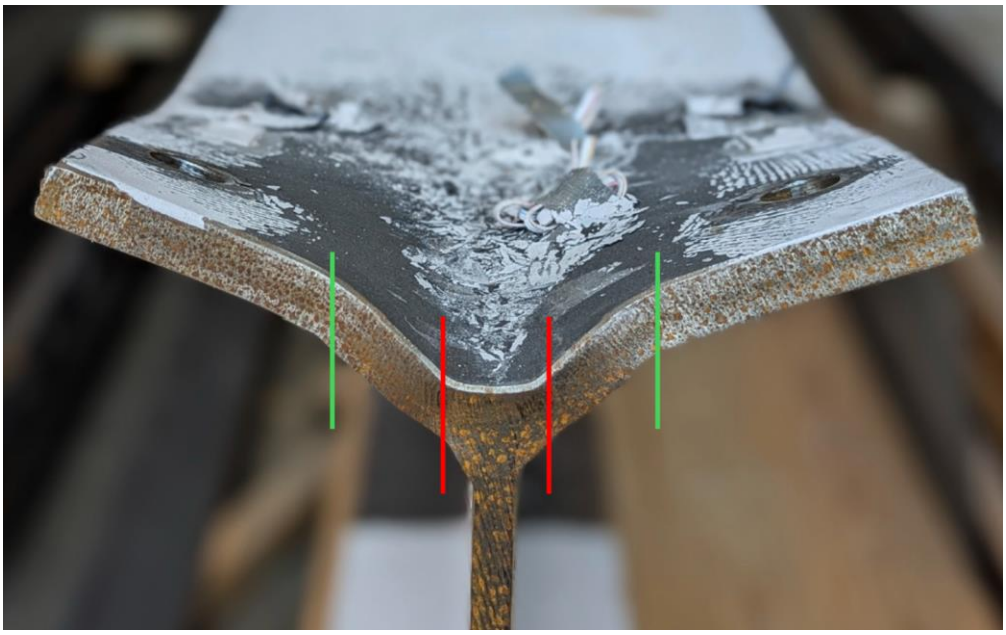

Figure 89: Failed Girder Plastic Hinge Locations

- In design, the engineer has direct knowledge of the location of the two hinges formed at the interior angle edges; however, the exact location of the hinges that form near the fillet of the girder may be unknown as the listed fillet size is a maximum value reported by steel-mills.

- According to the test results, the distance between the hinges to the left or right of the web can be approximated as 75% of the listed k_1 value for the girder in the AISC Dimensions and Properties tables (AISC, 2022). This distance provides the engineer with the ability to estimate the probable location of the other yield lines. Note that one may reduce this distance by utilizing encroachment of the angles into the fillet zone of the girder.
- The final length (in the longitudinal direction of the girder/beam) of the transverse bending yield lines varied significantly with the DIC data during testing. This was partly due to data being analyzed via monocular vision (creating biases) and the testing being stopped before complete flange bending failure.

- For all sufficiently stiff angles, a secondary failure mode of longitudinal yielding of the girder top flange was initiated at high shears, in which bending about the transverse edge of the angles occurred, allowing for a substantial increase in rotation.

For a single-sided beam-to-column drop-in connections, the following conclusion and recommendation were determined from the produced strain fields utilizing DIC at the column web:

- Though not likely to be the initial failure mode, significant plastic deformation did occur at the column web at high connection shears as the connection angles deformed. As with many other beam-to-column connections, an exceptionally thin column web is not recommended for use unless the section is stiffened.
- Further full-scale testing of beam-to-column drop-in connection is recommended to understand the behavior and yield line formation of the column web during loading.

References

AISC. (2018). Office: Conventional Steel Framing Study. In (pp. 1-12): AISC Steel Solutions Center.

AISC. (2022). Specification for Structural Steel Buildings (ANSI/AISC 360-22). In. Chicago, IL: American Institute of Steel Construction.

Astaneh, A. (1989). Demand and Supply of Ductility in Steel Shear Connections. *Journal of Constructional Steel Research*, *14*, 1-19. https://doi.org/https://doi.org/10.1016/0143-974X(89)90067-9

Astaneh, A., Call, S. M., & McMullin, K. M. (1989). Design of Single Plate Shear Connections. *Engineering Journal*, *26*(1), 21-32. https://doi.org/https://doi.org/10.62913/engj.v26i1.513

ASTM. (2024). Standard Specification for General Requirements for Rolled Structural Steel Bars, Plates, Shapes, and Sheet Piling. In *Permitted Variations in Dimensions and Weight [Mass]*.

Bjorhovde, R., Colson, A., & Brozzetti, J. (1990). Classification System for Beam-to-Column Connections. *Journal of Structural Engineering*, *116*(11), 3059-3076. https://doi.org/doi:10.1061/(ASCE)0733-9445(1990)116:11(3059)

Blikharsky, Y., & Kopiika, N. (2024). Digital Image Correlation for Assessment of Bridges' Technical State and Remaining Resource. *Structural Control and Health Monitoring*, *2024*, 23. https://doi.org/https://doi.org/10.1155/2024/1763285

Boake, T. M.). https://www.tboake.com/SSEF1/bolt.shtml

Carter, C. J., Thornton, W. A., & Murray, T. M. (1997). Discussion: The Behavior and Load-Carrying Capacity of Unstiffened Seated Beam Connections. *Engineering Journal*, *34*(4), 151-156. https://doi.org/https://doi.org/10.62913/engj.v34i4.1237

Chen, W.-F., Bowman, M. D., & Yang, W. H. (1997). The Behavior and Load-Carrying Capacity of Unstiffened Seated Beam Connections. *Engineering Journal*, *34*(3), 89-103. https://doi.org/https://doi.org/10.62913/engj.v34i3.684

Correlated Solutions, I. (2020a). *Digital Image Correlation (DIC): Overview of Principles and Software*. Correlated Solutions. https://www.youtube.com/watch?v=kfP9XRz2vo0&list=PLKk1tDmnghhfp1sCBOzX3bi3zvmZPuFsJ

Correlated Solutions, I. (2020b). Strain Tensors and Criteria in Vic. In M. Simonsen (Ed.).

Correlated Solutions, I. (2020c). VIC-3D Testing Guide. In I. Adkins (Ed.).

Correlated Solutions, I. (2021). *Introduction to Digital Image Correlation - Guest lecture at Oregon State University April 22, 2021*. https://www.youtube.com/watch?v=GtZjxx55Pis

Correlated Solutions, I. (2022). VIC-3D Software Manual Version 9.2. In.

Correlated Solutions, I. (2023). Speckle Kit User Manual. In (pp. 1-13).

Desai, N. (2016). Small-Strain Measurement in Bridge Connections Using the Digital Image Correlation (DIC) Technique. SPIE Smart Structures and Materials + Nondestructive Evaluation and Health Monitoring, Las Vegas, Nevada.

Elhadary, M., Bediwy, A., & Ahmed Elshaer. (2024). Novel steel connection for modular houses in indigenous communities: An experimental study. *Journal of Constructional Steel Research*, *220*. https://www.sciencedirect.com/science/article/pii/S0143974X24004000

Ellifritt, D. S., & Sputo, T. (1999). Design Criteria for Stiffened Seated Connections to Column Webs. *Engineering Journal*, *36*, 160-168. https://doi.org/https://doi.org/10.62913/engj.v36i4.729

Geschwinder, L. F., Liu, J., & Carter, C. J. (2017). Chapter 11: Simple Connections. In *Unified Design of Steel Structures, Third Edition*.

Jones, E. M. C., & Iadicola, M. A. (2018). *A Good Practices Guide for Digital Image Correlation*.

McCormick, N., & Lord, J. (2010). Digital Image Correlation. *Materials Today*, *13*(12), 52-54. https://doi.org/10.1016/S1369-7021(10)70235-2

Mousa, M. A., Yussof, M. M., Hussein, T. S., Assi, L. N., & Ghahari, S. (2023). A Digital Image Correlation Technique for Laboratory Structural Tests and Applications: A Systematic Literature Review. *Sensors*, *23*(23). https://doi.org/10.3390/s23239362

Muir, L. S., & Thornton, W. A. (2004). A Technical Note: A Direct Method for Obtaining the Plate Buckling Coefficient for Double-Coped Beams. *Engineering Journal*, *41*, 133-134. https://doi.org/https://doi.org/10.62913/engj.v41i3.830

Muir, L. S., & Thornton, W. A. (2011). The Development of a New Design Procedure for Conventional Single-Plate Shear Connections. *Engineering Journal*, *48*(2). https://doi.org/https://doi.org/10.62913/engj.v48i2.1006

Niezrecki, C., Baqersad, J., & Sabato, A. (2018). Digital Image Correlation Techniques for Non-Destructive Evaluation and Structural Health Monitoring. In N. Ida & N. Meyendorf (Eds.), *Handbook of Advanced Non-Destructive Evaluation*. https://doi.org/10.1007/978-3-319-30050-4_47-1

Oats, R. C., Dai, Q., & Head, M. (2022). Digital Image Correlation Advances in Structural Evaluation Applications: A Review. *Practice Periodical on Structural Design and Construction*, *27*(4). https://doi.org/10.1061/(ASCE)SC.1943-5576.0000725

Shih, M.-H., & Sung, W.-P. (2014). Developing Dynamic Digital Image Correlation Technique to Monitor Structural Damage of Old Buildings under External Excitation. *Shock and Vibration*, 1-15. https://doi.org/https://doi.org/10.1155/2014/954840

Sutton, M. A., Orteu, J.-J., & Schreier, H. W. (2009). *Image Correlation for Shape, Motion and Deformation Measurements*. Springer Science+Business Media, LLC. https://doi.org/10.1007/978-0-387-78747-3

Appendix 1: Design Drawings

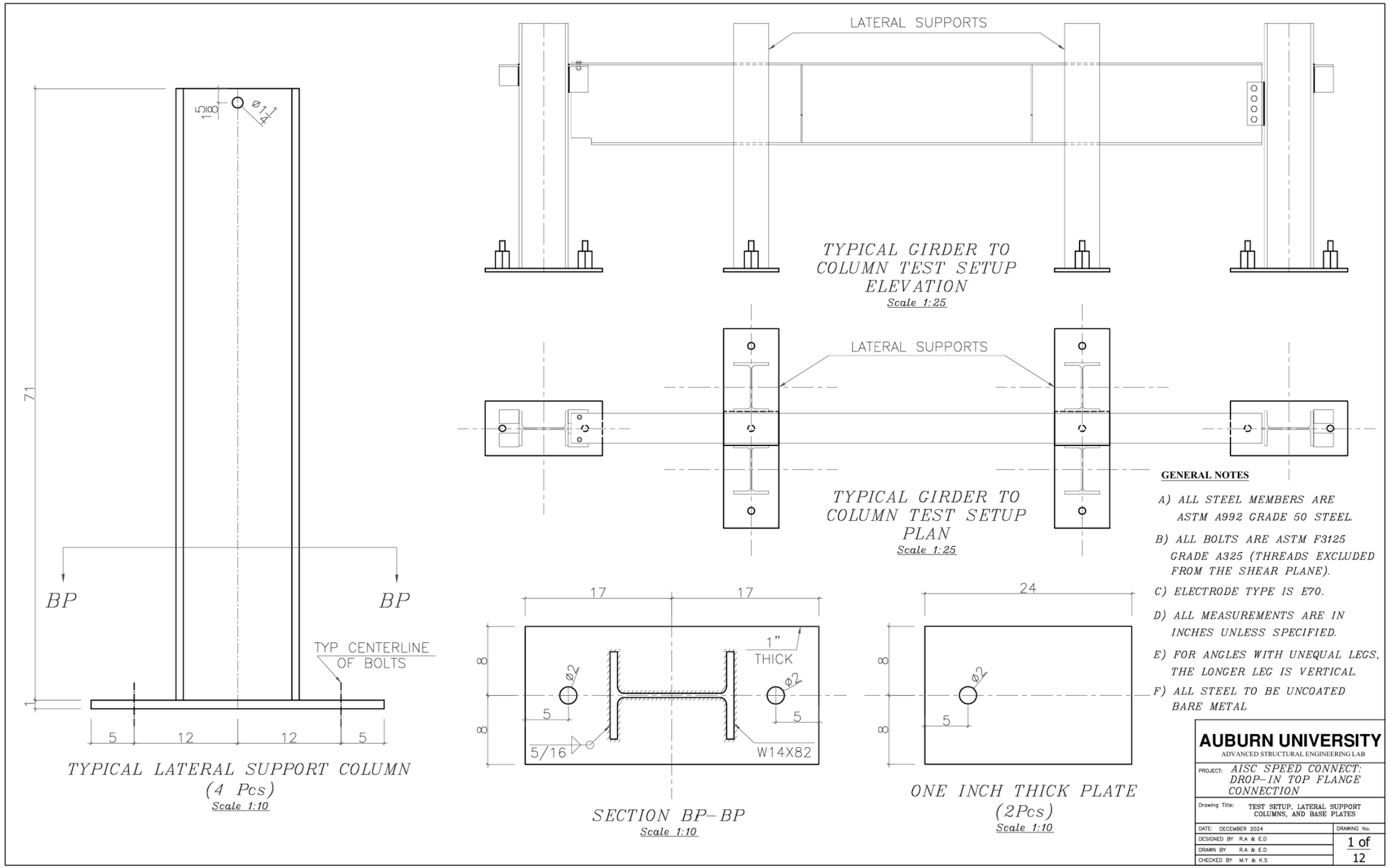

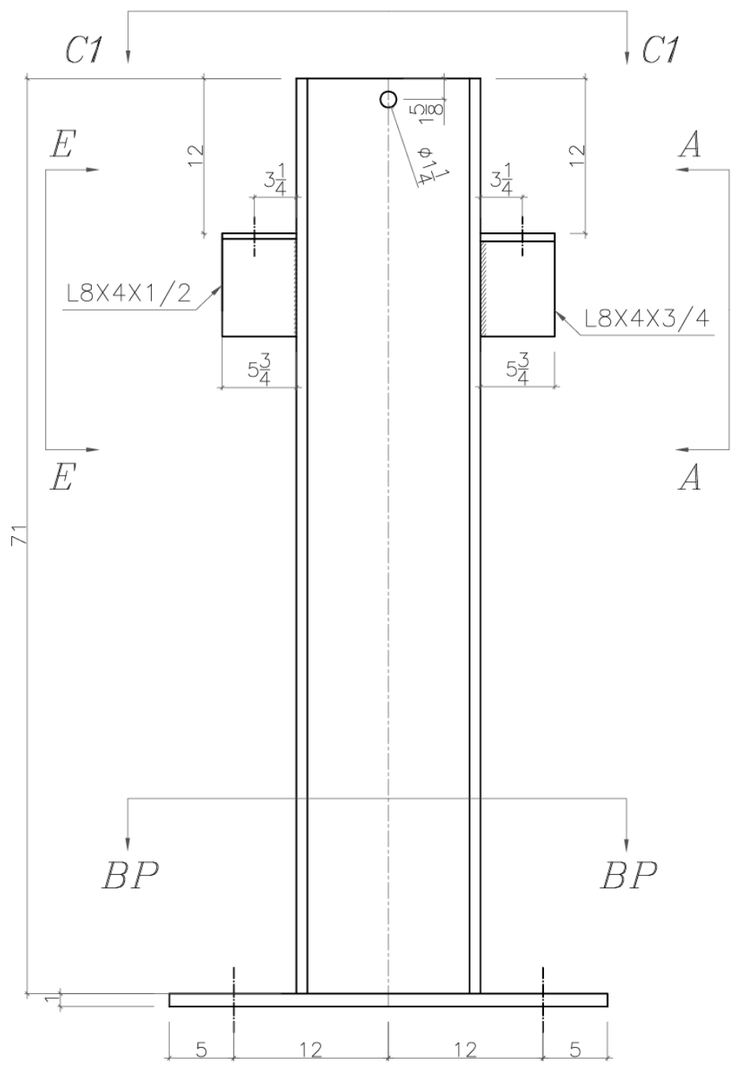

COLUMN 1 – W14X82

Scale 1:10

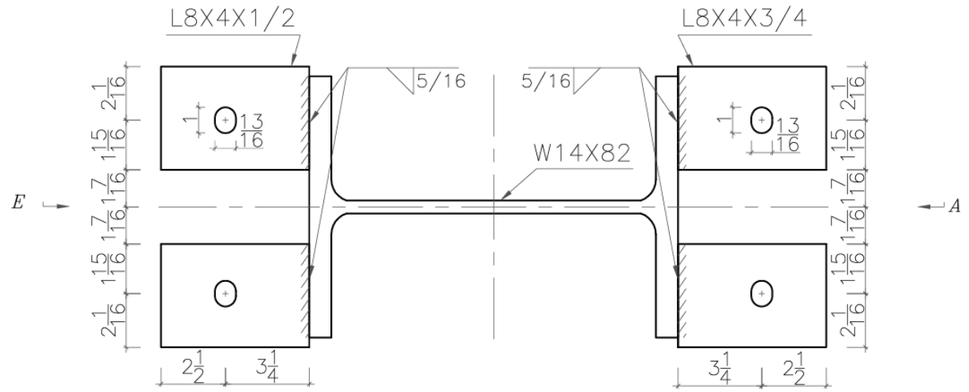

VIEW C1–C1

Scale 1:5

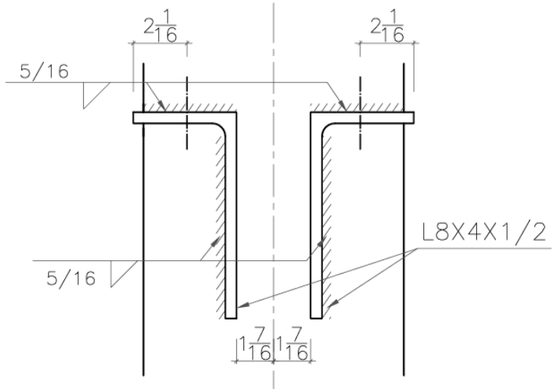

VIEW E–E

Scale 1:5

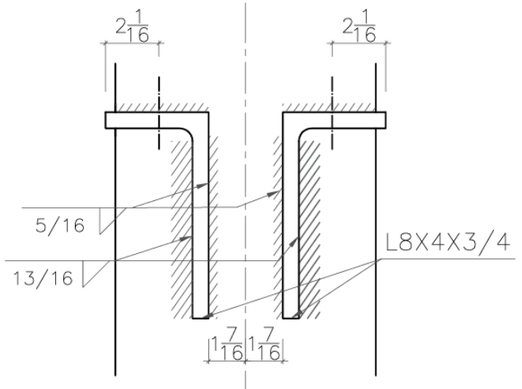

VIEW A–A

Scale 1:5

AUBURN UNIVERSITY

ADVANCED STRUCTURAL ENGINEERING LAB

PROJECT: *AISC SPEED CONNECT: DROP-IN TOP FLANGE CONNECTION*

Drawing Title: COLUMN 1

DATE: DECEMBER 2024	DRAWING No.
DESIGNED BY R.A & E.D	2 of 12
DRAWN BY R.A & E.D	
CHECKED BY M.Y & K.S	

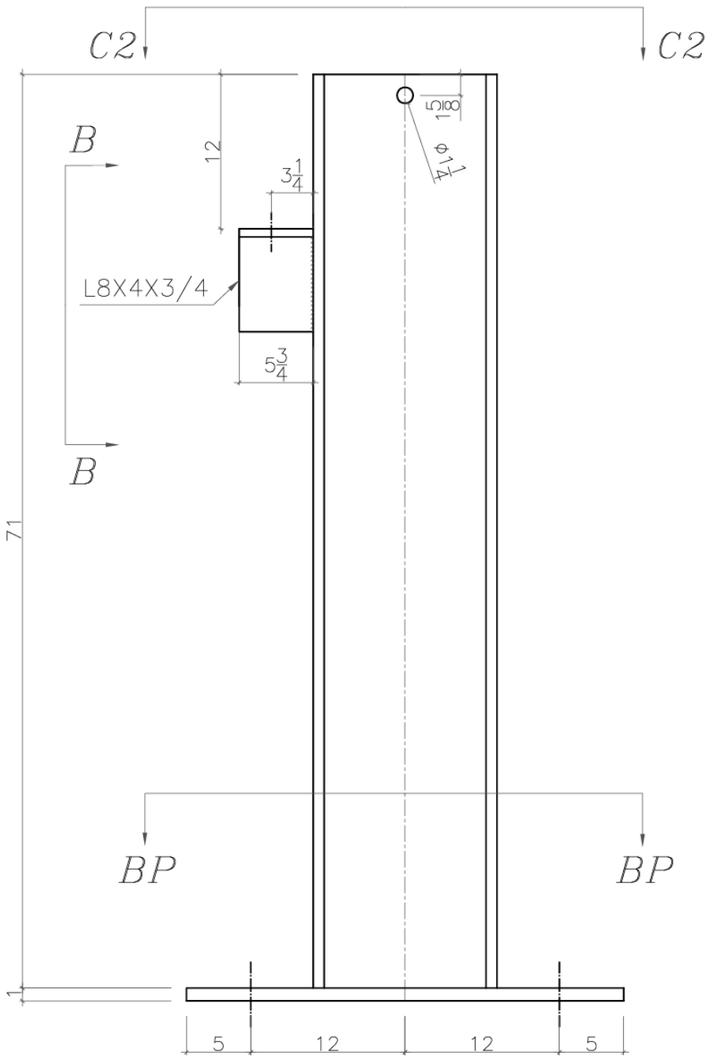

COLUMN 2 – W14X82

Scale 1:20

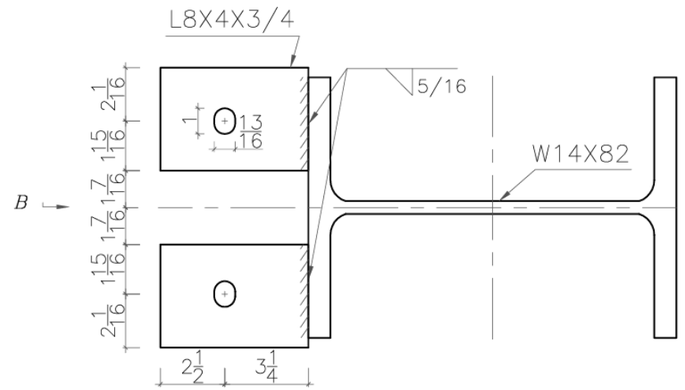

VIEW C2–C2

Scale 1:5

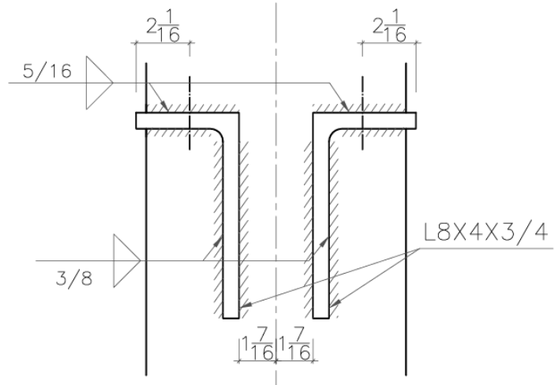

VIEW B–B

Scale 1:5

AUBURN UNIVERSITY
ADVANCED STRUCTURAL ENGINEERING LAB

PROJECT: AISC SPEED CONNECT: DROP-IN TOP FLANGE CONNECTION

Drawing Title: COLUMN 2

DATE: DECEMBER 2024	DRAWING No.
DESIGNED BY R.A & E.D	3 of 12
DRAWN BY R.A & E.D	
CHECKED BY M.Y & K.S	

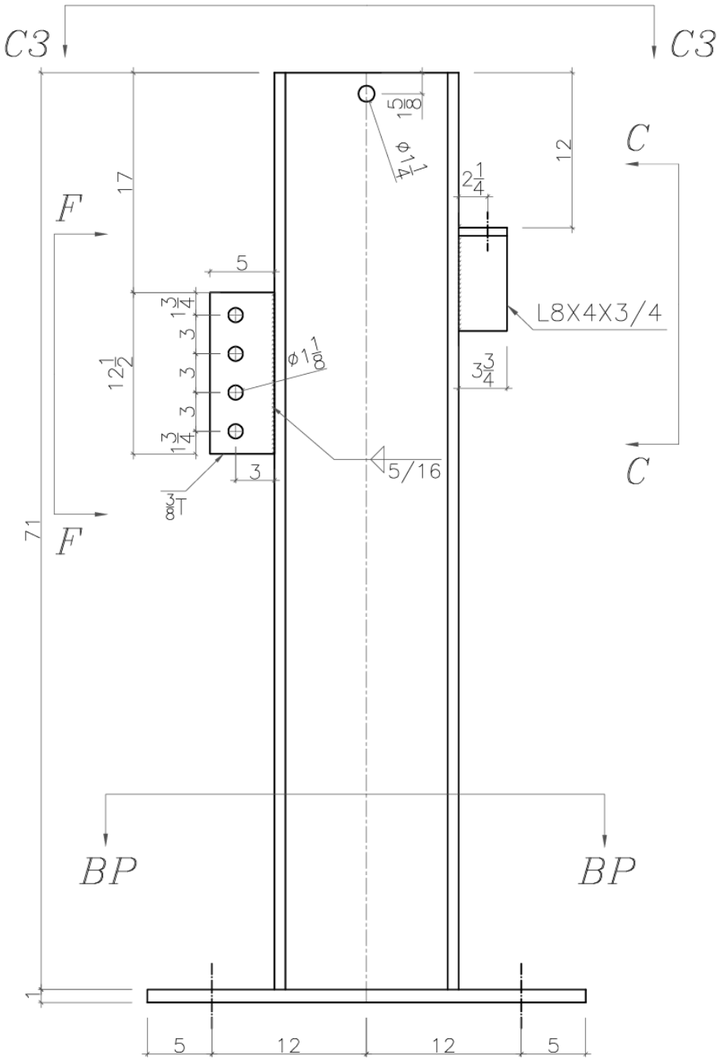

COLUMN 3 – W14X82

Scale 1:10

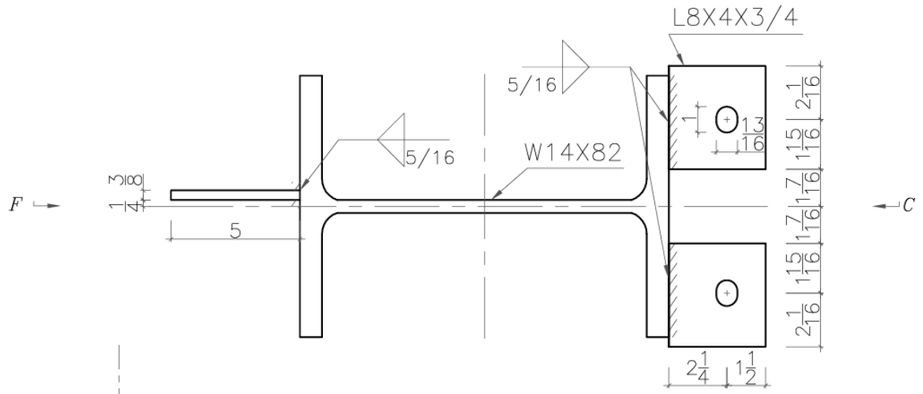

VIEW C3–C3

Scale 1:5

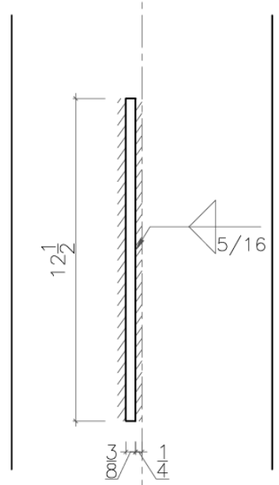

VIEW F–F

Scale 1:5

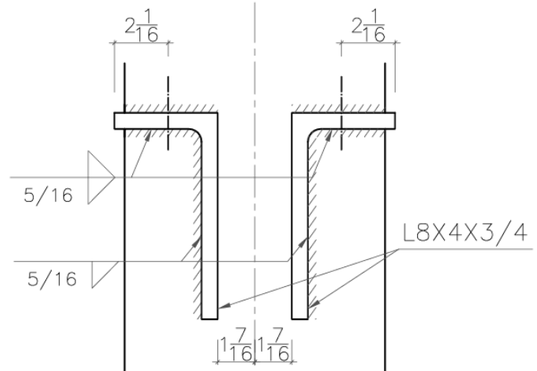

VIEW C–C

Scale 1:5

AUBURN UNIVERSITY

ADVANCED STRUCTURAL ENGINEERING LAB

PROJECT: *AISC SPEED CONNECT: DROP-IN TOP FLANGE CONNECTION*

Drawing Title: COLUMN 3

DATE: DECEMBER 2024	DRAWING No.
DESIGNED BY R.A & E.D	4 of 12
DRAWN BY R.A & E.D	
CHECKED BY M.Y & K.S	

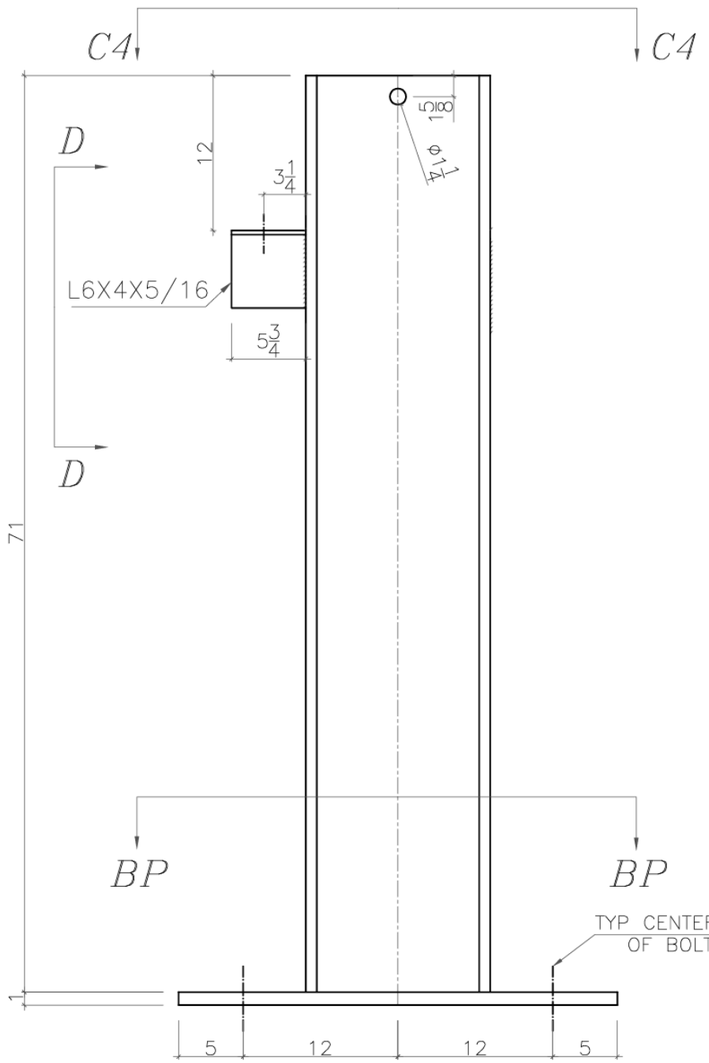

COLUMN 4 – W14X82

Scale 1:10

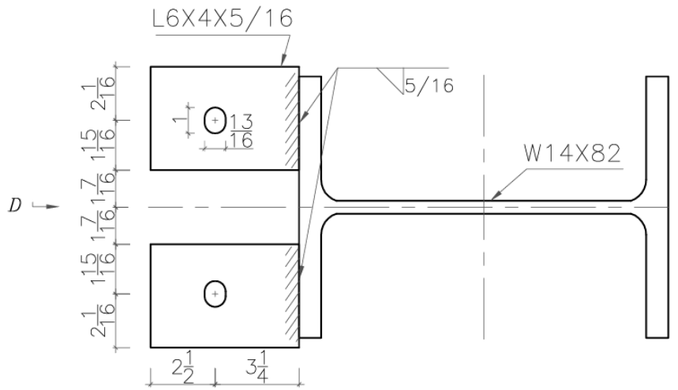

VIEW C4–C4

Scale 1:5

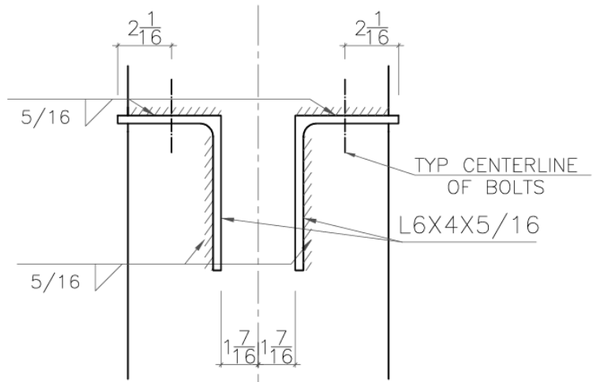

VIEW D–D

Scale 1:5

AUBURN UNIVERSITY

ADVANCED STRUCTURAL ENGINEERING LAB

PROJECT: *AISC SPEED CONNECT: DROP-IN TOP FLANGE CONNECTION*

Drawing Title: COLUMN 4

DATE: DECEMBER 2024	DRAWING No.
DESIGNED BY R.A & E.D	5 of 12
DRAWN BY R.A & E.D	
CHECKED BY M.Y & K.S	

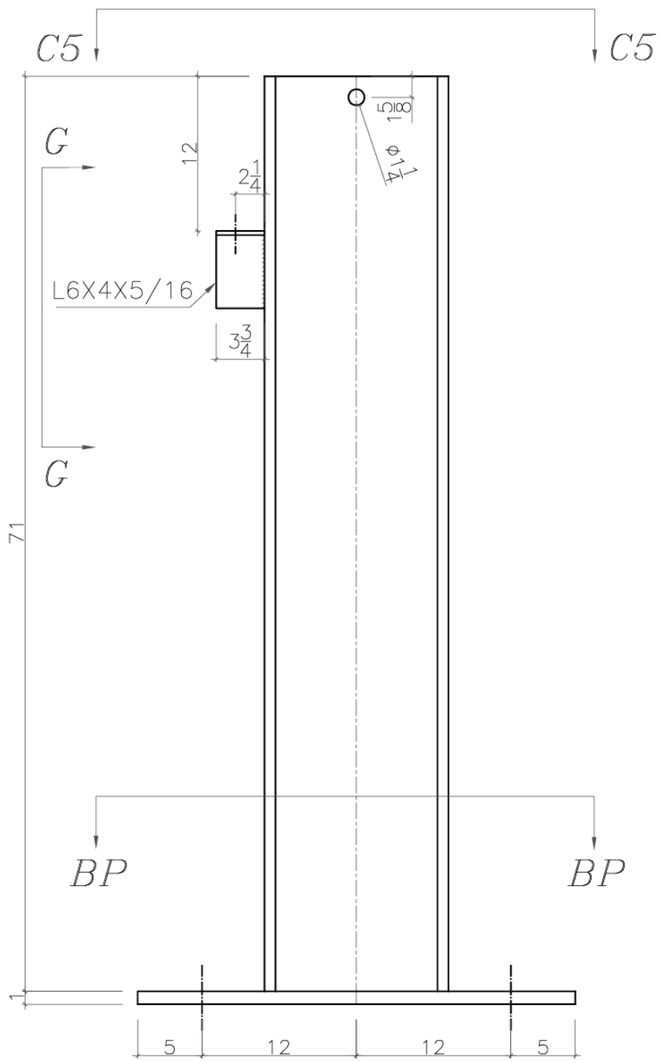

COLUMN 5 – W14X82

Scale 1:20

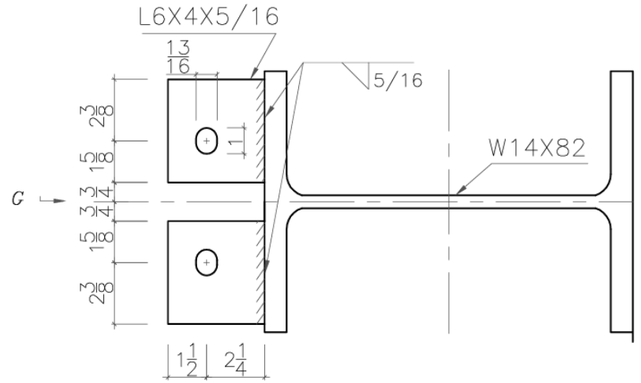

VIEW C5–C5

Scale 1:5

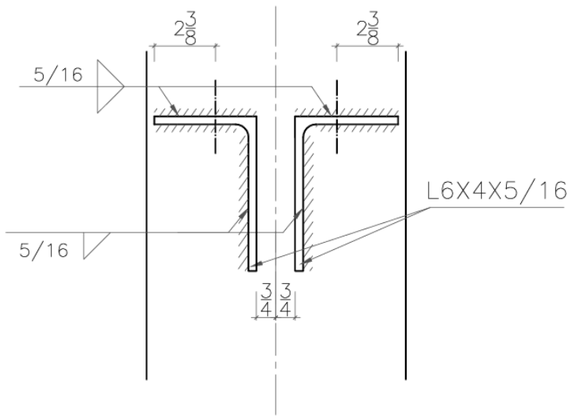

VIEW G–G

Scale 1:5

AUBURN UNIVERSITY
ADVANCED STRUCTURAL ENGINEERING LAB

PROJECT: AISC SPEED CONNECT: DROP-IN TOP FLANGE CONNECTION

Drawing Title: COLUMN 5

DATE: DECEMBER 2024	DRAWING No.
DESIGNED BY R.A & E.D	6 of 12
DRAWN BY R.A & E.D	
CHECKED BY M.Y & K.S	

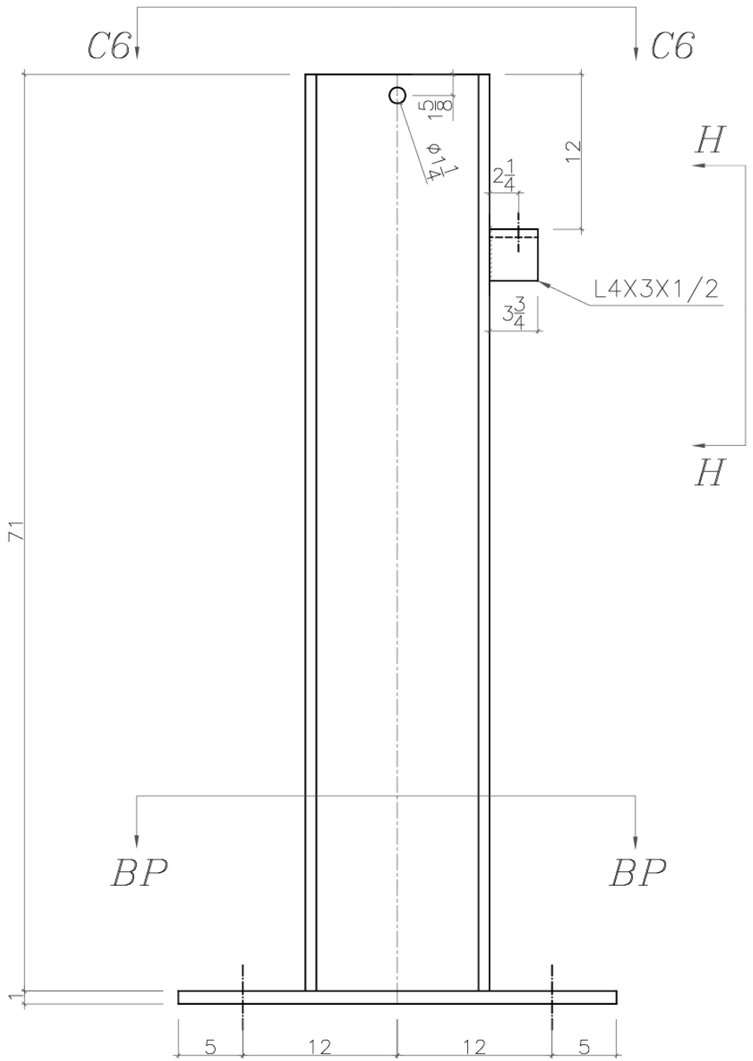

COLUMN 6 – W14X82

Scale 1:10

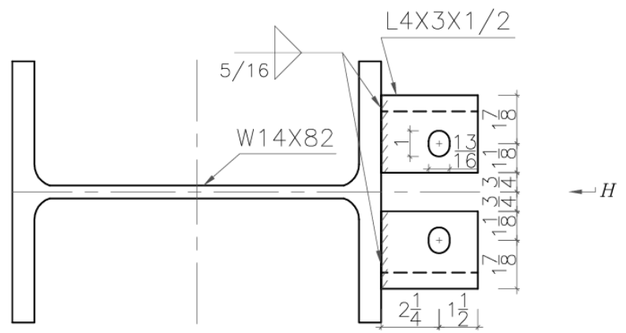

VIEW C6–C6

Scale 1:5

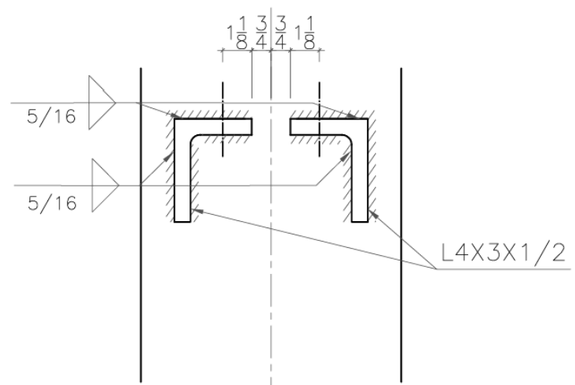

VIEW H–H

Scale 1:5

AUBURN UNIVERSITY ADVANCED STRUCTURAL ENGINEERING LAB	
PROJECT: AISC SPEED CONNECT: DROP–IN TOP FLANGE CONNECTION	
Drawing Title: COLUMN 6	
DATE: DECEMBER 2024	DRAWING No.
DESIGNED BY R.A & E.D	7 of 12
DRAWN BY R.A & E.D	
CHECKED BY M.Y & K.S	

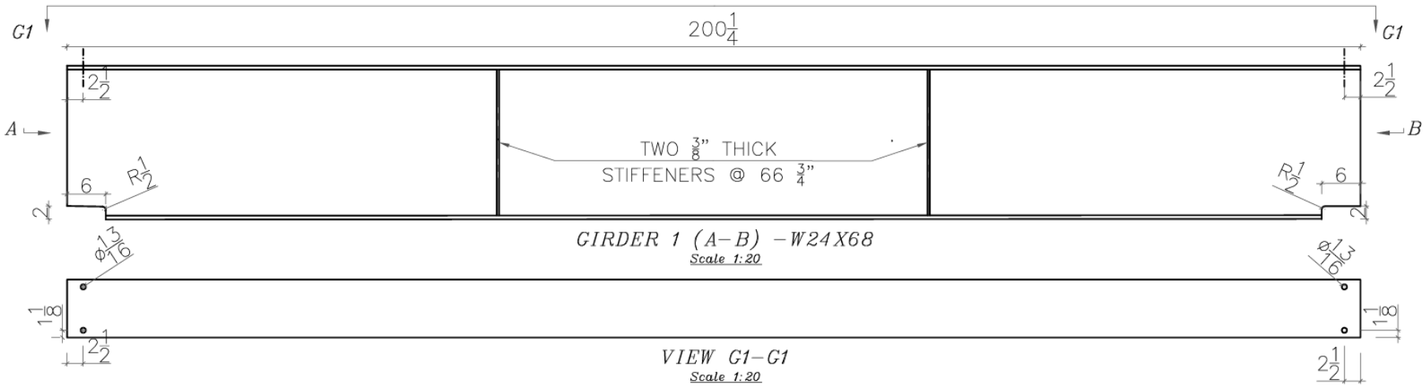

GIRDER 1 (A–B) –W24X68
Scale 1:20

VIEW G1–G1
Scale 1:20

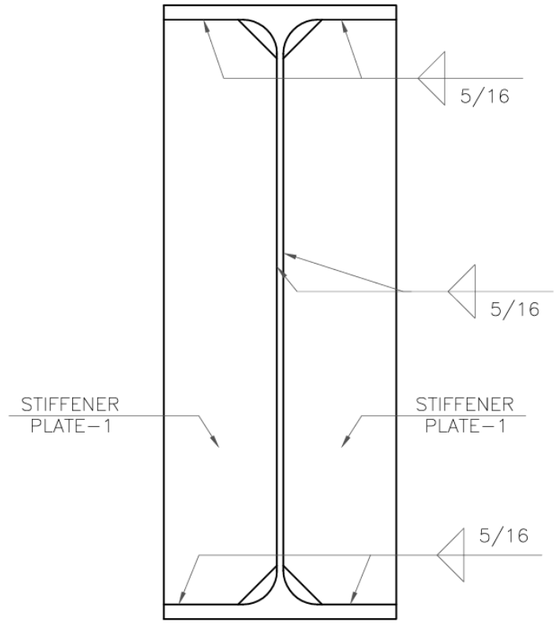

TYPICAL STIFFENER DETAIL FOR BEAMS 1 TO 5
Scale 1:5

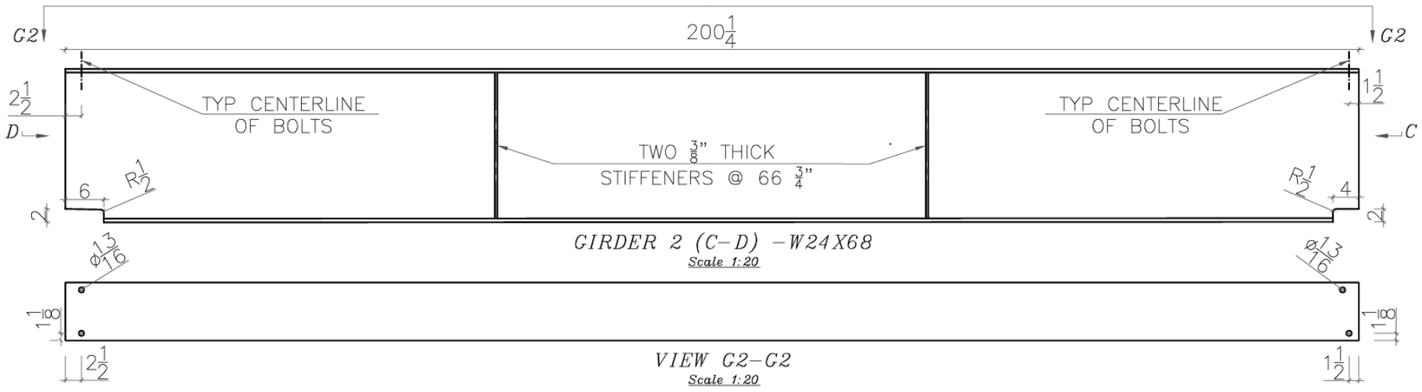

GIRDER 2 (C–D) –W24X68
Scale 1:20

VIEW G2–G2
Scale 1:20

STIFFENER PLATE–1
(20 Pcs)
Scale 1:5

AUBURN UNIVERSITY
ADVANCED STRUCTURAL ENGINEERING LAB

PROJECT: AISC SPEED CONNECT: DROP–IN TOP FLANGE CONNECTION

Drawing Title: GIRDERS 1 & 2 AND BEAM STIFFENER DETAIL

DATE: DECEMBER 2024	DRAWING No.
DESIGNED BY R.A & E.D	8 of 12
DRAWN BY R.A & E.D	
CHECKED BY M.Y & K.S	

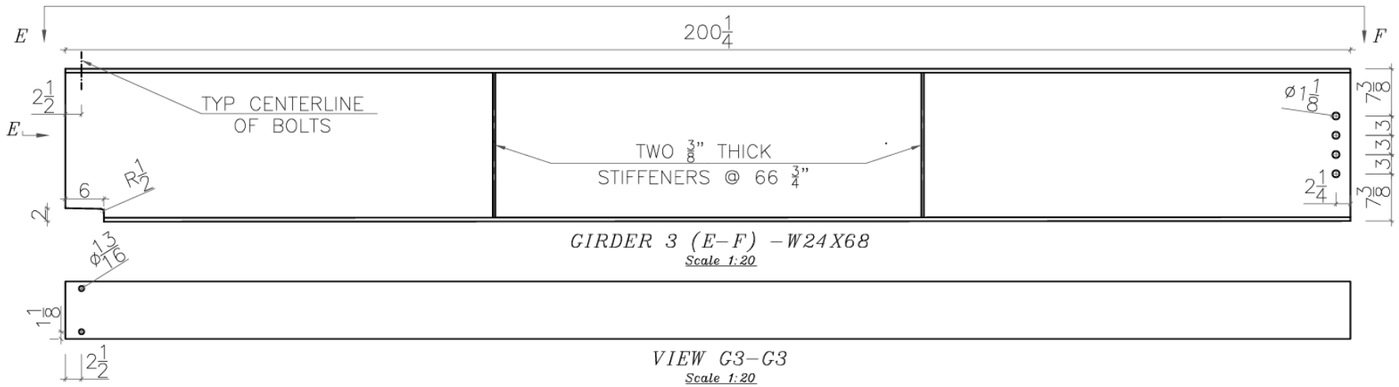

GIRDER 3 (E–F) –W24X68

Scale 1:20

VIEW G3–G3

Scale 1:20

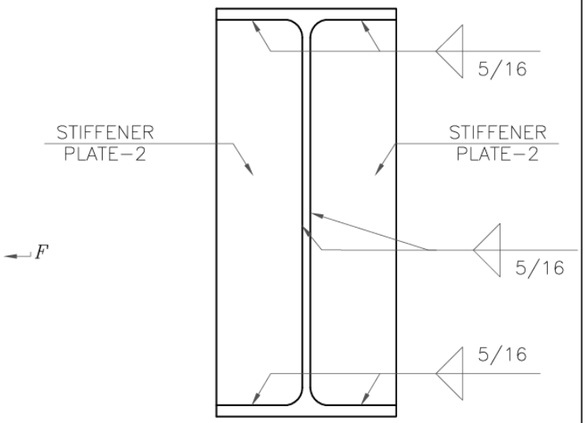

TYPICAL STIFFENER DETAIL
FOR BEAM 6

Scale 1:5

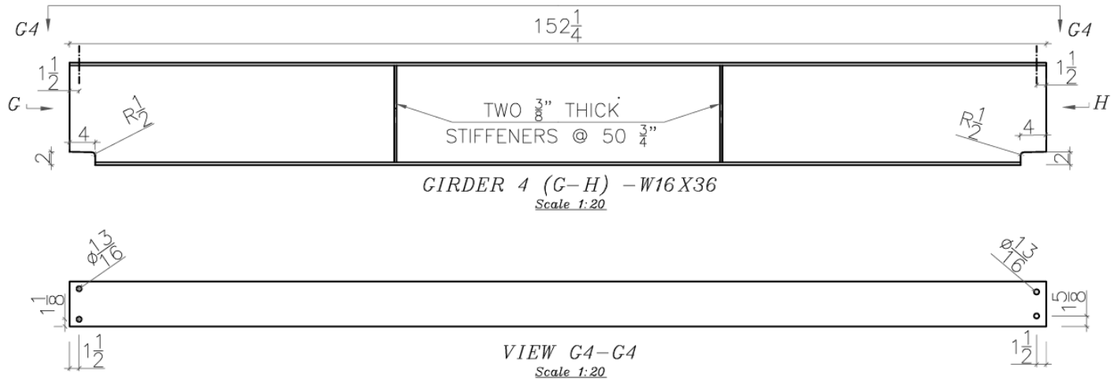

GIRDER 4 (G–H) –W16X36

Scale 1:20

VIEW G4–G4

Scale 1:20

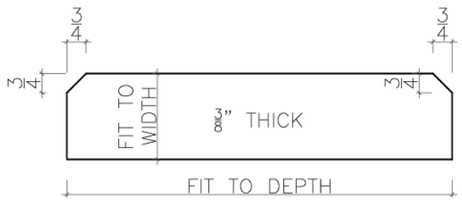

STIFFENER PLATE–2
(4 Pcs)

Scale 1:5

AUBURN UNIVERSITY ADVANCED STRUCTURAL ENGINEERING LAB	
PROJECT: AISC SPEED CONNECT: DROP–IN TOP FLANGE CONNECTION	
Drawing Title: GIRDERS 3 & 4 AND BEAM STIFFENER DETAIL	
DATE: DECEMBER 2024	DRAWING No.
DESIGNED BY R.A & E.D	9 of 12
DRAWN BY R.A & E.D	
CHECKED BY M.Y & K.S	

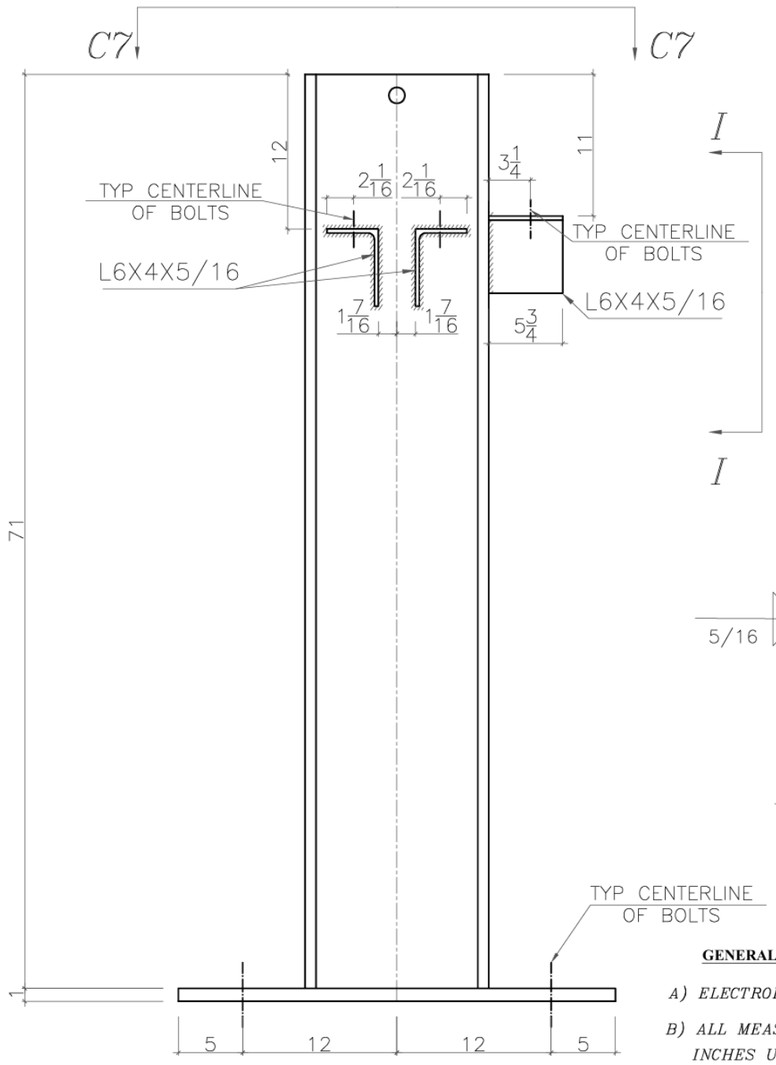

COLUMN 7 – W14X82

Scale 1:10

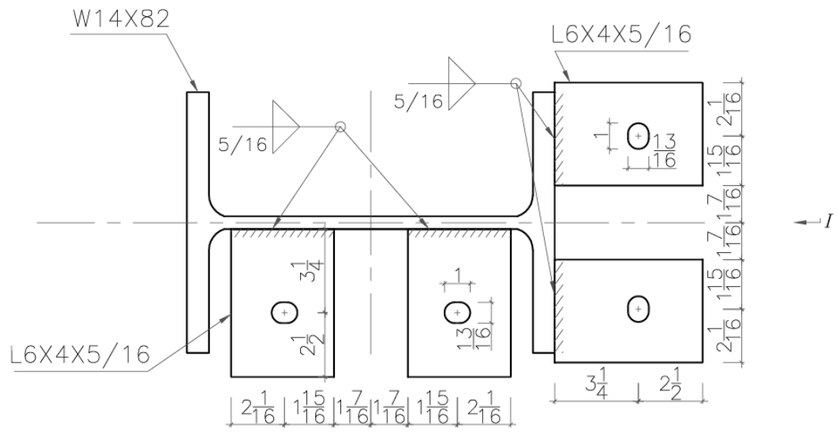

VIEW C7–C7

Scale 1:5

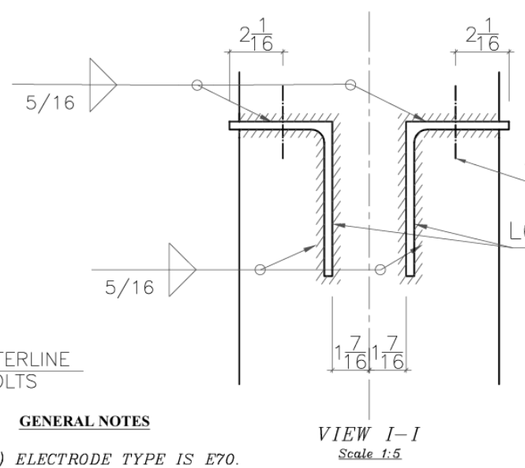

VIEW I–I

Scale 1:5

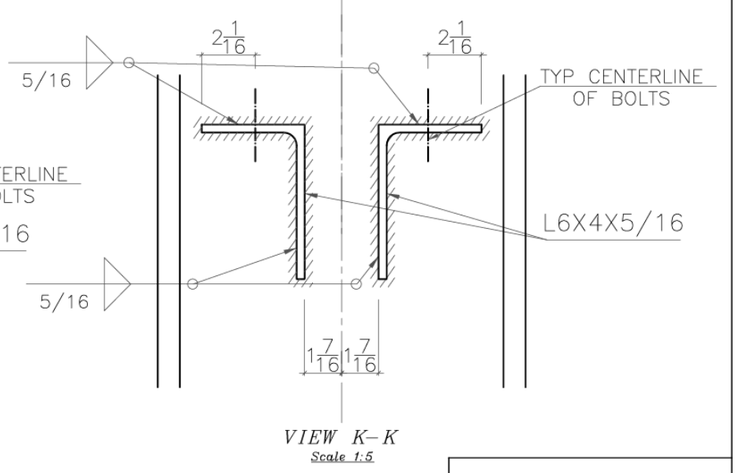

VIEW K–K

Scale 1:5

GENERAL NOTES

A) ELECTRODE TYPE IS E70.

B) ALL MEASUREMENTS ARE IN INCHES UNLESS SPECIFIED.

C) FOR ANGLES WITH UNEQUAL LEGS, THE LONGER LEG IS VERTICAL.

D) ALL STEEL TO BE UNCOATED BARE METAL

AUBURN UNIVERSITY
ADVANCED STRUCTURAL ENGINEERING LAB

PROJECT: AISC SPEED CONNECT: DROP–IN TOP FLANGE CONNECTION

Drawing Title: COLUMN 7

DATE: DECEMBER 2024

DESIGNED BY R.A & E.D

DRAWN BY R.A & E.D

CHECKED BY M.Y & K.S

DRAWING No. 10 of 12

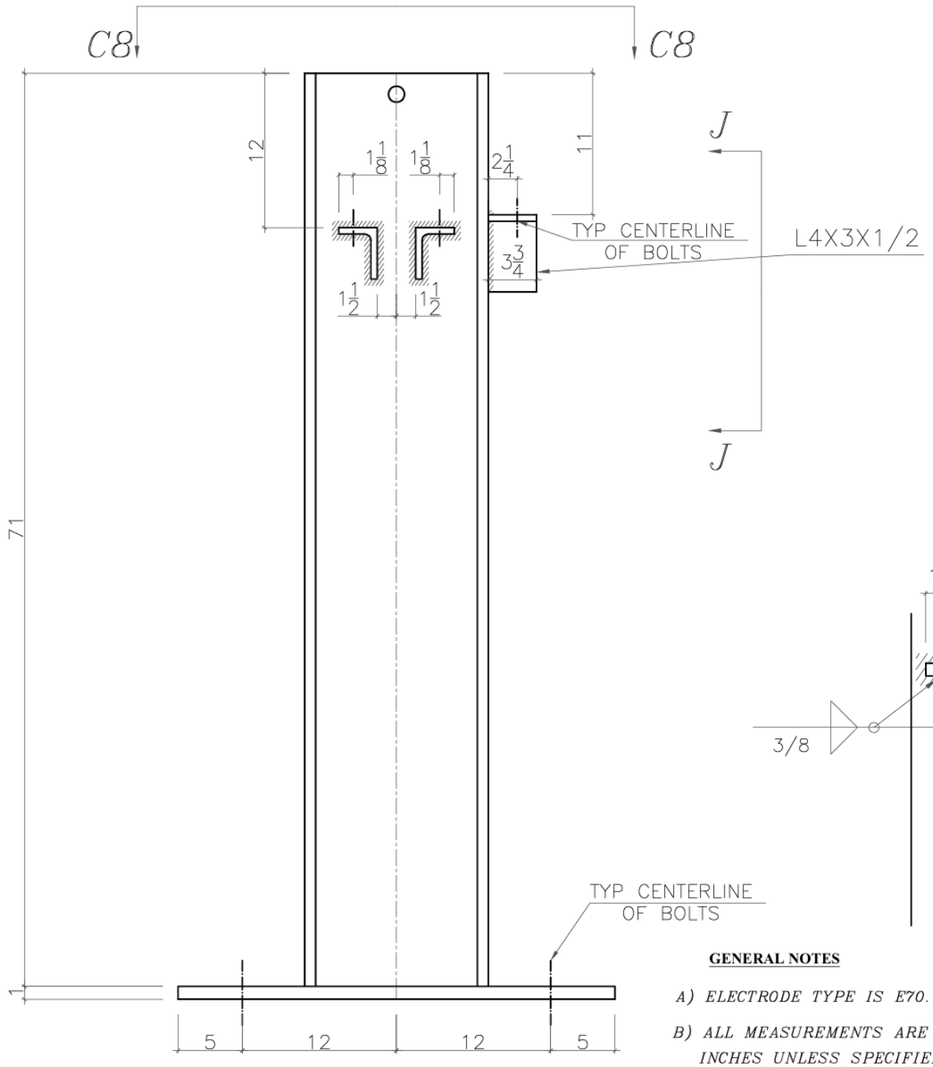

COLUMN 8 – W14X82

Scale 1:10

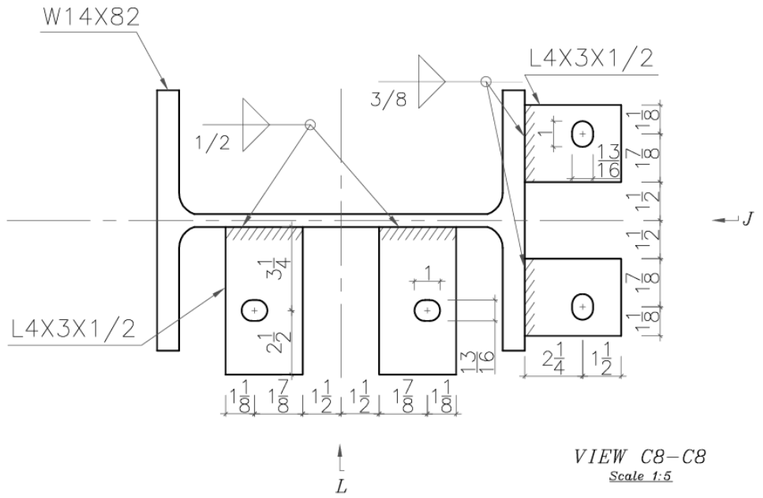

VIEW C8–C8

Scale 1:5

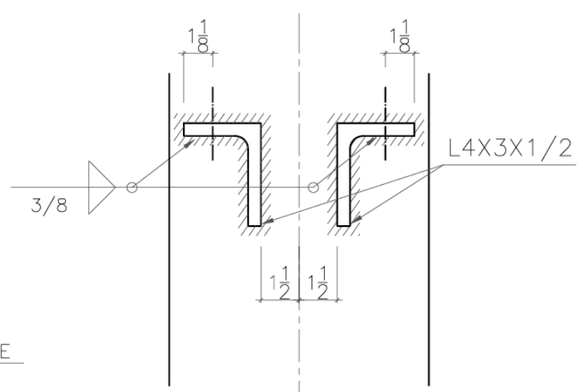

VIEW J–J

Scale 1:5

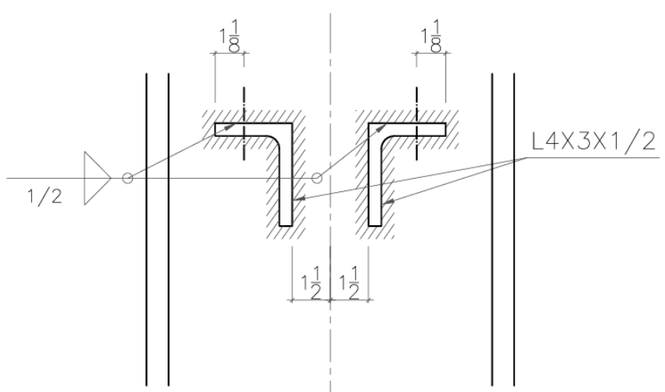

VIEW L–L

Scale 1:5

GENERAL NOTES

A) ELECTRODE TYPE IS E70.

B) ALL MEASUREMENTS ARE IN INCHES UNLESS SPECIFIED.

C) FOR ANGLES WITH UNEQUAL LEGS, THE LONGER LEG IS VERTICAL.

D) ALL STEEL TO BE UNCOATED BARE METAL

AUBURN UNIVERSITY

ADVANCED STRUCTURAL ENGINEERING LAB

PROJECT: AISC SPEED CONNECT: DROP–IN TOP FLANGE CONNECTION

Drawing Title: COLUMN 8

DATE: DECEMBER 2024

DESIGNED BY R.A & E.D

DRAWN BY R.A & E.D

CHECKED BY M.Y & K.S

DRAWING No. 11 of 12

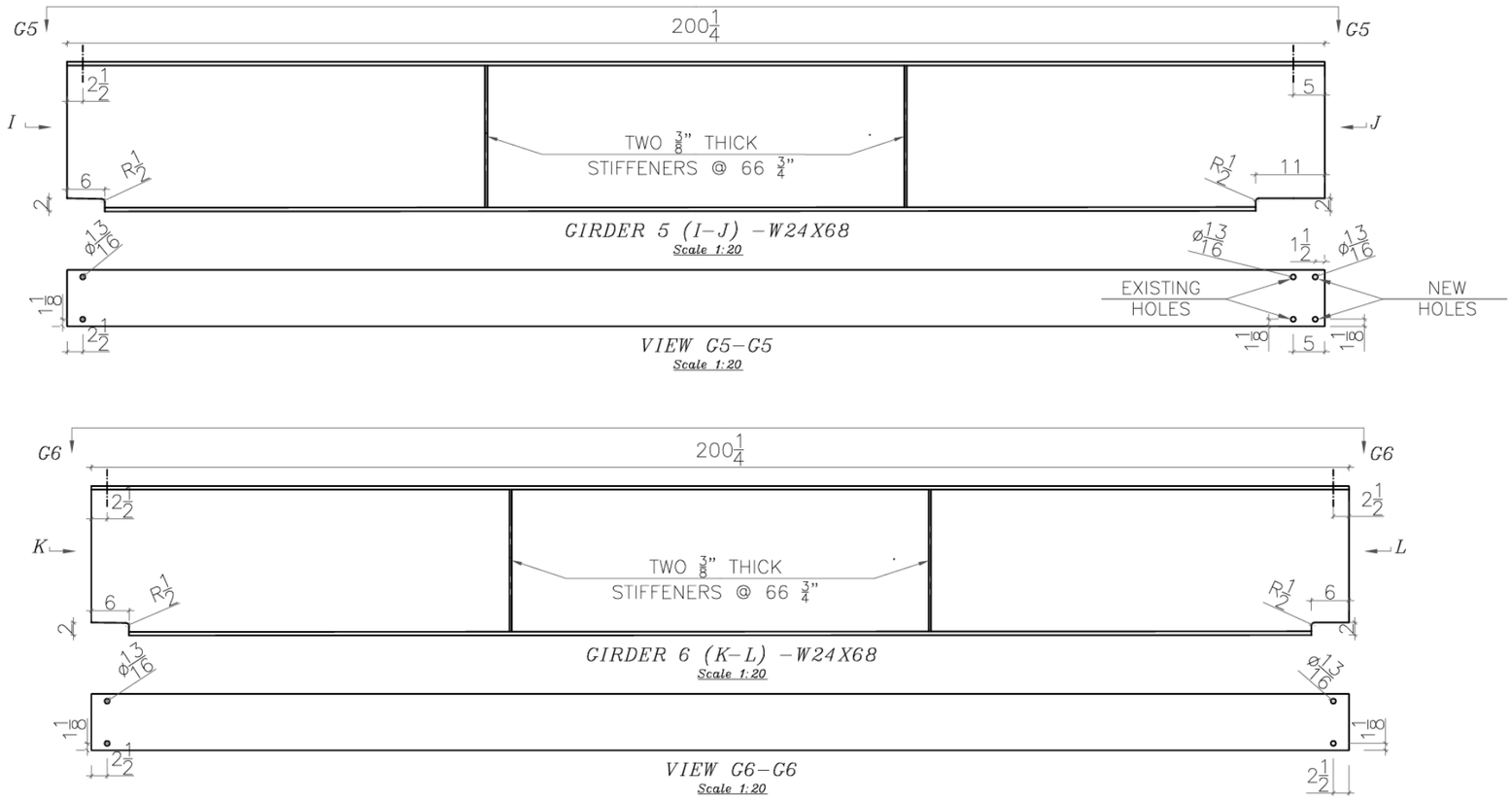

GENERAL NOTES

A) ALL STEEL MEMBERS ARE ASTM A992 STEEL.

B) ALL BOLTS ARE ASTM F3125 GRADE A325 (THREADS EXCLUDED FROM THE SHEAR PLANE).

C) ELECTRODE TYPE IS E70.

D) ALL MEASUREMENTS ARE IN INCHES UNLESS SPECIFIED.

E) FOR ANGLES WITH UNEQUAL LEGS, THE LONGER LEG IS VERTICAL.

F) ALL STEEL TO BE UNCOATED BARE METAL

AUBURN UNIVERSITY
ADVANCED STRUCTURAL ENGINEERING LAB

PROJECT: AISC SPEED CONNECT: DROP-IN TOP FLANGE CONNECTION

Drawing Title: GIRDERS 5 & 6

DATE: DECEMBER 2024	DRAWING No.
DESIGNED BY R.A & E.D	12 of 12
DRAWN BY R.A & E.D	
CHECKED BY M.Y & K.S	

Appendix 2: Mill Test Reports

Mill Test Report - Cover Sheet

Siskin Order No.
600477H

FROM: SISKIN STEEL & SUPPLY CO., INC. - NASHVILLE

SOLD TO
AMERICAN INSTITUTE OF STEEL
130 E RANDOLPH ST STE 2000
CHICAGO IL 60601

CONSIGNED TO
NORTH ALABAMA FAB CO. (NAFCC
1540 COUNTY RD 222
DEVIN HUBER 312.848.1961
CULLMAN, AL 35057

Customer Order No.
ENG090123A

Date Shipped	Account No.
20230918	103500

Thank You for Your Business

See Us For All Of Your Metal Needs

Heat numbers shown below subject to change at time of shipment.

Line Number	Quantity	Code	Description	Weight	Heat Numbers
005	2	177104	W 14" X 82# A572/A992 40' HT# 58057418	6560.00	58057418
010	3	180994	W 24" X 68# A572/A992 40' HT# 59113023 SAW TABLE	8160.00	59113023
015	1	132004	L 8 X 4 X 3/4" A572 40' HT# 55083511 SAW TABLE	1148.00	55083511
020	1	129504	L 4 X 3 X 1/2" A36/50 40' HT# 63224054 SAW TABLE	444.00	63224054

GERDAU

US-MI-CARTERSVILLE
384 OLD GRASSDALE ROAD NE
CARTERSVILLE, GA 30121
USA

CERTIFIED MATERIAL TEST REPORT

Page 1 / 1

CUSTOMER SHIP TO	CUSTOMER BILL TO	GRADE GGM50LTI	SHAPE / SIZE Angle / 8X6X3/4	DOCUMENT ID 0000608999
		LENGTH 40'00"	WEIGHT 9,184 LB	HEAT / BATCH 5508351I/02
SALES ORDER 1299833/0000060	CUSTOMER MATERIAL N°	SPECIFICATION / DATE or REVISION ASTM A529-14, A572-15 ASTM A6-17,A36-14, ASME SA-36 ASTM A709-18, AASHTO M270-15 CSA G40 20-13/G40 21-13		
CUSTOMER PURCHASE ORDER NUMBER GA-656762	BILL OF LADING 1323-0000237488	DATE 05/26/2023		

CHEMICAL COMPOSITION												
C (%)	Mn (%)	P (%)	S (%)	Si (%)	Cu (%)	Ni (%)	Cr (%)	Mo(%)	V (%)	Nb (%)	N (%)	CEqvA6 (%)	Sn (%)
0.09	0.96	0.017	0.027	0.22	0.26	0.10	0.14	0.031	0.001	0.027	0.0093	0.31	0.012

MECHANICAL PROPERTIES					
Elong (%)	G/L (inches)	UTS (PSI)	UTS (MPa)	YS 0.2% (PSI)	YS (MPa)
26.50	8.000	79080	517	53700	370
25.70	8.000	75660	521	55500	383

COMMENTS / NOTES

This grade meets the requirements for the following grades.
ASTM Grades A36, A529-50, A572-50, A709-36, A709-50
CSA Grades 44W, 50W
AASHTO Grades M270-36, M270-50
ASME Grades SA36

Gerdau's steel is 100% recyclable. Support the circular economy through our Metals Recycling Partnership. For details, visit www2.gerdau.com/metals-recycling, or contact metalsrecycling@gerdau.com.

The above figures are certified chemical and physical test records as contained in the permanent records of the company. We certify that these data are correct and in compliance with specified requirements. No weld repair was performed on this material. The material has not been in contact with mercury while in Gerdau possession. For all products other than billets or beam blanks, this material was produced (Electric Arc Furnace, Melted, Continuously Cast, Hot Rolled and, if applicable, Cold-Drawn) in the USA. For billets or beam blanks, this material was produced (Electric Arc Furnace, Melted and Continuously Cast) in the USA. CMTR complies with EN 10204 3.1.

BHASKAR YALAMANCHILI
QUALITY DIRECTOR
Phone (469) 267-1071 Email: Bhaskar.Yalamanchili@gerdau.com

YAN WANG
QUALITY ASSURANCE MGR.
Phone (770) 387 5718 Email: yan.wang@gerdau.com

Customer Name
SISKIN STEEL & SUPPLY CO INC

Customer PO#
N6004477-B

Shipper No
2217549

Heat Number
5508351I

Heat: 5508351I CustPO: ENG090123A Page 1 of 1
10350O AMERICAN INSTITUTE OF STEEL 6004477H 600477

Customer Name	Customer PO#	Shipper No	Heat Number
SISKIN STEEL & SUPPLY CO INC	N600477-B	2217550	58057418

CERTIFIED MATERIAL TEST REPORT

GERDAU

US-ML-MIDLOTHIAN
300 WARD ROAD
MIDLOTHIAN, TX 76065
USA

CUSTOMER SHIP TO	CUSTOMER BILL TO	GRADE	SHAPE / SIZE	DOCUMENT ID
		A992/A572-50	Wide Flange Beam / 14 X 82# / 360 X 122	0000956290

LENGTH	PCS	WEIGHT	HEAT / BATCH
49'00"	3	9,840 LB	58057418/04

SALES ORDER	CUSTOMER MATERIAL N°	SPECIFICATION / DATE or REVISION
133346200/000010		ASTM A6-17 ASTM A709-21 GR50 ASTM A992-20, A572-21 CSA G40.21-13 345W54, 50W

CUSTOMER PURCHASE ORDER NUMBER	BILL OF LADING	DATE
GA-663656	1327-0000545721	09/12/2023

CHEMICAL COMPOSITION	C (%)	Mn (%)	P (%)	S (%)	Si (%)	Cu (%)	Ni (%)	Cr (%)	Mo(%)	Sn (%)	V (%)	Nb (%)	Al (%)	CEqvA6 (%)
	0.68	0.98	0.017	0.038	0.23	0.34	0.09	0.16	0.019	0.005	0.002	0.021	0.001	0.30

MECHANICAL PROPERTIES	UTS (PSI)	YS (MPa)	UTS (MPa)	Y/T rati (%)	G/L (inches)	G/L (mm)	Elong (%)
YS 0.2% (PSI)	70828	367	488	0.750	8.000	200.0	24.60
53265	71376	379	492	0.770	8.000	200.0	24.70
54957							

COMMENTS / NOTES

Gerdau's steel is 100% recyclable. Support the circular economy through our Metals Recycling Partnership. For details, visit www2.gerdau.com/metals-recycling, or contact metalsrecycle@gerdau.com.

The above figures are certified chemical and physical test records as contained on the permanent records of the company. We certify that these data are correct and in compliance with specified requirements. No weld repair was performed on this material. The material has not been in contact with mercury while at Gerdau possession. For all products other than billets or beam blanks, this material was produced (Electric Arc Furnace, Melted, Continuously Cast, Hot Rolled and, if applicable, Cold-Drawn) in the USA. For billets or beam blanks, this material was produced (Electric Arc Furnace, Melted and Continuously Cast) in the USA. CMTR complies with EN 10204 3.1.

BHASKAR VALAVANDHELI
QUALITY DIRECTOR
Phone: (469) 267-1071 Email: Bhaskar.Valavandhli@gerdau.com

WADE LUMPKINS
QUALITY ASSURANCE MGR.
Phone: 972-779-5118 Email: Wade.Lumpkins@gerdau.com

Heat: 59113023 CustPO: ENG090123A Page 1 of 1
103500 AMERICAN INSTITUTE OF STEEL 600477H 600477

Heat Number 59113023

Shipper No 2217549

Customer PO# N600477-B

Customer Name SISKIN STEEL & SUPPLY CO INC

Page 1 / 1

CERTIFIED MATERIAL TEST REPORT

GERDAU

US-ML-MIDLOTHIAN
300 WARD ROAD
MIDLOTHIAN, TX 76065
USA

CUSTOMER SHIP TO	CUSTOMER BILL TO	GRADE	SHAPE / SIZE	DOCUMENT ID
		A992/A572-50	Wide Flange Beam / 24 X 68# / 610 X 101	0000987562

LENGTH	PCS	WEIGHT	HEAT / BATCH
40'00"	3	8,160 LB	59113023/02

SALES ORDER	CUSTOMER MATERIAL N°	SPECIFICATION / DATE or REVISION
1328496/7030040		ASTM A6-17 ASTM A709-21 GR50 ASTM A992-20, A572-21 CSA G40.21-13 345W/A, 50W

CUSTOMER PURCHASE ORDER NUMBER	BILL OF LADING	DATE
GA-662574	1327-0000542912	08/22/2023

CHEMICAL COMPOSITION

C (%)	Mn (%)	P (%)	S (%)	Si (%)	Cu (%)	Ni (%)	Cr (%)	Mo(%)	Sn (%)	V (%)	Nb (%)	CEqvA6 (%)
0.07	0.97	0.012	0.036	0.19	0.28	0.10	0.17	0.025	0.006	0.002	0.021	0.30

MECHANICAL PROPERTIES

YS 0.2% (PSI)	UTS (PSI)	YS (MPa)	UTS (MPa)	Y/T ratio (%)	G/L (inches)	G/L (mm)	Elong. (%)
56314	72288	388	499	0.780	8.000	200.0	23.40
55326	72452	383	500	0.770	8.000	200.0	23.90

COMMENTS / NOTES

Gerdau's steel is 100% recyclable. Support the circular economy through our Metals Recycling Partnership. For details, visit www2.gerdau.com/metals-recycling, or contact metalsrecycling@gerdau.com.

The above figures are certified chemical and physical test records as contained in the permanent records of the company. We certify that these data are correct and in compliance with specified requirements. No weld repair was performed on this material. The material has not been in contact with mercury while at Gerdau possession. For all products other than billets or beam blanks, this material was produced (Electric Arc Furnace, Melted, Continuously Cast, Hot Rolled and, if applicable, Cold-Drawn) in the USA. For billets or beam blanks, this material was produced (Electric Arc Furnace, Melted and Continuously Cast) in the USA. CMTR complies with EN 10204 3.1

BHASKAR YALAMANCHILI
QUALITY DIRECTOR
Phone (469) 267-1071 Email: Bhaskar.Yalamanchili@gerdau.com

WADE LUMPKINS
QUALITY ASSURANCE MGR
Phone: 972-779-5118 Email: Wade.Lumpkins@gerdau.com

Heat: 63224054 CustPO: ENG090123A Page 1 of 1
10350O AMERICAN INSTITUTE OF STEEL 600477H 553036

Customer Name SISKIN STEEL & SUPPLY CO INC

Customer PO# N553036-B

Shipper No 2164720

Heat Number 63224054

GERDAU

US-MI-JACKSON TN
801 GERDAU AMERISTEEL ROAD
JACKSON, TN 38305
USA

CERTIFIED MATERIAL TEST REPORT

Page 1 / 1

CUSTOMER SHIP TO	CUSTOMER BILL TO	GRADE G63MULTI	SHAPE / SIZE Angle / 4X3X1/2	DOCUMENT ID: 0000528445
		LENGTH 40'00"	WEIGHT 9,768 LB	HEAT / BATCH 63224054/04
SALES ORDER 128124/4000070	CUSTOMER MATERIAL N°	SPECIFICATION / DATE or REVISION ASTM A529-14, A572-15 ASTM A6-17,A36-19, ASME SA-36 ASTM A709-18, AASHTO M270-15 CSA G40.20-13/G40 21-13		
CUSTOMER PURCHASE ORDER NUMBER GA-652932	BILL OF LADING 1333-0000212291	DATE 03/27/2023		

CHEMICAL COMPOSITION													
C (%)	Mn (%)	P (%)	S (%)	Si (%)	Cu (%)	Ni (%)	Cr (%)	Mo(%)	V (%)	Nb (%)	Al (%)	CEqvA29 (%)	Sn (%)
0.13	0.70	0.013	0.025	0.22	0.34	0.11	0.19	0.030	0.003	0.006	0.001	0.36	0.017

MECHANICAL PROPERTIES					
Elong. (%)	G/L (inches)	G/L (mm)	UTS (PSI)	UTS (MPa)	YS (PSI)	YS (MPa)
28.00	8.000	200.0	72836	502	54460	376
30.00	8.000	200.0	74131	511	55645	384

GEOMETRIC CHARACTERISTICS
R R
934

COMMENTS / NOTES

This grade meets the requirements for the following grades
ASTM Grades A36, A529-50, A572-50, A709-36, A709-50
CSA Grades 44W, 50W
AASHTO Grades M270-36, M270-50
ASME Grades SA36

The above figures are certified chemical and physical test records as contained in the permanent records of the company. We certify that these data are correct and in compliance with specified requirements. No weld repair was performed on this material. The material has not been in contact with mercury while at Gerdau possession. For all products other than billets or beam blanks, this material was produced (Electric Arc Furnace, Melted, Continuously Cast, Hot Rolled and, if applicable, Cold-Drawn) in the USA. For billets or beam blanks, this material was produced (Electric Arc Furnace, Melted and Continuously Cast) in the USA. CMTR complies with EN 10204 3.1

BHASKAR YALAMANCHILI
QUALITY DIRECTOR
Phone (469) 267-1071 Email: Bhaskar.Yalamanchili@gerdau.com

BEN LOVELL
QUALITY ASSURANCE MGR.
Phone (731) 423-5213 Email: benjamin.lovell@gerdau.com

Mill Test Report - Cover Sheet

Siskin Order No.
600480

FROM: SISKIN STEEL & SUPPLY CO., INC. - NASHVILLE

SOLD TO

AMERICAN INSTITUTE OF STEEL
130 E RANDOLPH ST STE 2000

CHICAGO IL 60601

CONSIGNED TO

NORTH ALABAMA FAB CO. (NAFCC
1540 COUNTY RD 222
DEVIN HUBER 312.848.1961
CULLMAN, AL 35057

Customer Order No.
ENG090123A

Date Shipped	Account No.
20230918	103500

Thank You for Your Business

See Us For All Of Your Metal Needs

Heat numbers shown below subject to change at time of shipment.

Line Number	Quantity	Code	Description	Weight	Heat Numbers
005	2	448576	A572 GR.50 HSLA(YELLOW)TYPE2 1" X 48 X 96	2614.00	M3D825
010	1	443576	A572 GR.50 HSLA (YELLOW) TYPE2 3/8" X 48 X 96	490.00	23B4757

Heat: 23B4757 CustPO: ENG090123A Page 1 of 1
103500 AMERICAN INSTITUTE OF STEEL 600480 133840

NUCOR®

NUCOR STEEL TUSCALOOSA, INC.

MILL TEST CERTIFICATE

Nucor Steel Tuscaloosa, Inc.
1700 HOLT RD N.E.
Tuscaloosa, AL 35404-1000 USA
800 800-8204
customerservice@nucortusk.com

Load Number	Tally	Mill Order Number	PO NO | Line NO	Part Number	Certificate Number	Prepared
T331185	00000001139319	N-204771-001	N133840-S 1	443576.	S13931901-1	08/21/2023 14:19

Grade

Order Description:
Hot Roll Plate From Coil
A572 50, 0.3750 IN x 96.000 IN x 240.000 IN
Quality Plan Description:
A57250T2/A70950: ASTM A572-15 GR 50T2/A709-15 GR 50T2/M270-50

Customer:

Sold TO:
SISKIN STEEL AND SUPPLY CO INC Nashville TN
Ship TO:
SISKIN STEEL & SUPPLY CO., INC. NASHVILLE TN
Sent TO:

Shipped Item	Heat/Slab Number	Certified By	C	Mn	P	S	Si	Cu	Ni	Cr	Mo	Cb	V	Al	Ti	N2	B	Ca	Sn	CEV	ACI
3H0821C	23B4757-05 ***	23B4757	0.05	1.15	0.010	0.002	0.06	0.23	0.05	0.07	0.017	0.002	0.041	0.030	0.002	0.006	0.0002	0.0018	0.007	0.29	
3H0821D	23B4757-05 ***	23B4757	0.05	1.15	0.010	0.002	0.06	0.23	0.05	0.07	0.017	0.002	0.041	0.030	0.002	0.006	0.0002	0.0018	0.007	0.29	

Shipped Item	Certified By	Heat/Slab Number	Yield ksi	Tensile ksi	Y/T %	ELONGATION % 2"	8"	Bend OK?	Hard HB	Charpy Impacts (ft-lbs) Size mm	1	2	3	Avg	Shear % 1	2	3	Avg	Test Temp
3H0821C	S3H0821FTT	23B4757-05 ***	64.5	76.0	84.9	31.8													
3H0821C	S3H0821MTT	23B4757-05 ***	69.5	79.4	87.5	30.2													
3H0821D	S3H0821FTT	23B4757-05 ***	64.5	76.0	84.9	31.8													
3H0821D	S3H0821MTT	23B4757-05 ***	69.5	79.4	87.5	30.2													

Items: 2 PCS: 10 Weight: 24503 LBS

Mercury has not come in contact with this product during the manufacturing process nor has any mercury been used by the manufacturing process. Certified in accordance with EN 10204 3.1. No weld repair has been performed on this material. Yield strength is determined by the 0.2% offset method unless otherwise noted. Manufactured to a fully killed fine grain practice.
NUTEMPER TEMPER PASSED plate from coil
ISO 9001:2015 Registered, PED Certified

"***" indicates Heats melted and Manufactured in the U.S.A.

We hereby certify that the product described above passed all of the tests required by the specifications.

Jon Walton - Metallurgist

Heat: M3D825 CustPO: ENG090123A Page 1 of 1
103500 AMERICAN INSTITUTE OF STEEL 600480 130191

SSAB

12400 Highway 43 North, Axis, Alabama 36505, US

Test Certificate

Form TC1: Revision 4: Date 6 Feb 2019

Customer:
SISKIN STEEL & SUPPLY CO.
1901 RIVERFRONT PARKWAY
BOX 1191
CHATTANOOGA
TN 37401

Customer P.O. No.: C 130191-S
Mill Order No.: 41-706553-19
Shipping Manifest : AT378730
Product Description: ASTM A572-50/M345(21)/A709-50/M345(21) TYPE 2
Ship Date: 02 May 23
Cert Date: 02 May 23
Cert No: 081109769
(Page 1 of 1)
Size: 1.000 X 96.00 X 240.0 (IN)

Tested Pieces				Tensiles						Charpy Impact Tests									
Heat Id	Piece Id	Tested Thickness	Tst Loc	YS (KSI)	UTS (KSI)	%RA	Elong % 2in 8in	Tst Dir	Hardness	Abs. Energy(FTLB) 1 2 3 Avg				% Shear 1 2 3 Avg				Tst Tmp	Tst Dir	Tst Siz (mm)	BDWTT Tmp %Shr
M3D825	A13	0.999 (DISCRT)	L	58	78		45	T													

Chemical Analysis

Heat Id	C	Mn	P	S	Si	Tot Al	Cu	Ni	Cr	Mo	Cb	V	Ti	N	IIW	ORGN
M3D825-A13	.17	1.03	.009	.002	.19	.023	.28	.10	.10	.03	.000	.025	.001	.0061	.39	USA

KILLED STEEL
MERCURY IS NOT A METALLURGICAL COMPONENT OF THE STEEL AND NO MERCURY WAS INTENTIONALLY ADDED DURING THE MANUFACTURE OF THIS PRODUCT.
CEV (IIW) = C + MN/6 + (CR+MO+V)/5 + (NI+CU)/15
MTR EN 10204:2004 INSPECTION CERTIFICATE 3.1 COMPLIANT
100% MELTED, POURED, AND ROLLED IN THE USA
PRODUCTS SHIPPED:
M3D825 A13 PCES: 6, LBS: 39204

(P) Cust Part # : 448576

WE HEREBY CERTIFY THAT THIS MATERIAL WAS TESTED IN ACCORDANCE WITH, AND MEETS THE REQUIREMENTS OF, THE APPROPRIATE SPECIFICATION

Jason Thomas
Director Technical Services

Mill Test Report - Cover Sheet

Siskin Order No.
600483

FROM: SISKIN STEEL & SUPPLY CO., INC. - NASHVILLE

SOLD TO

AMERICAN INSTITUTE OF STEEL
130 E RANDOLPH ST STE 2000

CHICAGO IL 60601

CONSIGNED TO

NORTH ALABAMA FAB CO. (NAFCC
1540 COUNTY RD 222
DEVIN HUBER 312.848.1961
CULLMAN, AL 35057

Customer Order No.
ENG090123A

Date Shipped	Account No.
20230918	103500

Thank You for Your Business

See Us For All Of Your Metal Needs

Heat numbers shown below subject to change at time of shipment.

Line Number	Quantity	Code	Description	Weight	Heat Numbers
005	1	177794	W 16" X 36# A572/A992 20' 0" AS IS LOC D7	720.00	A224376
010	1	130504	L 8 X 4 X 1/2" A36/572 40'	784.00	577210
015	1	126204	L 6 X 4 X 5/16" A36 40' MEETS A572 GR50	412.00	1087377

Heat: 1087377 CustPO: ENG090123A Page 1 of 1
103500 AMERICAN INSTITUTE OF STEEL 600483 974252

CMC STEEL ALABAMA
101 S 50TH STREET
BIRMINGHAM AL 35212-3525

CERTIFIED MILL TEST REPORT
For additional copies call
800-637-3227

We hereby certify that the test results presented here are accurate and conform to the reported grade specification

Marcus W. McCluney - CMC Steel AL
Quality Assurance Manager

1SERIES-BPS ®

HEAT NO.:1087377 SECTION: ANG 6 X 4x5/16 40'0" A36/52950 GRADE: ASTM A36-19/A529-19 Gr 50 ROLL DATE: 07/16/2023 MELT DATE: 07/07/2023 Cert. No.: 85519984 / 087377B236	SOLD TO	Siskin Steel & Supply 1901 RIVERFRONT PKWY CHATTANOOGA TN US 37408-1037 4237563671 4237562734	SHIP TO	Siskin Steel & Supply Co 4040 Jordonia Rd Nashville TN US 37218-0000 6152424444	Delivery#: 85519984 BOL#: 75518580 CUST PO#: 974252 CUST P/N: 126204 DLVRY LBS / HEAT: 9888.000 LB DLVRY PCS / HEAT: 24 EA

Characteristic	Value
C	0.14%
Mn	0.67%
P	0.019%
S	0.022%
Si	0.16%
Cu	0.37%
Cr	0.22%
Ni	0.13%
Mo	0.037%
V	0.004%
Cb	0.012%
Sn	0.011%
B	0.0003%
Ti	0.001%
N	0.0077%
Carbon Eq A6	0.34%
Carbon Eq A529	0.37%
Yield Strength test 1	57.9ksi
Tensile Strength test 1	75.9ksi

Characteristic	Value
Elongation test 1	25%
Elongation Gage Lgth test 1	8IN
Yield to tensile ratio test1	0.76
Yield Strength test 2	57.8ksi
Tensile Strength test 2	76.2ksi
Elongation test 2	25%
Elongation Gage Lgth test 2	8IN
Yield to tensile ratio test2	0.76

ALABAMA LICENSED PUBLIC WEIGH-MASTER No. 608607 ALABAMA FACTORY STUDIOVANT

The Following is true of the material represented by this MTR:
*Material is fully killed and is Hot Rolled Steel
*100% melted, rolled, and manufactured in the USA
*EN10204:2004 3.1 compliant
*Contains no weld repair
*Contains no Mercury contamination
*Manufactured in accordance with the latest version of the plant quality manual
*Meets the "Buy America" requirements of 23 CFR635.410, 49 CFR 661
*Warning: This product can expose you to chemicals which are known to the State of California to cause cancer, birth defects or other reproductive harm. For more information go to www.P65Warnings.ca.gov

REMARKS : ALSO MEETS ASTM GRADE A36 REV 08, A572-50, A709-36, A709-50, A992, AASHTO GRADE M270-36, M270-50, CSA G40.21-04 GRADE 44W, 50W, ASME SA-36 2008A ADDEND A.

Heat: 577210 CustPO: ENG090123A Page 1 of 1
103500 AMERICAN INSTITUTE OF STEEL 600483 133922

Invoice No.	256747
Bill of Lading	597991
Customer No.	7895
Customer P.O	N0133922-S

NUCOR-YAMATO STEEL CO.

P.O. BOX 1228: BLYTHEVILLE, AR 72316

CERTIFIED MILL TEST REPORT

100% Melted and Manufactured in U.S.A

All Shapes produced by Nucor-Yamato Steel are cast and rolled to a fully killed and fine grain practice

Date: 07/20/2023 5:14 AM

SOLD TO:
SISKIN STEEL & SUPPLY CO., INC.
BOX 1191
1901 RIVERFRONT PKWY
CHATTANOOGA TN 37401
USA

SHIP TO:
SISKIN STEEL & SUPPLY CO., INC.
4040 JORDONIA STATION RD.
NASHVILLE WAREHOUSE
NASHVILLE TN 37218
USA

ASTM A992/A992M-20 A572/A572M GR50-18
ASTM A709/A709M-18 GR50 (345)
ASTM A709/A709M-18 GR50S (345S)
CSA G40.21-13 50WM (345WM)
ASTM A6/A6M-19

Item	Item Description	QTY	Heat#	Mechanical Properties								Chemical Properties														
				Yield to Tensile Ratio	Yield Strength	Tensile Strength	ELONG	Charpy Impact				C	Mn	P	S	Si	Cu	Ni	Cr	Mo	V	Cb	CE	Sn	Pcm	Cl
								Temp	Impact Energy		Loc															
					KSI	KSI	%	°F	ft-lbf																	
					MPa	MPa	%	°C	J																	
1	L08X019.6 L8X4X1/2" 40 ft 0 in L203X29 L203x102x12.7 (12.19 m)	12	577210	0.77	56	73	26					.07	1.10	.012	.027	.24	.27	.14	.14	.05	.00	.017	.32	.01	.16	
				0.77	57	73	26																			
					383	500																				
					390	507																				

ELONGATION BASED ON 8.00 INCH GAUGE LENGTH

Pcm= C+Si/30+Mn/20+Cu/20+Ni/60+Cr/20+Mo/15+V/10+5B(B=Approx .0005)

Corrosion Index= 26.01(%Cu)+3.88(%Ni)+1.2(%Cr)+1.49(%Si)+17.28(%P)-7.29(%Cu)(%Ni)-9.10(%Ni)(%P)-33.39(%Cu)^2

ISO 9001:2015 certified (Registration # 0985-07).

Meets mechanical lab independence requirements of EN10204 type 3.1.

The Charpy machine striker geometry used by Nucor-Yamato Steel is the 8 mm (0.315") striker (KV_8) per ASTM A370 Section 22.1.2 and ISO 148-1 Section 7.3.

CARBON EQUIVALENT CE= C+Mn/6+(Cr+Mo+V)/5+(Ni+Cu)/15

Mercury has not been used in the direct manufacturing of this material

Boron has not been intentionally added and will not exceed 0.0008%

This material was produced in accordance with the Nucor-Yamato Steel Quality Manual.

I hereby certify that the contents of this report are accurate and correct. All test results and operations performed by this material manufacturer are in compliance with the requirements of the material specifications, and when designated by the purchaser, meet the applicable specifications.

Doug Lennell

Chief Metallurgist

State of Arkansas
County of Mississippi
Sworn to and subscribed before me

Amanda Stockman

on 2023-07-20

AMANDA F STOCKMAN
NOTARY PUBLIC - ARKANSAS
MISSISSIPPI COUNTY
My Commission Expires 03-25-2032
Commission # 12397835

Heat: A224376 CustPO: ENG090123A Page 1 of 1
103500 AMERICAN INSTITUTE OF STEEL 600483 129266

Steel Dynamics, Inc.
Long Products Group
Structural and Rail Division
01 S. County Road 700 East
lumbia City, Indiana 46725
30) 625-8100 (260) 625-8950 FAX

CERTIFIED MILL TEST REPORT

Printed: 03 / 01 / 2023
Produced: 02 / 16 / 2023

Ship to:
Siskin Steel & Supply
4040 Jordonia Station Road
Nashville TN, 37218 US
Attn: Receiving

Customer # 000172

Bill to:
Siskin Steel & Supply
1901 Riverfront Parkway
P.O. Box 1191
Chattanooga TN, 37401 US
Attn: Receiving

uality Steel 100% EAF Melted and Manufactured in the USA
O 9001:2015 and ABS Certified
VTR complies with EN 10204 3.1.

GENERAL INFORMATION

Product	Wide Flange Beam
Size	W16X36
	W410X53
Heat Number	A224376
Condition(s)	As-Rolled
	Fine Grained
	Fully Killed
	No Weld Repair

SPECIFICATIONS

Standards	Grades*
ASTM A6/A6M - 21	
» ASTM A992/A992M - 20	A992 / A992M
ASTM A572/A572M - 21	A572 gr50/gr345
ASTM A709/A709M - 21	A709 gr50/gr345
AASHTO M270M/M270 - 20	M270 gr345/gr50
CSA G40.21-13	50WM/345WM
ASTM A36/A36M - 19	A36 / A36M

*SDI-MULTI meets the requirements of ASTM A992, A572-50, A709-50, A529-50, A36 and A709-36; AASHTO M270-50 and M270-36; CSA 300W, 345W and 350W.

SHIPMENT DETAILS

BOL # 0000757889 - 7200.00 lbs

Bundle / ASN #	Length	pcs	Cust PO	Job/Ref	Part/Ref
061826473	40' 0"	5	N 129266-S		

CHEMICAL ANALYSIS (weight percent)

C	Mn	P	S	Si	Cu	Ni	Cr	Mo	Sn	V	Nb/Cb	Al	N	B	*CE1	*CE2	*CE3	*I	Analysis Type
.08	1.27	.015	.022	.23	.31	.10	.14	.04	.015	.034	<.001	.003	.0110	.0003	.36	.400	.32	5.76	Heat

MECHANICAL TESTING

Test	Yield (fy) Strength ksi / MPa	Tensile (fu) Strength ksi / MPa	fy / fu ratio	% Elong. (8" gage)
1	57 / 395	72 / 495	.79	28
2	59 / 405	74 / 510	.79	25
3				
4				

CHARPY IMPACT TESTS (available only when specified at time of order)

Absorbed Energy ft-lbf / J

Test	Temp F / C	Specimen 1	Specimen 2	Specimen 3	Average	Minimum
1						
2						
3						
4						
5						
6						
7						

Notes: *Calculated Chemistry Values: Carbon Equivalents (C1, C2, C3, PC), Corrosion Index (I) (ASTM G101)= 26.01(Cu)+3.88(Ni)+1.20(Cr)+1.49(Si)+17.29(P)-7.29(Cu)(Ni)-9.10(Ni)(P)-33.39(Cu²)
CE1 (IIW)=C+Mn/6+(Cr+Mo+V)/5+(Ni+Cu)/15 CE2 (AWS)=C+(Mn+Si)/6+(Cr+Mo+V)/5+(Ni+Cu)/15 CE3 (CET) = C + (Mn/6) + (Si/24) + (Cr/5) + (Ni/40) +(Mo/4) + (V/14)

hereby certify that the material described herein has been made to the applicable pecification by the electric arc furnace/continuous cast process and tested in accordance ith the requirements of American Bureau of Shipping Rules with satisfactory results.

Signed:

ABS CERTIFICATION

hereby certify that the content of this report are accurate and correct. All tests and operations performed by this material manufacturer are in compliance with the equirements of the material specifications and applicable purchaser designated requirements.

Signed: **Valoree Varick** Valoree Varick
orm F-6100-002-054 rev 8 Quality Manager

State of Indiana, County of Whitley Sworn to and subscribed before me this day of

Signed: Notary Public

My commission expires:

ASTM A6 - 14.6: A signature is not required on the test report; however, the document shall clearly identify the organization submitting the report. Notwithstanding the absence of a signature, the organization submitting the report is responsible for the content of the report

Appendix 3: Measured Weld Sizes

Connection	Weld Size/Position Measured																							
	1			2			3			4			5			6			7			8		
	Left	Mid	Right	Left	Mid	Right	Bott	Mid	Top	Bott	Mid	Top	Left	Mid	Right	Left	Mid	Right	Bott	Mid	Top	Bott	Mid	Top
A	3/8	3/8	5/16	5/16	5/16	5/16	13/16	13/16	13/16	5/16	1/4	1/4	1/4	1/4	1/4	5/16	5/16	5/16	3/4	3/4	3/4	1/4	1/4 [1]	1/4
B	5/16	5/16	5/16	5/16	5/16	3/8	3/8	3/8	3/8	3/16	3/16	1/4	3/8	3/8	3/8	3/8	3/8	3/8	3/8	3/8	3/8	1/4	1/4	1/4
C	1/4	1/4	1/4	1/4	1/4	1/4	5/16	5/16	5/16	-	-	-	1/4	1/4	1/4	5/16	5/16	1/4	1/4	1/4	5/16	-	-	-
D	1/4	3/8	5/16	-	-	-	5/16	5/16	5/16	-	-	-	5/16	5/16	5/16	-	-	-	3/8	3/8	3/8	-	-	-
E	5/16	5/16	1/16	1/4	5/16	5/16	5/16	5/16	5/16	-	-	-	5/16	5/16	5/16	5/16	5/16	5/16	5/16	5/16	5/16	-	-	-
F	-	-	-	-	-	-	5/16	5/16	5/16	5/16	5/16	5/16	-	-	-	-	-	-	-	-	-	-	-	-
G	1/4	5/16	5/16	5/16	5/16	5/16	5/16	5/16	5/16	-	-	-	5/16	5/16	5/16	5/16	5/16	5/16	1/4	5/16	5/16	-	-	-
H	5/16	5/16	5/16	5/16	5/16	5/16	1/4	5/16	5/16	5/16	5/16	5/16	5/16	5/16	5/16	5/16	5/16	1/4	5/16	5/16	5/16	5/16	5/16	5/16
I	1/4	5/16	5/16	5/16	5/16	5/16	5/16	5/16	5/16	1/4	5/16	5/16	5/16	5/16	5/16	5/16	5/16	5/16	5/16	5/16	5/16	5/16	5/16	5/16
J	3/8	3/8	3/8	5/16	5/16	5/16	5/16	5/16	5/16	5/16	5/16	5/16	5/16	5/16	5/16	5/16	5/16	5/16	5/16	5/16	5/16	3/8	5/16	5/16
K	1/4	5/16	5/16	5/16	5/16	5/16	5/16	5/16	5/16	5/16	1/4	1/4	5/16	5/16	5/16	5/16	5/16	5/16	5/16	5/16	5/16	5/16	5/16	5/16
L	5/16 [2]	5/16 [2]	5/16 [2]	5/16 [2]	5/16 [2]	5/16 [2]	5/16 [2]	3/8 [2]	3/8 [2]	5/16 [2]	5/16 [2]	5/16 [2]	5/16 [2]	5/16 [2]	5/16 [2]	5/16 [2]	5/16 [2]	5/16 [2]	1/2	3/8 [2]	3/8 [2]	5/16 [2]	5/16 [2]	5/16 [2]

[1] Weld discontinuous at two points, between middle and top

[2] Increased to 1/2'' via in-house welding

As seen from the girder/beam towards the column

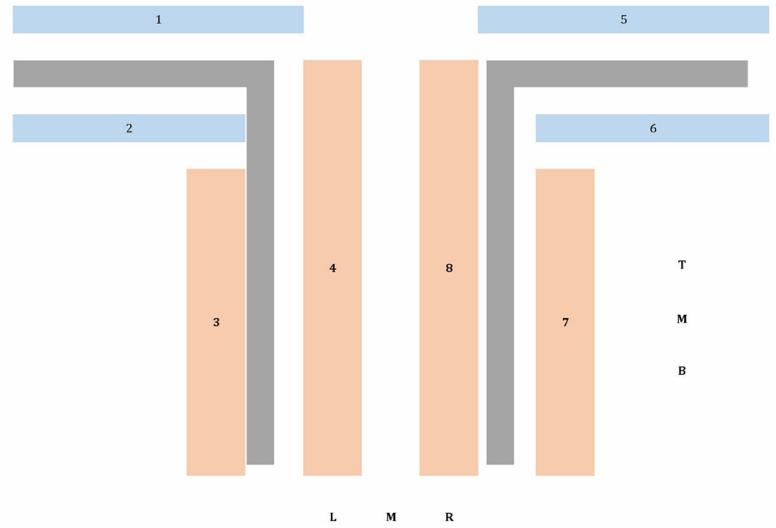

Appendix 4: Girder/Beam Test Length

Finding Length of W24x68 Test Girder

"Reality" Fully Composite Girder:
W24x68

Girder & Beam Properties:

Realistic Length of Girder: $L_{reality} := 30\ ft$

Cross-Sectional Area of Girder: $A_{girder} := 20.1\ in^2$

Beam Spacing: $s_{beam} := 10\ ft$

Depth of Girder: $d_{girder} := 23.7\ in$

MoE of Girder: $E_s := 29000\ ksi$

MoI of Girder: $I_{xgirder} := 1830\ in^4$

Loads:

$DL := 56\ psf$

$LL := 65\ psf$

Deck Properties:

Height of concrete: $h_{conc} := 3.25\ in$

Height of deck: $h_{deck} := 3\ in$

Total height of system: $h_{sys} := d_{girder} + h_{conc} + h_{deck} = 29.95\ in$

Weight of regular concrete (pcf): $w_c := 145$

Strength of regular concrete (ksi): $f'_c := 4$

Point Load: $P_{beam} := 77.896\ kip$

Factored Loading per foot:

$$W_{tot} := \frac{\left(P_{beam} \cdot 2\right)}{L_{reality}} = 5.193\ \frac{kip}{ft}$$

$$W_{tot} \cdot L_{reality} = 155.792\ kip$$

Effective width of concrete contribution:

$$b'_{eff} := min\left(\frac{L_{reality}}{8}, \frac{s_{beam}}{2}\right) = 3.75\ ft$$

$$b_{eff} := 2 \cdot b'_{eff} = 7.5\ ft$$

Modulus of Elasticity of Concrete:

$$E_c := w_c^{1.5} \cdot \sqrt[2]{f'_c} \cdot 1\ ksi = \left(3.492 \cdot 10^3\right)\ ksi$$

Modular ratio:

$$n' := \left(\frac{E_s}{E_c}\right) = 8.305$$

$$n := \mathrm{trunc}\left(n'\right) = 8$$

Note: round actual modular ratio to closest whole integer

Finding Length of W24x68 Test Girder

"Reality" Fully Composite Girder:
W24x68

Girder & Beam Properties:

Realistic Length of Girder: $L_{reality} := 30\ ft$

Cross-Sectional Area of Girder: $A_{girder} := 20.1\ in^2$

Beam Spacing: $s_{beam} := 10\ ft$

Depth of Girder: $d_{girder} := 23.7\ in$

MoE of Girder: $E_s := 29000\ ksi$

MoI of Girder: $I_{xgirder} := 1830\ in^4$

Loads:

$DL := 56\ psf$

$LL := 65\ psf$

Deck Properties:

Height of concrete: $h_{conc} := 3.25\ in$

Height of deck: $h_{deck} := 3\ in$

Total height of system: $h_{sys} := d_{girder} + h_{conc} + h_{deck} = 29.95\ in$

Weight of regular concrete (pcf): $w_c := 145$

Strength of regular concrete (ksi): $f'_c := 4$

Point Load: $P_{beam} := 77.896\ kip$

Factored Loading per foot:

$$W_{tot} := \frac{\left(P_{beam} \cdot 2\right)}{L_{reality}} = 5.193\ \frac{kip}{ft}$$

$$W_{tot} \cdot L_{reality} = 155.792\ kip$$

Effective width of concrete contribution:

$$b'_{eff} := min\left(\frac{L_{reality}}{8}, \frac{s_{beam}}{2}\right) = 3.75\ ft$$

$$b_{eff} := 2 \cdot b'_{eff} = 7.5\ ft$$

Modulus of Elasticity of Concrete:

$$E_c := w_c^{1.5} \cdot \sqrt[2]{f'_c} \cdot 1\ ksi = \left(3.492 \cdot 10^3\right)\ ksi$$

Modular ratio:

$$n' := \left(\frac{E_s}{E_c}\right) = 8.305$$

$$n := \mathrm{trunc}\left(n'\right) = 8$$

Note: round actual modular ratio to closest whole integer

Transformed concrete width:

$$b_{trans} := \frac{b_{eff}}{n} = 11.25\ in$$

Area of girder:

$$A_{girder} = 20.1\ in^2$$

Area of concrete:

$$A_{conc} := b_{trans} \cdot h_{conc} = 36.563\ in^2$$

Y bar of girder from top of system:

$$y_{girder} := h_{conc} + h_{deck} + \frac{d_{girder}}{2} = 18.1\ in$$

Y bar of concrete from top of system:

$$y_{conc} := \frac{h_{conc}}{2} = 1.625\ in$$

Y bar from top of system:

$$y_{bar} := \frac{\left(A_{girder} \cdot y_{girder}\right) + \left(A_{conc} \cdot y_{conc}\right)}{A_{girder} + A_{conc}} = 7.469\ in$$

Moment of inertia of concrete:

$$I_{conc} := \left(\frac{1}{12} \cdot b_{eff} \cdot {h_{conc}}^3\right) = 257.461\ in^4$$

Distance from centroid of concrete to overall centroid:

$$d_{conc.} := y_{bar} - \frac{h_{conc}}{2} = 5.844\ in$$

Moment of inertia of steel beam:

$$I_{xgirder} = \left(1.83 \cdot 10^3\right)\ in^4$$

Distance from centroid of steel beam to overall centroid:

$$d_{girder.} := h_{sys} - y_{bar} - \frac{d_{girder}}{2} = 10.631\ in$$

Transformed moment of inertia of composite section:

$$I_{trans} := \left(I_{conc} + \left(A_{conc} \cdot {d_{conc.}}^2\right)\right) + \left(I_{xgirder} + \left(A_{girder} \cdot {d_{girder.}}^2\right)\right) = \left(5.608 \cdot 10^3\right)\ in^4$$

Angle of rotation of beam at support:

$$\theta_{reality} := \frac{W_{tot} \cdot {L_{reality}}^3}{24\ E_s \cdot I_{trans}} = 0.005$$

"Simulated" Non-Composite Beam:
W24x68

$$\theta_{sim} := \theta_{reality}$$

$$W_{tot} := 9.09 \ \frac{kip}{ft}$$ <---Distributed Load

Final suggested length of simulated beam:

$$L_{sim} := \sqrt[3]{\frac{\theta_{sim} \cdot 24 \cdot E_s \cdot I_{xgirder}}{W_{tot}}} = 17.138 \ ft$$

$$W_{tot} \cdot L_{sim} = 155.784 \ kip$$

$$Reaction_{support} := \frac{W_{tot} \cdot L_{sim}}{2} = 77.892 \ kip$$ <--- Confirmed this value matches desired shear

Appendix 5: Required Design Strength Calculations

Girder-Column & Beam-Column Loading Calcs

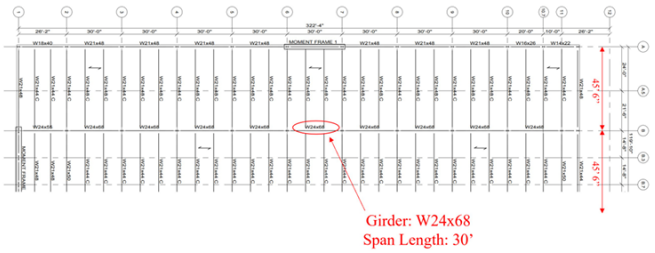

Loading Summary

Criteria are based on the 2012 *International Building Code (IBC)* and a project location of Minneapolis, Minn.

Gravity Loading	
Live Loads	
Office	65 psf (including 15 psf partition loading)
Roof Deck	100 psf
Roof Snow	50 psf
Dead Loads	
Typical Floor	46 psf (3 in. metal deck with 3½ in. LW Concrete)
Roof	4 psf (3 in. metal deck)
Superimposed Dead Loads	
Office	10 psf (CMEP, etc.)
Occupied Roof	45 psf (CMEP, pavers, roofing, etc.)
Unoccupied Roof	20 psf (CMEP, roofing, etc.)
Cladding	
Brick Façade	770 plf
Wind Loading	
Basic Wind Speed	115 mph
Exposure Category	C
Drift Limit	H/500

Seismic Loading	
Seismic Design Category	A
Seismic Importance Factor	1.00
Spectral Response Acceleration, Short Period, S_s	0.048 g
Spectral Response Acceleration, One Second Period, S_1	0.027 g
Site Class	D
Building Period Coefficient, C_t	0.02
Response Modification Factor, R	3.00
System Overstrength Factor, Ω_0	3.00
Deflection Amplification Factor, C_d	3.00
Allowable Story Drift Coefficient	0.02
Lateral Force Resisting System	
Steel Systems Not Specifically Detailed For Seismic Resistance	
Risk Category	II

Beam Dimensions:

$L_{beam} := 45.5\ ft$ $S_{beam} := 10\ ft$

Unfactored Loads:

$LL := 65\ psf$ $LL' := LL \cdot S_{beam} = 650\ plf$

$DL := 56\ psf$ $DL' := DL \cdot S_{beam} = 560\ plf$

Factored Loads:

$$W_{factored} := (1.2 \cdot DL') + (1.6 \cdot LL') = (1.712 \cdot 10^3)\ plf$$

Reactions:

$$M_{maxbeam} := \frac{W_{factored} \cdot {L_{beam}}^2}{8} = 443.034\ kip \cdot ft$$

Beam-to-Column Shear Reaction:

$$V_{beam} := \frac{W_{factored} \cdot L_{beam}}{2} = 38.948\ kip$$

Girder Dimensions:

$L_{girder} := 30\ ft$ $S_{girder} := 45.5\ ft$

Reactions:

$$P_{beam} := 2 \cdot V_{beam} = 77.896\ kip$$

$$M_{maxgirder} := P_{beam} \cdot S_{beam} = 778.96\ kip \cdot ft$$

Girder-to-Column Shear Reaction:

$$V_{girder} := P_{beam} = 77.896\ kip$$

W16x36 Girder Loading Calcs

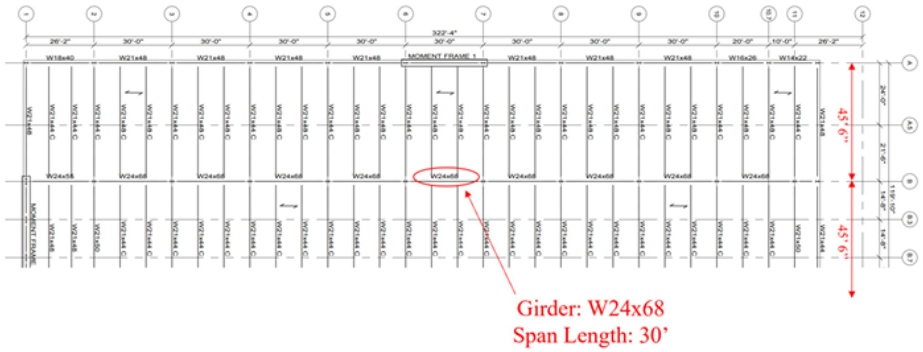

Beam Dimensions:

$L_{beam} := 30\ ft$ $S_{beam} := 10\ ft$

Unfactored Loads:

$LL := 65\ psf$ $LL' := LL \cdot S_{beam} = 650\ plf$

$DL := 56\ psf$ $DL' := DL \cdot S_{beam} = 560\ plf$

Factored Loads:

$$W_{factored} := (1.2 \cdot DL') + (1.6 \cdot LL') = (1.712 \cdot 10^3)\ plf$$

Reactions:

$$M_{maxbeam} := \frac{W_{factored} \cdot L_{beam}^{\ 2}}{8} = 192.6\ kip \cdot ft$$

$$V_{beam} := \frac{W_{factored} \cdot L_{beam}}{2} = 25.68\ kip$$

Girder Dimensions:

$L_{girder} := 30\ ft$ $S_{girder} := 30\ ft$

Reactions:

$$P_{beam} := 2 \cdot V_{beam} = 51.36\ kip$$

$$M_{maxgirder} := P_{beam} \cdot S_{beam} = 513.6\ ft \cdot kip$$

$$V_{girder} := P_{beam} = 51.36\ kip$$